



BRNO UNIVERSITY OF TECHNOLOGY

VYSOKÉ UČENÍ TECHNICKÉ V BRNĚ

FACULTY OF MECHANICAL ENGINEERING

FAKULTA STROJNÍHO INŽENÝRSTVÍ

INSTITUTE OF SOLID MECHANICS, MECHATRONICS AND BIOMECHANICS

ÚSTAV MECHANIKY TĚLES, MECHATRONIKY A BIOMECHANIKY

ANALYSIS OF IMPACT OF EXPERIMENT REALISATION ON MECHANICAL CHARACTERISTICS OF BIOMATERIALS

ANALÝZA VLIVU REALIZACE EXPERIMENTU
NA MECHANICKÉ CHARAKTERISTIKY BIOMATERIÁLŮ

AUTHOR

AUTOR PRÁCE

ING. MARTIN SLAŽANSKÝ

SUPERVISOR

ŠKOLITEL

PROF. ING. JIŘÍ BURŠA, PH.D.

CO-SUPERVISOR

ŠKOLITEL SPECIALISTA

ING. PAVEL SKÁCEL, PH.D.

BRNO 2017

Abstract

The dissertation thesis focuses on the plausibility of mechanical testing of soft biological tissues and on the predictive capabilities of different material models, all assessed using finite element method.

The first part of the thesis is dedicated to an introduction into the problem. Next soft biological tissues related to the problem and the ways of their mechanical testing are described according to the most recent knowledge.

The second part of the thesis deals with finding the optimal experimental setup using computational modelling by virtual simulation of the mechanical testing.

Results have confirmed that two narrow clamps per edge as well as commonly used hooks are applicable for biaxial tension testing of different soft tissues using square shape specimens. Use of clamps is therefore a time efficient, easy and reliable alternative not inferior to hooks. The analysis focused on recommendations for the choice of type, number and size of gripping elements for different specimen size was also carried out in the thesis.

The third part of the thesis examines the predictive capabilities of material models of soft tissues and their dependencies. It can be concluded that the resulting mechanical behaviour of a fitted material model depends on starting parameters and there are no “ideal” starting parameters to be used when fitting experimental data. Despite the absence of “ideal” starting parameters, the most efficient way of achieving the best approximation of experimental data from many data sets is proposed. Furthermore, it is also concluded that a constraint of the fitted parameters results in unpredictable influence on the quality of the fit.

Finally, the presumption of affine and non-affine deformation of material models was analysed in order to explain the large contradictions between the structure-based constitutive models and the results of biaxial tests under different testing protocols. Although certain differences between the analysed models were found out, they were not significant enough to explain those large contradictions.

Further possible areas of investigation are mentioned as the last part of the thesis.

Key words: soft biological tissues, biaxial mechanical testing, computational modelling, constitutive model, sensitivity analysis, predictive capability, affine deformation

Abstrakt

Dizertační práce se zabývá věrohodností mechanického testování měkkých biologických tkání a predikčními schopnostmi různých modelů materiálů. Obě oblasti byly zkoumány užitím metody konečných prvků.

První část práce je věnována úvodu do problému a popisu měkkých biologických tkání, které s problémem souvisí, a rešerši nynějšího způsobu jejich mechanického testování.

Druhá část práce se zabývá hledáním optimálního nastavení experimentálního zařízení za použití počítačového modelování pomocí virtuální simulace mechanických testů.

Výsledky analýzy potvrdily, že dvě úzké svorky po délce hrany, stejně jako běžně používané háčky, jsou použitelné pro dvouosé tahové zkoušky různých měkkých tkání za použití čtvercového vzorku. Použití svorek je proto časově úsporná, jednoduchá a spolehlivá alternativa, která není podřadná použití háčků. V práci byla rovněž provedena analýza, jejímž výsledkem jsou doporučení ohledně typu, počtu a velikosti uchycení pro různě velké vzorky.

Třetí část práce zkoumá predikční schopnosti modelů materiálů měkkých tkání a závislosti těchto schopností. Lze shrnout, že výsledné mechanické chování proloženého modelu materiálu závisí na počátečních parametrech a že neexistují „ideální“ počáteční parametry při prokládání experimentálních dat. Navzdory absenci „ideálních“ počátečních parametrů je navržen v rámci možností nejefektivnější způsob aproximace experimentálních dat z mnoha jejich souborů. Dále je možné shrnout, že omezení hodnot parametrů modelu při prokládání experimentálních dat ústí v nepředvídatelný vliv na kvalitu aproximace.

V závěrečné části práce byl analyzován předpoklad afinní a neafinní deformace modelů materiálů za účelem vysvětlení velkých rozporů mezi výsledky strukturně založených modelů a výsledky dvouosých testů při různých testovacích protokolech. Ačkoli byly zjištěny určité rozdíly mezi výsledky analyzovaných modelů, přece nebyly dostatečně významné, aby vysvětlily výše uvedené velké rozpory.

V poslední části práce jsou zmíněny další možné oblasti výzkumu.

Klíčová slova: měkké biologické tkáně, dvouosé mechanické testování, počítačové modelování, konstitutivní model, citlivostní analýza, predikční schopnost, afinní deformace

I declare herewith that I have personally penned this doctoral thesis. I have only used the mentioned sources and utilities and have marked parts copied from elsewhere, either literally or by content as such. I have also used texts and information from my own co-authored publications.

The doctoral thesis is written in English language.

Prohlašuji, že tuto dizertační práci jsem vypracoval samostatně s použitím odborné literatury a dalších informačních zdrojů, které jsou všechny citovány. V dizertační práci jsem také použil texty a informace z článků, kterých jsem autor nebo spoluautor.

Práce je psána v anglickém jazyce

Ing. Martin Slažanský

Bibliographic quote

SLAŽANSKÝ, M. Analysis of impact of experiment realisation on mechanical characteristics of biomaterials. Brno University of Technology, Faculty of Mechanical Engineering, 2018. 122 p. Supervisor: prof. Ing. Jiří Burša, Ph.D.

Dizertační práce je dostupná v tištěné podobě na oddělení vědy a výzkumu Fakulty strojního inženýrství Vysokého učení technického v Brně, Technická 2896/2, 616 69 Brno.

Acknowledgement

I wish to express my deep gratitude to my supervisor prof. Ing. Jiří Burša, Ph.D. for all his guidance and support throughout my research. I also want to thank Ing. Stanislav Polzer, Ph.D., Ing. Vojtěch Man, Ing. Kamil Novák and Ing. Pavel Skácel, Ph.D. who all helped me with an immense number of problems in both experimental and computational fields.

Last but not least I am thankful to my family and my wife Markéta who supported me for the whole time of my doctoral study.

This thesis would not exist without any of these people.

Table of Content

1	Introduction	10
1.1	Motivation	11
1.2	Goals of the thesis.....	11
2	Soft biological materials.....	12
2.1	Abdominal aortic wall	12
2.2	Main components of aortic wall	14
2.3	Properties of aortic wall.....	15
3	Mechanical tests of soft biological tissues	16
3.1	Uniaxial tension tests.....	18
3.2	Biaxial tension tests	18
3.3	Compressibility tests.....	23
4	Sensitivity analysis of gripping method - Methodology	25
4.1	FE parametric study.....	25
4.1.1	Geometry	26
4.1.2	Applied material models	29
4.1.3	Numerical problems of anisotropic material models	32
4.1.4	Contacts	32
4.1.5	Mesh specifics	33
4.2	Evaluation of accuracy of biaxial tension tests	36
4.3	Evaluation of the parametric study	40
4.4	Limitations of the computational model.....	41
5	Sensitivity analysis of gripping method - Results	42
5.1	Influence of 2D vs. 3D modelling	42
5.2	Influence of dimensions and numbers of grips.....	43
5.3	Influence of the loading protocol.....	45
5.4	Influence of the specimen size.....	46

5.5	Summary of results	48
6	Predictive capabilities of different material models	50
6.1	Process of fitting the measured data using the program Hyperfit	51
6.2	Dependence of coeff. of det. on starting and constrained parameters	54
6.2.1	Starting parameters	54
6.2.2	Constrained parameters	56
6.2.3	Overview	59
6.3	Conclusion	62
7	The influence of affine deformation between matrix and fibres	63
7.1	Motivation	63
7.2	Objective.....	63
7.3	Methods	64
7.3.1	Geometry	64
7.3.2	Applied material models	65
7.3.3	Mesh specifics, connections	67
7.3.4	Loads and other boundary conditions, testing protocol	68
7.3.5	Parametric study	69
7.3.6	Examples of deformed state	70
7.3.7	Evaluation of virtually measured data	71
7.4	Results	72
7.5	Discussion, limitations.....	75
8	Conclusion.....	76
9	Future work	78
9.1	Experimental estimation of radial stiffness	78
9.2	Using other anisotropic material models	79
9.3	Analysis of gripping with rakes	79
9.4	Inaccurate positioning of gripping elements	80

10	References	81
11	List of Figures	93
12	List of Tables.....	97
13	Authors publications	98
14	Appendix A.....	100
15	Appendix B	101
16	Appendix C	104

1 Introduction

Design, realisation and evaluation of mechanical tests have a significant influence on quality of the measured and modelled stress-strain data. Reliable and accurate description of mechanical behaviour of the tested material is fundamental for further calculations of any structure (e.g. carrying capacity of a bridge, economic design of a bicycle, or rupture risk of an aortic aneurysm).

For classical structural materials (crystalline) just uniaxial tests are sufficient. Standardisation of the experimental setup ensures high accuracy of their results. Materials showing large strains (e.g. rubber or soft tissues) need biaxial tests which are not standardized and are influenced by load transmission to the specimen due to St. Venant's principle. Their accuracy is therefore lower.

In order to find the optimal experimental setup we can use computational modelling to virtually simulate the mechanical testing with the aim to evaluate the influence of various experimental setups on the resulting stress-strain data. Also operator's influence causing inaccuracies in the setup is significant and should be examined.

Especially finite element (FE) models can help us to simulate mechanical behaviour of soft tissues and other materials showing large strains [1][2][3][4][5] which are the object of interest in this thesis. FE models enable us to simulate real tests of soft tissues. The main advantage of virtual testing is the inherent knowledge of the mechanical properties (characteristics) and behaviour of the virtually tested material specimen. Thus you can compare the virtually measured data with the input material model to evaluate the inaccuracy of the results obtained using the chosen testing setup which is, to the author's best knowledge, a novel approach. This principle is almost impossible in real testing due to the mostly unknown exact material properties of the measured material. Another positive of computational modelling is the absence of measurement noise and unwanted operator's influence on the testing and also the possibility of large amount of simulations with different experimental setups.

The measured stress-strain data are implemented into the following FE analyses via material models. The predictive capabilities of material models, which are based on measured data, are capable to influence the results of FE analyses significantly. Thus the predictive capability and its dependencies should be also examined.

1.1 Motivation

Our research group at the Brno University of Technology, Institute of Solid Mechanics, Mechatronics and Biomechanics, was focusing on calculation of the rupture risk of abdominal aortic aneurysm. Uniaxial and biaxial tension tests of healthy porcine aorta, of the human aortic aneurysm wall and of intraluminal thrombus were performed here in order to obtain stress-strain data describing mechanical behaviour of these soft tissues. These data create a basis for material model identification.

Our experimental setup differs from those commonly used elsewhere in the way how the load is transferred onto the specimen. Instead of many hooks or one wide clamp we use two slim clamps per edge, see Figure 3. This approach was repeatedly dissented in the process of reviewing our articles by some researchers from other research groups as they were of the opinion that this approach cannot give reliable results. Therefore in this thesis I investigated the influence of different gripping methods on the measured biaxial stress-strain data using computational modelling, together with other possible influencing factors of experiment realisation.

To my best knowledge, such extensive analysis has not been performed till now. I investigated hooks used commonly to grip the specimen [1][7][8][12][13][15][16][21][22][24][25][26] as well as clamps which so far have been used by our group only [17][29].

Furthermore, different material models are commonly used which exhibit different predictive capabilities. Thus the predictive capability and its dependencies are also examined in this thesis.

1.2 Goals of the thesis

- a) To perform a literature review about mechanical testing of soft biological tissues and about the influence of experiment realisation on the mechanical characteristics of soft biological tissues.
- b) To investigate the influence of experiment realisation on mechanical characteristics of soft biological tissues using computational modelling of selected types of tests.
- c) To investigate the predictive capability of material models and its dependencies. This goal emerged from further scientific work under solved projects.

2 Soft biological materials

Accurate simulation of biaxial tension tests of soft biological tissues requires thorough knowledge of mechanical properties of those tissues which are the subject of testing. In my case it is specifically the abdominal aortic wall.

In this chapter only a rudimentary medical minimum is introduced for orientation in this work. An extensive description of the issue can be found in the literature [40], graduate works [41][42][43][44], online e-learning of Biomechanics course [45], or on the websites of medical faculties of the Czech and Slovak Republic [46]. Those sources form a basis for this chapter.

The knowledge of the basic properties of the measured tissue is a needed prerequisite for proper setup of the experiment. As examples we can mention the choice of type of mounting (gripping) the specimen or of a correct keeping of nonstandard boundary conditions, such as specimen immersion in physiological solution or maintaining a constant temperature corresponding to body temperature. Furthermore the knowledge of mechanical and structural properties of the tissue creates a solid basis for advanced structural material models such as Holzapfel 2000 [34] or Holzapfel 2005 [71] models, Gasser model [35], Martufi-Gasser model [70]. In addition to the results of biaxial tests, these models use also structural data such as, for example, fibre orientation and distribution, or waviness.

The most common tested soft tissues are the blood vessel wall (see references in the bibliography), skin [39], the bladder wall [47], small intestine [13] or tendon [48].

In the next chapter a wider description of the abdominal aortic wall is offered which is the subject of the simulated mechanical tests in this thesis.

2.1 Abdominal aortic wall

Abdominal aorta has the outer diameter of 20-25 mm [49] and a wall thickness of about 1,8 mm [50][51]. Abdominal aortic wall consists of three layers: tunica intima, tunica media and tunica adventitia.

The inner layer (tunica intima) is formed by a thin layer of endothelial cells, ensuring the smooth flow of blood. It has distinctly orthotropic behaviour and axial stiffness is greater than the circumferential [45]. Its thickness increases with age [54].

The middle layer (tunica media) is the thickest aortic layer formed by smooth muscle cells, elastin and collagen [45][55], see Figure 1. The picture represents the structure of abdominal aorta of a rat.

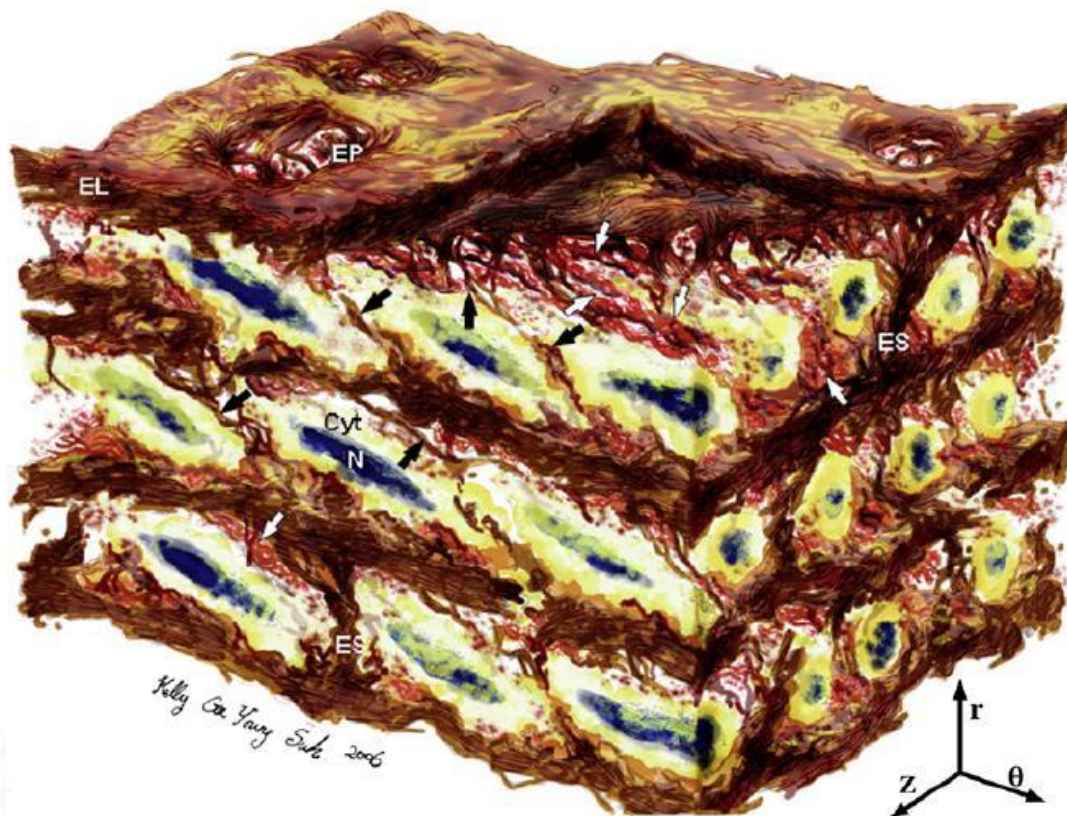


Figure 1 The microstructure of the tunica media including tunica intima. Coordinates r , z , and θ represent radial, axial, and circumferential directions, respectively. Dimensions of the specimen $\theta \times z \times r$ are $80 \mu\text{m} \times 60 \mu\text{m} \times 45 \mu\text{m}$. Elastin (white letters EL, IEF, ES and EP), smooth muscle cells (blue nucleus, cytoplasm white) and collagen (indicated by the black arrows) can be seen [56].

In a normal state the tunica media absorbs majority of the load caused by the blood pressure.

The outer layer (tunica adventitia) consists mainly of collagen fibres and fibroblasts. The collagen fibres are arranged in almost isotropic way [29].

The collagen fibres at a normal blood pressure and without external influence (overload, impact, etc.) are wavy [57].

It is clear that the most important building components of the wall are elastin, collagen and smooth muscle cells. Elastin and collagen are fibrillar components of the extracellular tissue. Together with binding cells they form a connective tissue [59]. In the following the function and structure of these essential components of the wall of the abdominal aorta are described.

2.2 Main components of aortic wall

Elastin

From a mechanical point of view elastin is very pliable with the ductility of about 70 % [61], the Young's modulus value differs according to different sources from 523 kPa [62] to 1200 kPa [91]. In FE simulations I use the value 900,8 kPa [32]. Elastin exhibits approximately linear response in the Green strain vs. Cauchy stress space. Elastin gradually degrades with age [54].

Collagen

Collagen fibres provide the vessel wall with tensile strength and stiffness [63] and are the stiffest part of the vessel wall. The ductility is in the range of 2–4 %, Young's modulus in units of GPa [64].

Smooth muscle cells

The function of smooth muscle cells is muscle contraction and protein synthesis for tissue remodelling. They are characterised by a wide hysteresis loop, significant relaxation and Young's modulus in the range between 15 to 25 kPa [45].

These cells are mainly responsible for the viscoelastic behaviour of the arterial wall [65]. With a greater loading speed the artery wall exhibits higher stiffness [66].

Smooth muscle cells can bring inaccuracies into measuring mechanical properties of the wall because of their changed state from in vivo to in vitro. The changes could be for example

due to different chemical environment or ceased innervation and nutrition and consequent death of the cells.

2.3 Properties of aortic wall

The aortic wall as a whole exhibits an approximately equal strain range under physiological load up to about 25÷30 % [29] and the strength of about 1 MPa [45]. Although it is commonly considered as incompressible, number of contradictive experimental results exists and it is still under investigation [74], see chapter 3.3 for more intense literature search on this topic.

The artery is axially prestressed, thereby reducing the risk of loss of shape stability when the artery is bent. This prestressing effect represents itself by longitudinal shortening after removal from the body. This effect influences the character of stress distribution in the arterial wall. In case of a healthy young (porcine) aorta, the value of axial pre-stretch can achieve 21÷43 % depending on the position of the specimen along the aorta [77]. In case of human abdominal aorta the value of about 40 % drops to a few percent with increasing age [92]. Another effect influencing the stress distribution in the wall is the residual stress [72].

3 Mechanical tests of soft biological tissues

Computational, especially finite element models (FEM) represent a relevant approach in biomechanics of soft tissues nowadays and help us to simulate mechanical behaviour of soft tissues. Quality of the model depends primarily on the quality of input data which are obtained from experiments. Credibility of the experiment thus defines the quality and plausibility of the computational model.

It was shown that the choice of experiment type and its various features can be decisive for accuracy of the results, may cause significant errors in some cases and thus negatively influence outputs of the computational models. In case of soft biological tissues the measured stress-strain data based on uniaxial or biaxial tension tests give different mechanical behaviour of the measured material. The apparent initial stiffness and overall anisotropy differs greatly, namely the material model proposed by Raghavan and Vorp [31] versus the Microfiber model [29] and the work of Vande Geest [30] or Tong [16].

The influence of the inaccurate or non-ideal realisation of the experiment with chosen features can also influence the results negatively.

An example of specimen preparation and biaxial testing is introduced below. In Figure 2 acquiring of the specimens of human and porcine aortic tissue is shown. Small specimen size (typically 15 x 15 mm) should be noted.

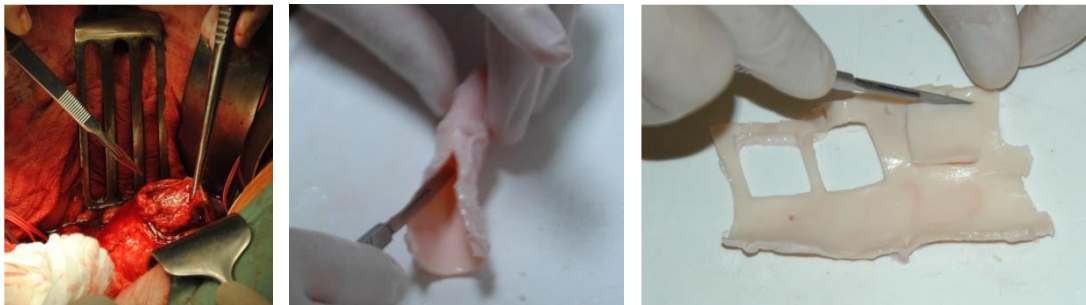


Figure 2 Acquiring of the specimen of the human aorta from a surgery (left) and from a porcine aorta (middle). Specimens are cut according to axial and circumferential directions (right).

Specimen is gripped with clamps or other gripping elements into the testing device, see Figure 3. Contrast points (markers) in the middle of the specimen serve as tracking points for off-line evaluation of the deformation of the specimen.

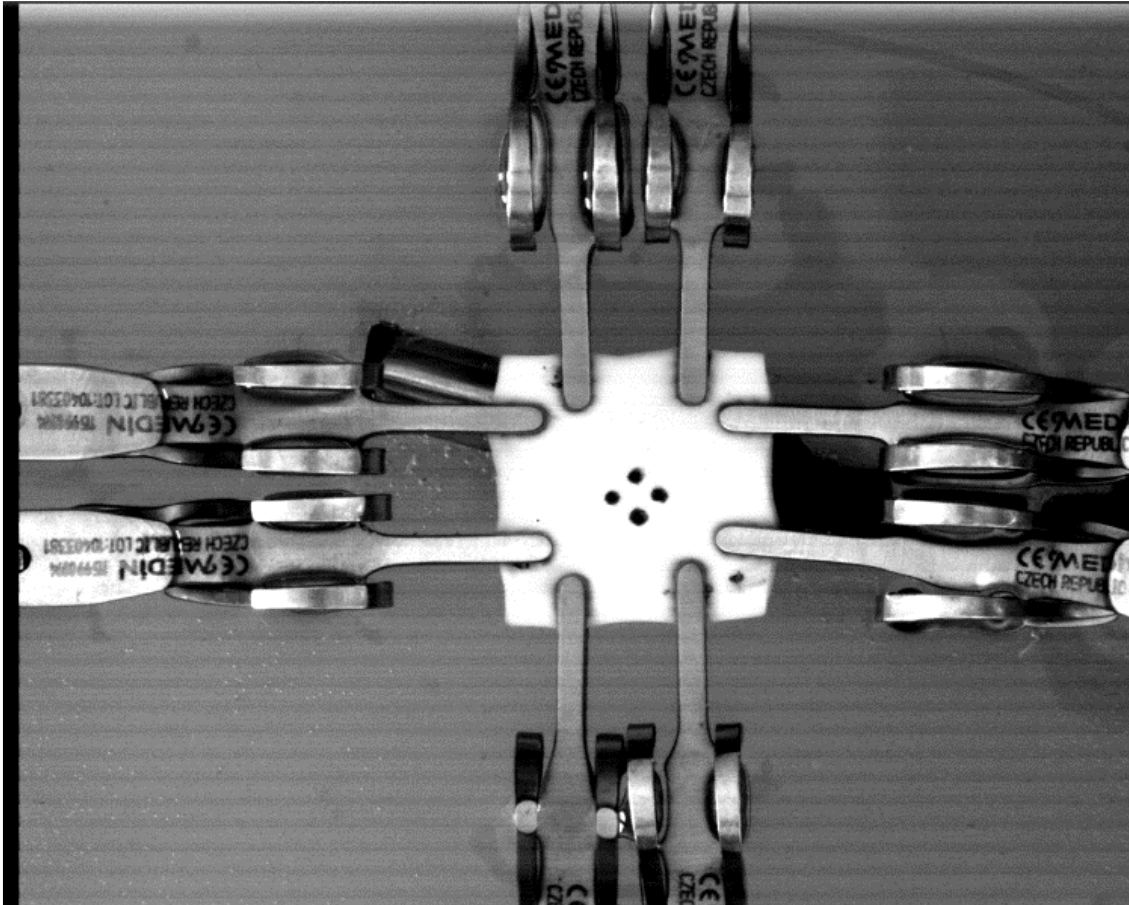


Figure 3 Gripped specimen with contrast points (markers) in the centre of the specimen.

In biaxial testing of soft tissues, stresses are calculated by dividing the total force by the undeformed cross section area. Intrinsicly the assumption of uniform stress distribution throughout the specimen cross section is introduced here. Strains, however, are calculated on the basis of the (optically recorded) undeformed and deformed positions of markers (contrast points) in the central part of the specimen called region of interest (ROI) below. Consequently, the calculated value represents an average throughout the ROI. This difference may have significant consequences on the accuracy of the stress-strain curves obtained from these tests, especially if using square shaped specimen. In these specimens the load acting at the specimen edges is not far enough from the ROI in the sense of Saint Venant's principle, therefore the stress and strain distribution throughout the evaluated region of the specimen is not uniform and the non-uniform load distribution along the specimen edge influences the measured data.

We cannot evaluate the accuracy of experimental data from the experiment itself because we are neither able to measure stresses nor evaluate (non)uniformity of their distribution. However, they can be easily evaluated in FE simulations where also dimensions, including the deformed ones, can be assessed with higher accuracy, and, moreover, we know the ideal (input) material properties for comparison. The goal of the FEM simulations is therefore to assess the inaccuracy of the measured data, to determine main influences on the measured data and to design the best setting of the testing device.

3.1 Uniaxial tension tests

Most engineering materials like steel or plastics are isotropic and usually undergo small strains, so a uniaxial tension test is sufficient to describe their mechanical behaviour in the range of small deformations. Soft tissues exhibit however large strains and an anisotropic behaviour due to their fibrous structure which is equivalent to composites. It has been shown by several authors that for credible constitutive models of soft tissues biaxial tension tests should be preferred to uniaxial ones because they correspond better to the physiological load of these tissues in human body [6][7].

Nevertheless, uniaxial tension test are still used to measure the strength and the mechanical behaviour of the material in different axes, typically in the direction of fibres and the direction perpendicular to fibres, and they are used to determine parameters of different material models [77][78][79][80].

3.2 Biaxial tension tests

As stated above, in soft tissue testing biaxial tension tests are preferred to uniaxial ones. In contrast to uniaxial tension tests there are no generally agreed standards for the execution of biaxial tensile tests; their arrangement, specimen shape and size, as well as the way of load transmission on the specimen (gripping elements used), are chosen solely by the staff or the designer of the respective testing machine. It has been shown that the chosen features can be decisive for accuracy of the results and may cause significant errors in some cases [8][9][10][37]. In all these papers the effect of specimen gripping was investigated using 2D simulations.

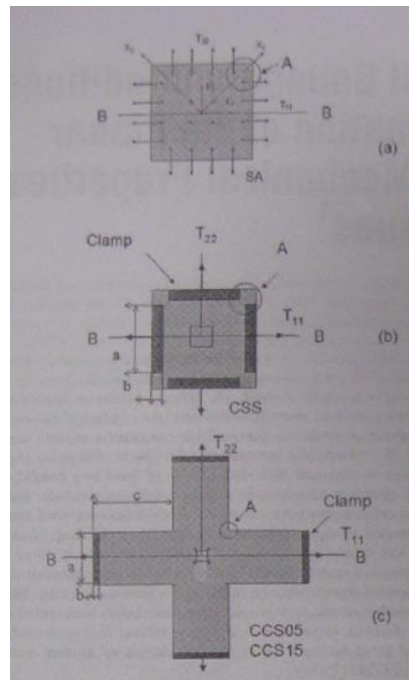


Figure 4 Different gripping methods and specimen shapes [8].

In [8] four, six and eight hooks or one wide clamp were used on square shaped (25 mm edge length) or cruciform specimens. The examined specimen shapes are shown in Figure 4. Only equibiaxial tests were simulated. Hooks were evaluated as the best gripping method according to more even stress distribution through the specimen. This approach to evaluation of the suitability of different experimental setups is indirect, as it only indicates a possible influence on the measured data, not the measurement error itself. More about the evaluation of the accuracy of biaxial tension tests is written in chapter 4.2. According to the conclusion of this paper, four hooks are sufficient; more hooks cannot offer better results. One clamp was not recommended to use as it constrains transversal deformation and therefore substantially redistributes the stresses, primarily by inducing high stress concentrations at the corners between the clamps and also by essential “stress-shielding” of the central region [8].

Similar cases were analysed also in [9] and [10], see Figure 5.

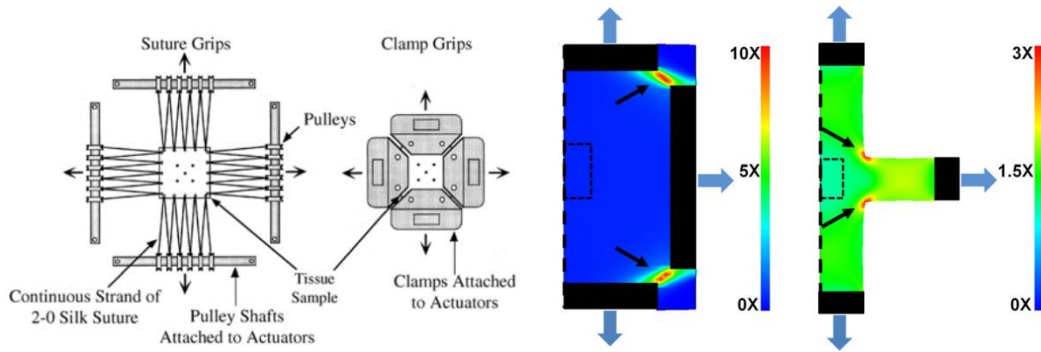


Figure 5 Different gripping methods using sutures or one wide clamp on square or cruciform specimen [9][10].

In all cases the boundary conditions affected the measured mechanical response of the tissue. Samples appeared to become less extensible and stiffer when clamped (using one broad clamp). The gripping method had no effect on the collagen fibre (re)distribution at the sample centre [9]. The shear strain inducted in tissue samples was negligible [9]. Broad clamps with their high stress concentrations between the clamps in the specimen corners redistribute the load from ROI significantly, resulting thus in a stress-shielding effect [10]. This effect is particularly notable in case of square specimen and less pronounced for cruciform specimen [10].

Although both square-shaped [6][7][8][9][12][13][14][15][16][17] and cruciform [7][8][18][19] specimens are commonly used for biaxial testing of soft tissues, the cruciform specimens require a much larger amount of tissue for the same ROI size compared to the square shaped ones [7]. Therefore square specimens are preferred if the specimen size is limited (e.g. for arterial tissues) although they are rather sensitive to the non-uniform load distribution along the specimen edges due to disruption of the Saint Venant's principle.

In contrast to cruciform specimens, however, it is not possible to keep a sufficient distance (in the sense of St. Venant's principle) between the gripping elements and the specimen centre for square shaped specimens; consequently, the assumption of uniform stress distribution throughout the specimen cross section is disturbed. On the contrary, strains (or stretches) are calculated on the basis of the (optically recorded) undeformed and deformed positions of markers (contrast points) in the central area of the specimen [11](ROI). The calculated components of deformation gradient tensor are then transformed into principal

coordinate system and polar decomposition is applied to obtain the principal components of stretch tensor. Thus the calculated values of stresses represent average values throughout the whole cross section of the specimen, while strains are averaged throughout the ROI only. This difference may have a significant impact on the accuracy of the stress-strain curves obtained from these tests because the values in the ROI can be overestimated or underestimated in comparison with the average values throughout the specimen; the difference depends on the number, shape, dimensions and position of the gripping elements. Typically, for two gripping elements the values of stresses and strains are lower in the ROI than the average throughout the specimen, while for three gripping elements they are higher because of the central gripping element. In general, clamps, sutures (threads), or hooks (sometimes joined into rakes) are commonly used as gripping elements introducing the load into the specimen in biaxial testing.

Examples of using hooks to grip the specimen are shown in Figure 6.

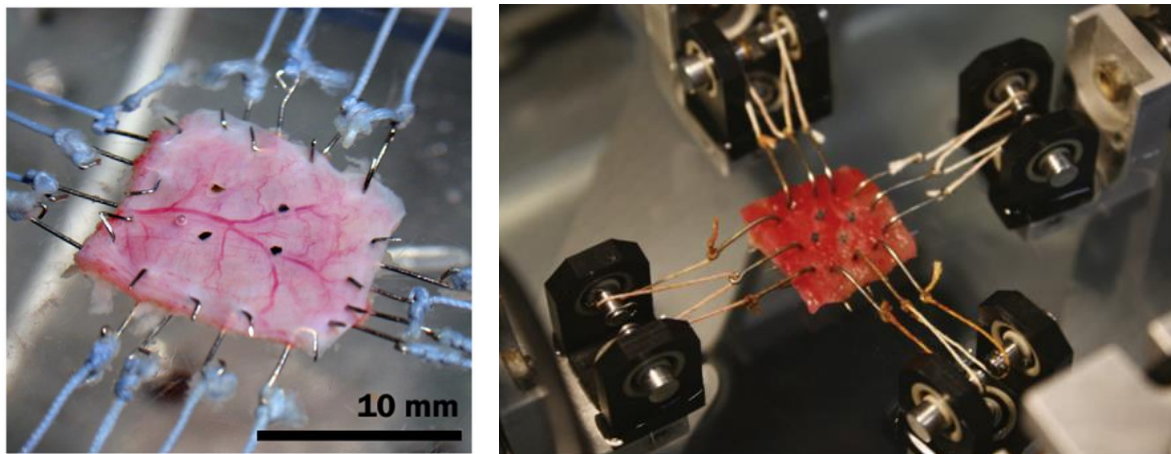


Figure 6 Example of gripped specimen using hooks (left [13], right [16]) and markers.

In some cases also rakes are used [25][37], see Figure 7. Rakes differ from hooks in the induced boundary conditions when constant displacement load is introduced by their individual pins instead of constant forces acting on every hook.

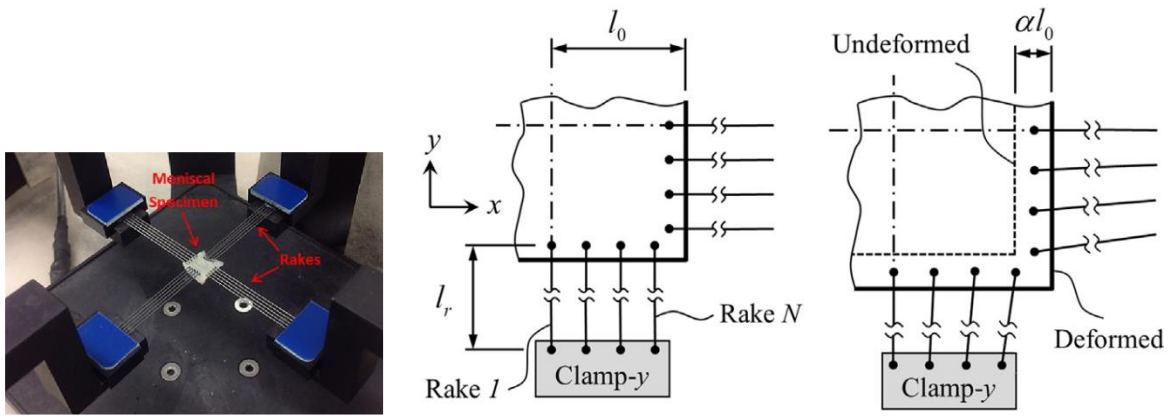


Figure 7 Specimen gripping using rakes (left [25], right [37]).

While hooks are applied most frequently and considered as a standard gripping method (see among others [20][21][22][23][24][25][26][27]), clamps were rejected as unacceptable by some authors [8][9][10][37]. However, this rejection was substantiated by numerical or experimental analyses done only for broad clamps used one per specimen edge, while two or more narrow clamps per edge were — according to our knowledge — presented by our group only [17][29], see Figure 8.

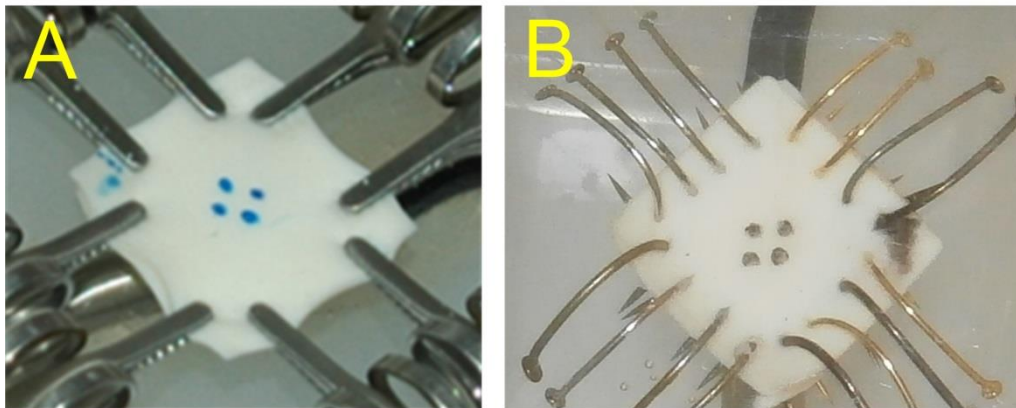


Figure 8 Real specimen of young porcine aortic tissue gripped using two clamps (A) or four hooks (B) per edge.

From a practical point of view, the application of clamps brings several advantages compared to hooks. Manipulation with clamps is easier and faster, it allows repeatable mounting and unmounting of the specimen without tearing it which is important for reaching the optimal spatial position of the clamps. Also avoidance of the risk of operator injury which exists when using sharp hooks is worth to be mentioned. On the other hand, any thorough

analysis has not yet been performed to compare the accuracy of the measured stress-strain curves when using several clamps or hooks per specimen edge. Therefore a comparison of these two methods is addressed in my doctoral thesis to assess advantages and drawbacks of both methods and to validate the application of clamps.

3.3 Compressibility tests

Arterial wall is commonly considered incompressible. In opposite to this fact some researchers still investigate this simplification [75] because number of contradictive experimental results exist, as stated in [74], see Table 1 for comparison of some of the results. In spite of these facts most of the constitutive models for arterial wall are defined as incompressible since this also simplifies analytical calculations [74] and ensures better convergence of numerical FE solution.

Table 1 Summary of experimental data from past studies on incompressibility of arterial wall [76]. NS – not specified, US - ultrasound

Publication	Year	Animal	Artery	Spec. quant.	V_0 (μL)	dV/V_0 (%)	Method
Lawton [81]	1954	Canine	Aorta	NS	1000	Negligible	Extension tests
Carew et al. [82]	1968	Canine	Various	31	426 – 2933	Negligible	Static inflation test
Tickner, Sacks [83]	1967	Human	Various	9	NS	Up to 35%	X-ray measurements
		Canine	Thoracic aorta	2			
			Femoral artery	2			
Dobrin, Rovick [85]	1967	Canine	Carotid	NS	NS	Negligible	X-ray measurements

Chuong, Fung [84]	1984	Rabbit	Thoracic aorta	4	41,9 – 53,9	Negligible	Strip compression
Girerg et al. [87]	1992	Human	Mammary, Radial	6	cca 32,3 (for 1 cm length)	Negligible	US measurements
Faury et al. [86]	1999	Mouse	Various	14	NS	15 – 18%	Transillumination
Boutouyrie et al. [88]	2001	Human	Carotid	15	103,5 (for 1 cm length)	4,7 ± 2,7%	US measurements
Chesler et al. [89]	2004	Mouse	Left pulmonary	12	cca 0,3	15 – 20%	Transillumination
Di Puccio et al. [90]	2012	Swine	Renal artery	2	78,5 – 251,3	6 – 20%	Dynamic inflation test

The experimental setup of incompressibility test is mostly based on a pressure load acting on a flat specimen [84] or on an internal pressure on a whole aorta tube [90][76], see the review article [76] for detailed description of different experimental setups.

4 Sensitivity analysis of gripping method - Methodology

I have stated above that experiments cannot be used to evaluate the influence of different clamping methods on the resulting measured mechanical behaviour of soft tissues. The main reasons are as follows:

1. In reality we do not know the true mechanical properties of the measured tissue. So I cannot compare measured results with the ground-truth (ideal) data.
2. Experiments suffer from different numerous errors caused by the operator, mechanism, material non-homogeneity, etc. These errors cannot be separated to evaluate only those of them we are interested in, e.g. the influence of different clamping method.

The preliminary simulations in chapter 4.2 have shown that assessment of strain non-homogeneity throughout the specimen (which is the only feasible way how to evaluate accuracy of experiments) may be misleading. Because of that I have chosen the approach based on computational modelling of the tests; in this work I simulate different mechanical tests using FE method where the input material properties are known at the beginning, so comparison of the (virtually) measured and true (input) data is feasible. This comparison enables me to assess the accuracy of the chosen experimental setup.

4.1 FE parametric study

Finite element simulations of biaxial tension tests were realized and the resulting stress-strain curves (evaluated in the same manner as in real experiments) compared with the input ones by means of coefficient of determination R^2 . The investigated parameters were type of gripping elements (hooks or narrow clamps), their number (2÷5) and size (0,25÷5 mm), specimen size (18÷35 mm), testing protocol (different displacement ratios), and specimen material (healthy artery, aneurysm wall tissue, elastin, intraluminal thrombus). In this study rakes were not analysed because of its limited use amongst research groups who prefer hooks. Further extension of this multiparameter study would require an excessive amount of computational time and is planned in future, see chapter 9.3.

The main goal of the study was to compare the most common gripping method (hooks) with the method applied by our research group (clamps).

At first 2D and 3D simulations using isotropic material model were created in the same manner as in previous studies [8][9][10] and resulting R^2 compared. The results for chosen isotropic materials differ significantly (see chapter 5.1), thus we assume that using 3D simulations is a more realistic approach which is then used throughout all this study. Other main reasons for not using 2D simulations emerged as well, firstly the impossibility of simulating radial pressing of the specimen by the clamps which means neglecting the effect of clamping. Moreover, no incompressible anisotropic material model was able to fit the material curves with sufficient accuracy; therefore a double layer model (with independent Holzapfel formulations used for media and adventitia) was used which naturally cannot be reduced to 2D. To the author's best knowledge, a 3D analysis of the effect of the above investigated parameters on results of biaxial tension tests of soft tissues was not yet published.

The description of the computational model below is relevant for the 3D modelling approach.

4.1.1 Geometry

First I have analysed the effect of number and size of the gripping elements. For this purpose a geometrical model of the tested specimen with dimensions 18x18x1,8mm (unless stated otherwise below) was created; in fact, only its 1/8 was modelled due to its assumed symmetries (see Figure 10). The dimensions were chosen according to a typical specimen size of the tested arterial tissues [16][29][30]. The load was transferred to the specimen by either clamps or hooks.

Although real **hooks** pierce the sample which leads to tissue damage and creates discontinuities, I have chosen a simpler way of how to model this interaction. A set of holes of the same diameter as the diameter of the hooks was created, and the hooks were modelled as straight cylinders put into these holes. A frictionless contact algorithm was used between the hooks and the specimen. This simplification ensures an easy convergence of the model without necessity of application of damage and failure models which are generally very time consuming. Numbers of hooks were chosen on the basis of literature search as summarized (with the specimen sizes) in Table 2. With the exception of one team [8], all researchers used between 2 and 5 hooks per specimen edge, therefore I kept the same numbers in the analysis.

In addition, I have also simulated the case with **clamps**, specifically with 2 clamps per edge. Here, instead of creating holes in the specimen model, a foregoing load step was applied in which the specimen was compressed by the clamps perpendicularly to the contact surface since the clamps only squeeze the tissue instead of penetrating it. Load transmission between the clamps and specimen was ensured by a rough contact algorithm (which assumes infinite friction in tangential direction) to simulate small teeth on the gripping surfaces of the clamps (Figure 10) which are omitted in the clamp geometry with the aim to improve convergence of the calculation, reduce the size of the model and, consequently, to reduce the computation time.

Table 2 Overview of parameters of experimental setups published in literature.

Number of hooks	Length of the edge	Reference	Number of hooks normalized per 18 mm edge
5	7 mm	[25]	12,9
4	7 mm	[21]	10,3
5	10 mm	[15]	9,0
4	10 mm	[13]	7,2
8	20 mm	[8]	7,2
6	20 mm	[8]	5,4
4	20 mm	[8][26]	3,6
5	25 mm	[22]	3,6
5	30 mm	[15]	3,0
3	20 mm	[16]	2,7
4	28 mm	[7]	2,6
2	15 mm	[12]	2,4
5	45 mm	[1]	2,0
4	39,5 mm	[24]	1,8
2	22 mm	[12]	1,6
2	35 mm	[12]	1,0

The diameter of hooks was varied between 0,25 and 1mm and the width of clamps was between 1,75mm and 5mm, both stepped by 0,25 mm. Length of gripping (distance of the hook or clamp tip from the specimen edge) was set to 2 mm. For each number of gripping

elements the specimen edge was virtually divided into the same number of intervals and each element was placed in the middle of this interval to ensure the most uniform load distribution along the specimen edge (see Figure 9). Only if the distance between the neighbouring elements in the corner tended to zero, their position was shifted away from the corner to keep a minimal distance of 1 mm between them as usual in the experimental practice. This disruption of uniform load distribution across the sample is applied in numerous studies [13][15][16][25] and aims at reduction of the stress concentrations in the corner, which would evoke tissue failure under lower loads.

In biaxial testing machines the load is usually distributed into individual gripping elements either via a system of balance levers [11] or via nylon threads [8][13][15][16][25][26]. Our machine employs balance levers so I mimic them also in our computational model. This setup allows me to apply the displacement on the base lever (see Figure 10), and the levers ensure a uniform force distribution into the individual gripping elements.

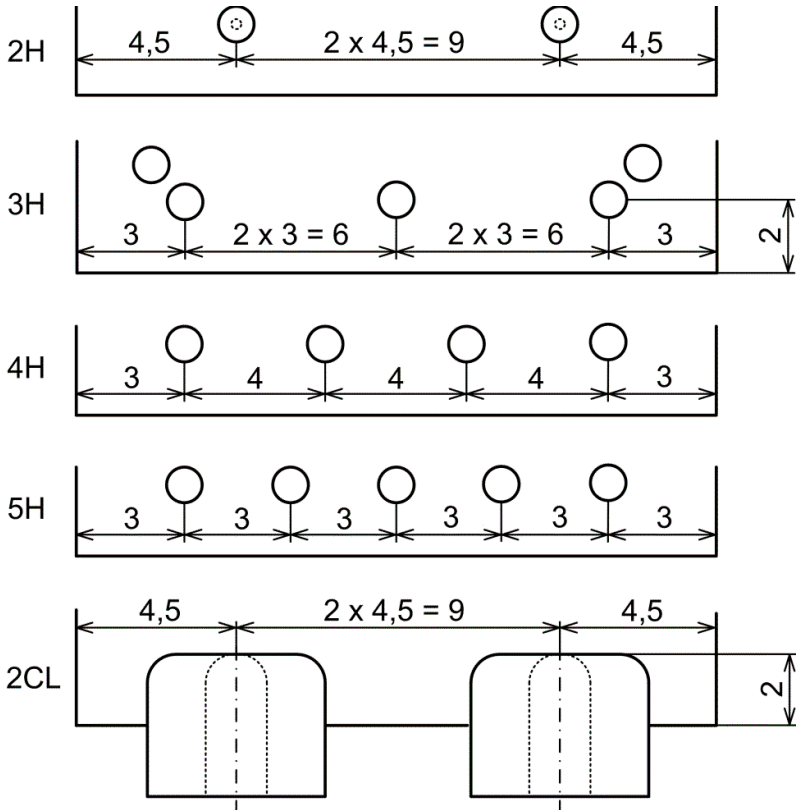


Figure 9 Geometry of emplacement of hooks and clamps according to their numbers. The solid lines represent the largest and the dotted lines the smallest investigated size of the gripping element.

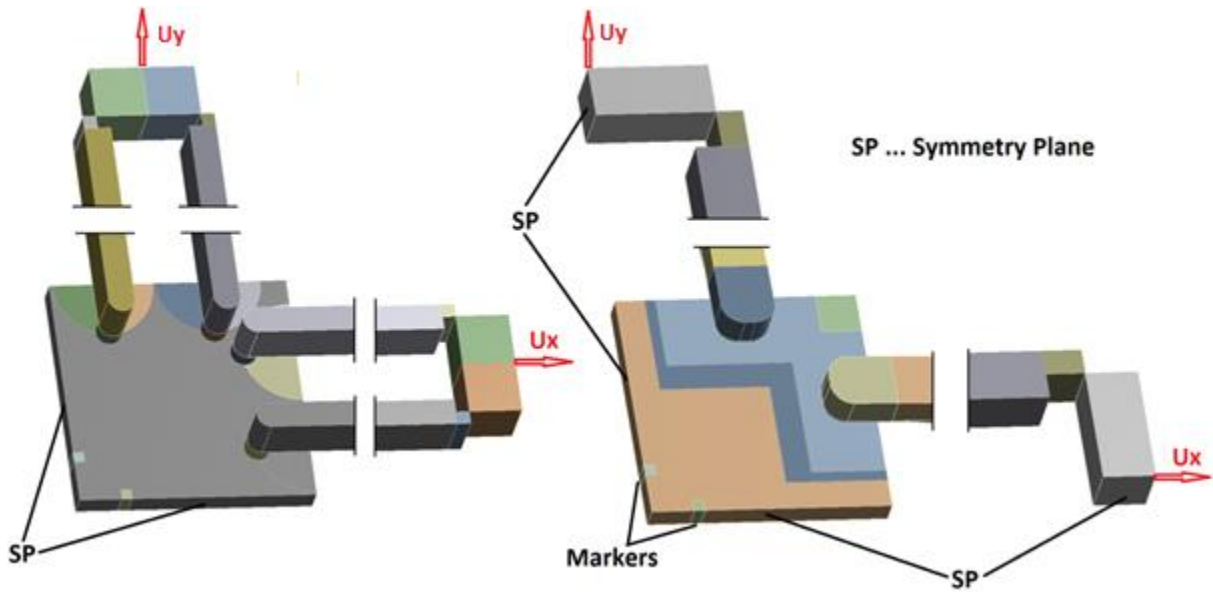


Figure 10 Geometry of 1/8 of the analysed experimental setup showing gripping via four hooks (left) and two clamps (right) per edge. The system of levers with knuckle joints ensures an even distribution of the load induced by the displacements U_x and U_y prescribed to the model as indicated by the red arrows in both figures.

Different types of displacement-controlled biaxial tests were simulated, with displacement ratios u_x/u_y of 1 (equibiaxial), 2 ($1/2$) and 4 ($1/4$); due to local deformation similar to a real experiment, strain components cannot keep a fixed ratio. All the models were tested for sufficient mesh density and optimized for computational efficiency.

4.1.2 Applied material models

Local effects in the vicinity of gripping elements may depend significantly on mechanical properties of the tested tissue such as initial stiffness, strain stiffening and anisotropy. Therefore I have considered several different material models with substantially different stress-strain curves related to tissues of healthy young (porcine) aortas and (human) aortic aneurysms.

(i) For healthy young porcine aortas I chose an (incompressible) isotropic constitutive model (denoted as material 1 below) based on the Yeoh strain energy density function (SEDF) [28]:

$$\psi_{iso} = \sum_{i=1}^n c_i (I_1 - 3)^i \quad (1)$$

where I_1 is invariant of right Cauchy-Green deformation tensor and c_i are material parameters. On the basis of stress-strain curves from different types of biaxial tests [29], their values were fitted for the 3rd order Yeoh model ($n=3$) with the resulting values of $c_1 = 17,4$ kPa, $c_2 = 0,0$ kPa, $c_3 = 13,8$ kPa. This model corresponds to mean population data for which the anisotropy is less pronounced due to individual differences.

(ii) Arterial wall can be more accurately modelled by anisotropic models. I chose the two-layered Holzapfel model [34] (denoted as material 2 below) with the following SEDF:

$$\psi_{aniso} = \mu(I_1 - 3) + \sum_{j=A,B} \frac{k_{1,j}}{2k_{2,j}} \sum_{m=4,6} \left(\exp(k_{2,j}(I_m - 1)^2) - 1 \right) \quad (2)$$

where μ is Neo-Hookean parameter related to stiffness of the isotropic component of arterial wall (mainly arterial elastin), $k_{i,j}$ are parameters ($i=1,2$) for the individual layers media ($j=A$) and adventitia ($j=B$) determining the anisotropic contribution of fibres to the strain energy density, and I_m are pseudoinvariants of the right Cauchy-Green deformation tensor (see [34]) related to stretches of the individual fibre families; in each layer the Holzapfel model assumes two families of fibres perfectly aligned in two directions $\pm\varphi_j$ symmetric with respect to the circumferential direction. Parameters were obtained by fitting this model to our mean population response of previously published experimental biaxial data [29]. The resulting parameters are $\mu = 10,0$ kPa, $k_{1A} = 9,68$ kPa; $k_{2A} = 1,32$; $\varphi_A = 0,97$ rad; $k_{1B} = 14,68$ kPa; $k_{2B} = 0,813$; $\varphi_B = 0,18$ rad. Let me note there were convergence problems using this material which prevented me from inducing higher strains than some 15% till now. Due to the very high compliance of the model in radial direction and shear, an excessive mesh distortion occurred much sooner than in case of the isotropic approximation of the same tissue (material 1). I tried to apply other anisotropic material models, but only this material model was able to converge to sufficient stretch magnitude, see chapter 4.1.3 for detailed information.

(iii) Abdominal aortic aneurysms exhibit significantly different mechanical behaviour compared to healthy aorta [30] and are often modelled also as a Yeoh-like material according

to eq.1 (for n=2) with constants $c_1 = 174$ kPa, $c_2 = 1881$ kPa (see [31], denoted as material 3 below).

(iv) Arterial elastin exhibits relatively high initial stiffness but it gradually softens [32] and is usually modelled via Neo-Hookean SEDF which can be defined by eq.1 with n=1 and $c_1 = 163$ kPa (denoted as material 4 below).

(v) Intraluminal thrombus (occurring frequently in abdominal aortic aneurysms) is a very compliant material compared to arterial wall [16] and I model it via Ogden-like SEDF:

$$\psi_{iso} = \frac{\mu}{4} (\lambda_1^4 + \lambda_2^4 + \lambda_3^4 - 3) \quad (3)$$

where parameter $\mu = 3,5$ kPa is estimated from uniaxial tensile tests [33] (denoted as material 5 below).

Equibiaxial stress-strain responses of all the described materials are presented in Figure 11.

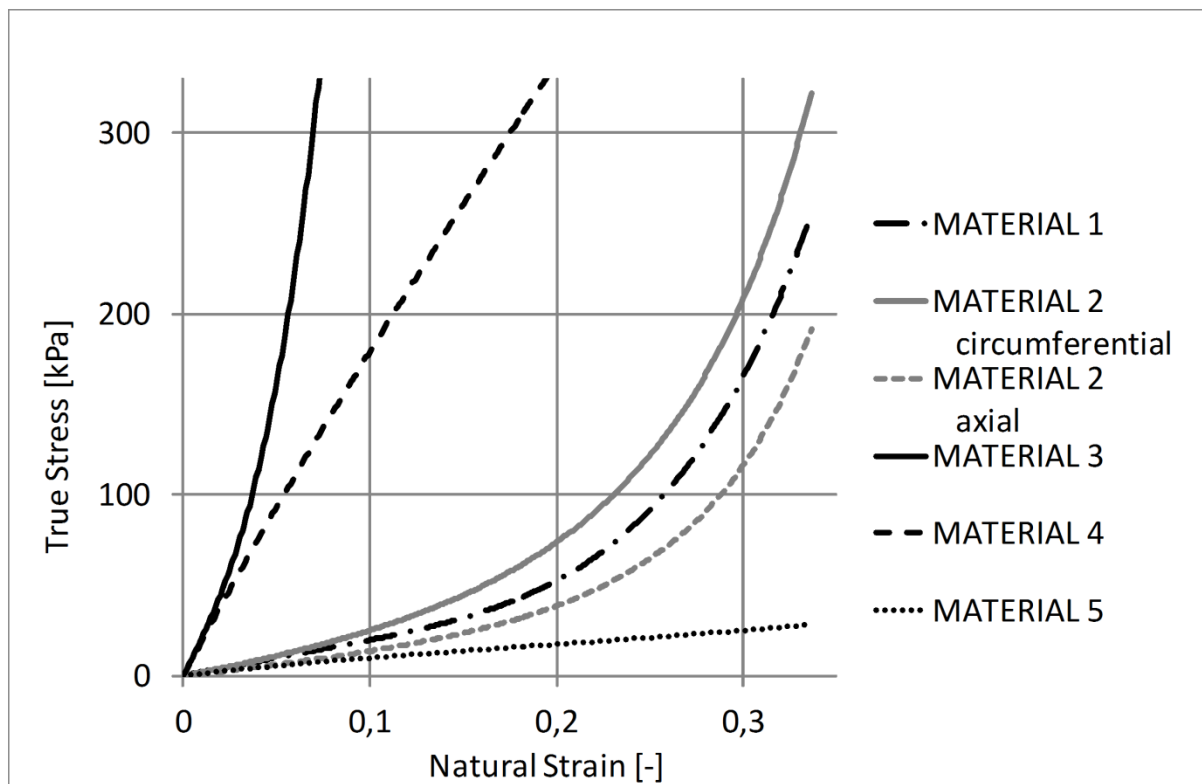


Figure 11 Equibiaxial stress-strain curves of all the investigated materials demonstrate fundamental differences in their behaviour.

4.1.3 Numerical problems of anisotropic material models

Different soft biological tissues can be characterised by different anisotropic material models. In the computational model used in this analysis various material models were tested in order to widen the applicability of the results.

I tried to apply the following models of compressible material:

- Holzapfel double layer 2000 [34]
- Gasser 2006 [35]

The used anisotropic models were nearly incompressible to simulate the nearly incompressible behaviour of soft tissues (see chapter 3.3). Their compressibility parameter influenced strongly the convergence of the computational model. With values in the range of nearly incompressible mechanical behaviour the model was either unable to converge to sufficient stretch magnitude or even failed in the first load step – radial pressing of the specimen with clamps.

Microfiber model [29] was not used due to much higher computational time and consequently excessive amount of time required for the high number of simulations needed.

4.1.4 Contacts

Clamps

Rough contact between specimen and clamp simulates the teeth on the clamp surface. The huge imbalance in material stiffness (steel-aorta) has also to be taken into consideration. Normal stiffness was manually changed according to radial load of the specimen in the first load step. Contact stiffness had to be updated in every iteration because of large strains of the soft tissue. The overall setup of the contact pair is described below.

Always used:

Behaviour: Asymmetric

Formulation: Augmented Lagrange

Time Step Controls: Automatic Bisection

Update Stiffness: Each Iteration, Aggressive

Sometimes used to improve convergence:

Normal Stiffness manually set to 0,1.

Penetration Tolerance manually to 0,0125 mm

Hooks

Contact between hook and specimen was modelled as frictionless. The imbalance of materials (steel-aorta) was also taken into consideration. Normal stiffness was manually changed in dependence on loading direction (protocol) and fibre orientation (for anisotropic models). Contact stiffness had to be updated in every iteration because of large strains of the soft tissue. The overall setup of the contact pair is described below.

Always used:

Behaviour: Asymmetric

Formulation: Augmented Lagrange

Time Step Controls: Automatic Bisection

Update Stiffness: Each Iteration, Aggressive

Interface Treatment: Adjust to Touch

Sometimes used to improve convergence:

Normal Stiffness manually set to 10.

4.1.5 Mesh specifics

The mesh requires special setting according to the expected large deformation in the vicinity of contact between the specimen and gripping element. Linear elements were used as they are better suited for hyperelastic behaviour of specimen.

Dense mesh was used only in the areas of contact; in the ROI the mesh was relatively rough as seen in Figure 12. The low mesh density in the measured region had negligible effect on results because of small deformation gradient.

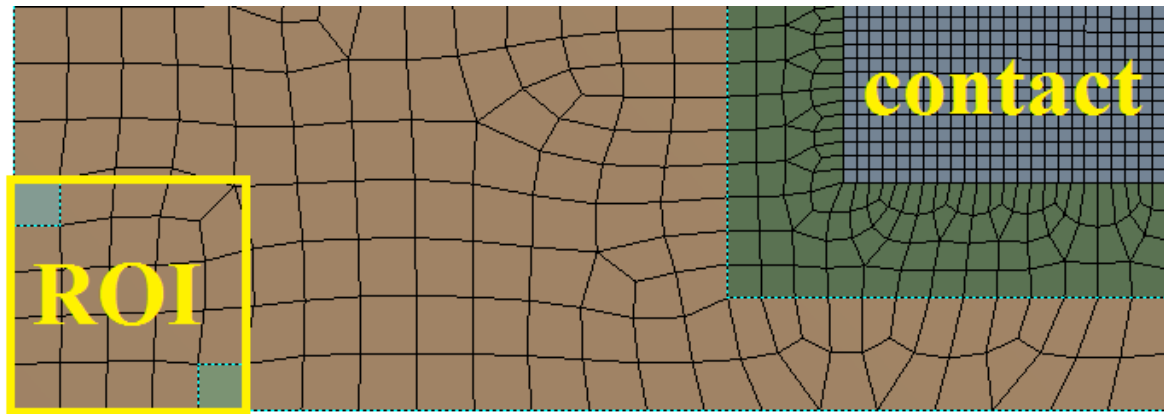


Figure 12 Different mesh sizing in the region of interest and in the contact region.

Elements in the contact area have to be specially shaped according to the expected deformation. In the case of clamps I prescribed compression of the specimen by roughly 50 %, so the elements had to be pillar-like shaped, see Figure 13, Figure 14. Similarly in the contact area with hooks the elements were elongated in the direction of their expected compression (see Figure 15).

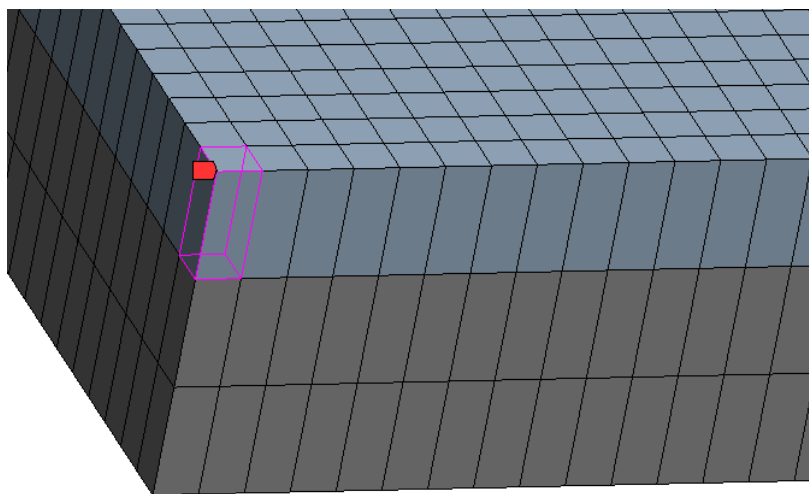


Figure 13 Pillar-like elements in the contact region under clamps.

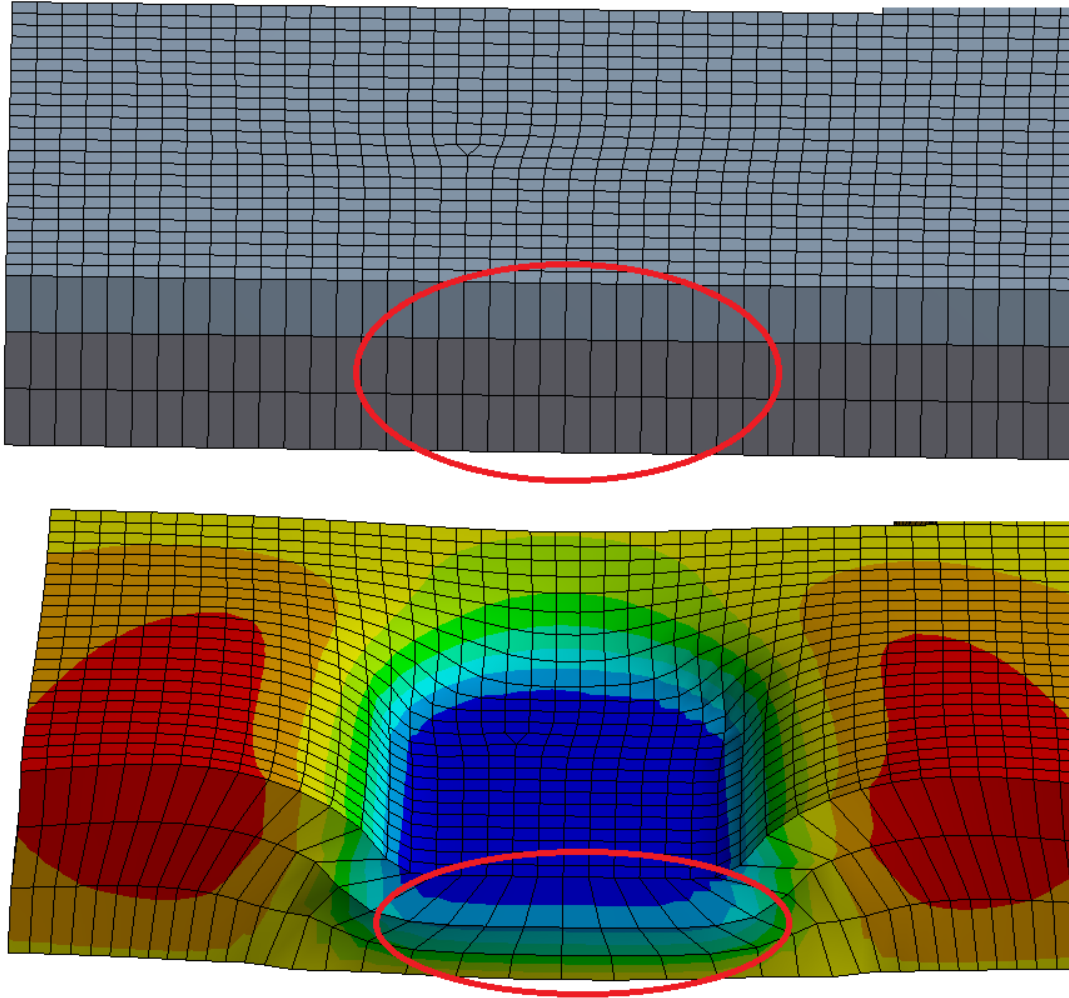


Figure 14 Long-shaped elements in the contact region under the clamp, before and after compression.

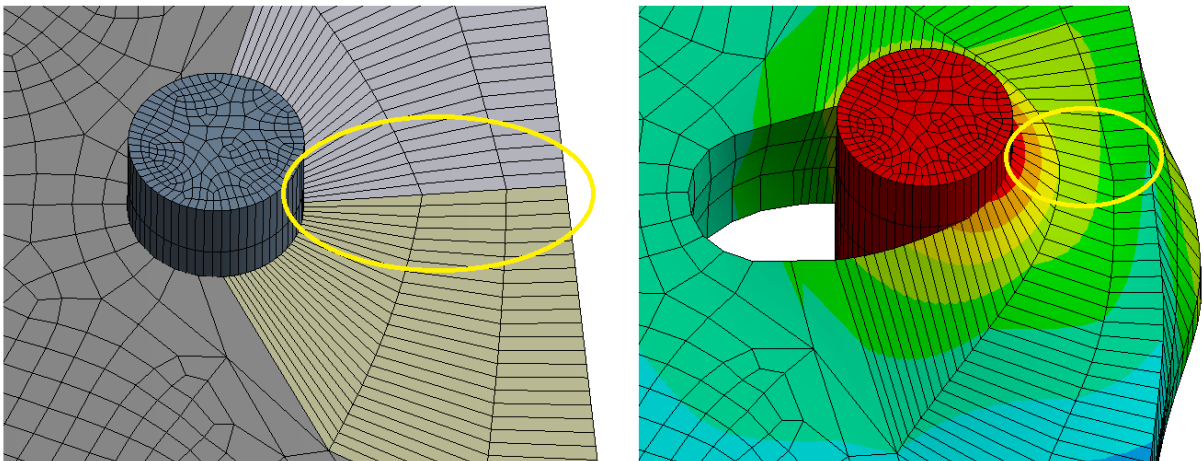


Figure 15 Long-shaped elements in the contact region with hooks

4.2 Evaluation of accuracy of biaxial tension tests

Typical strain distributions under load of 0,1 N in the equibiaxial test (with two materials) for setups with 2 clamps, 2 hooks and 4 hooks are shown in Figure 16 and reveal interesting differences in strain distribution across the specimen.

Use of 4 hooks gives a rather homogeneous strain (and consequently stress) distribution in a large part of the specimen (including the ROI), while both 2 hooks and 2 clamps result in much more non-homogeneous strain patterns showing a strip of higher strain values between the opposite gripping elements (outside of the ROI), in accordance with the expectation of major stress flow lines between them. In spite of these differences, however, the R^2 values representing the accordance between the resulting and theoretical responses are comparable in all of these cases (Figure 18) and surprisingly the lowest R^2 value corresponds to the most uniform strain distribution (4H).

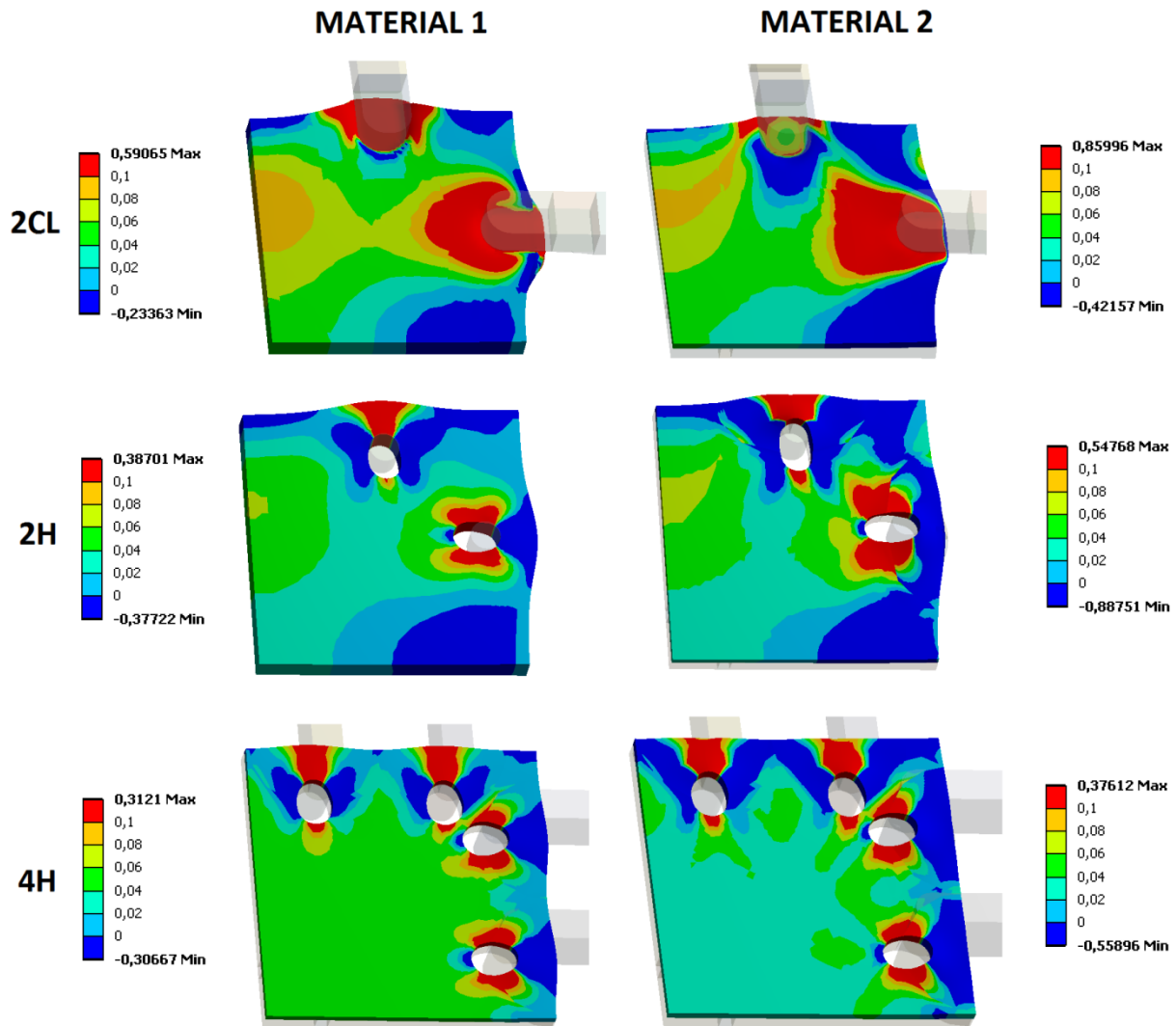


Figure 16 Distribution of natural strain ϵ_x for various gripping setups and two materials (isotropic and anisotropic) at the same load of 0,1 N during equibiaxial tensile test.

Two hooks and two clamps provide similar strain distributions for each material while four hooks provide more uniformly distributed strains in most of the specimen.

Instead of assessing the non-uniformity of stresses or their maximum values throughout the specimen or the non-uniformity of strains in the ROI, as done in the previous studies [7][8][9][12][21] (see Figure 17) or the comparison of averaged stress value in ROI with the loading stress as done in [10], I evaluated the results of simulations by a novel approach based on comparison of the resulting stress-strain curves obtained from the simulations with the corresponding theoretical responses of the original material models specified in chapter 4.1.2 by means of coefficient of determination R^2 ($R^2 = 1$ for identity).

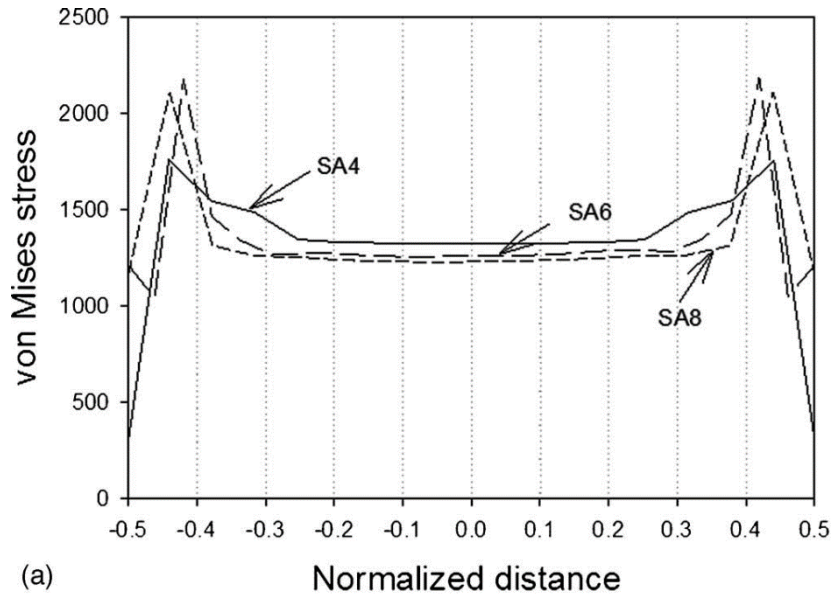


Figure 17 Von Mises stress distribution from the centre of the specimen (normalized distance = 0) to grippers (normalized distance = ± 0.5) [8].

Square specimen was gripped via 4 (SA4), 6 (SA6) and 8 (SA8) hooks. Normalized distance was used because of specimen size varied with different gripping methods.

Evaluation using non-uniformity of stresses throughout the specimen

The reason why the previous way of evaluation using the non-uniformity of stresses throughout the specimen was refused in this study is analysed below. According to the geometry of the specimen, the load of 1 N results in 123 kPa of (average engineering) stress independently of the experiment setup and material. For this analysis an isotropic model was used (model (iv) in chapter 4.1.2). The corresponding strain distributions along the specimen axis (from the centre to the edge) for different setups are presented in Figure 18 where the theoretical strain value (i.e. the natural strain calculated from the input equibiaxial stress-strain curve, using thus intrinsically the assumption of their uniform distribution throughout the whole specimen) corresponding to the stress of 123 kPa is depicted. While the curves represent distributions of strains along the symmetry plane, the straight lines (denoted as “eval.” in the legend) show the average strains evaluated throughout the ROI. Evidently the more homogeneous distribution of strains for 4 hooks induces overestimation of the strain evaluated in the ROI, while for 2 hooks or 2 clamps the strain in the ROI corresponds better to the theoretical value as documented also by R^2 values. It is evident, that the evaluated strain value (and thus the R^2 value) depends on the position of the marker and in the presented case the less uniform distributions of strains (and consequently stresses) give better accordance

with the theoretical value than the more uniform distribution (4H lines in Figure 18) which overestimates the strain value in the ROI due to its steep decrease towards the edge.

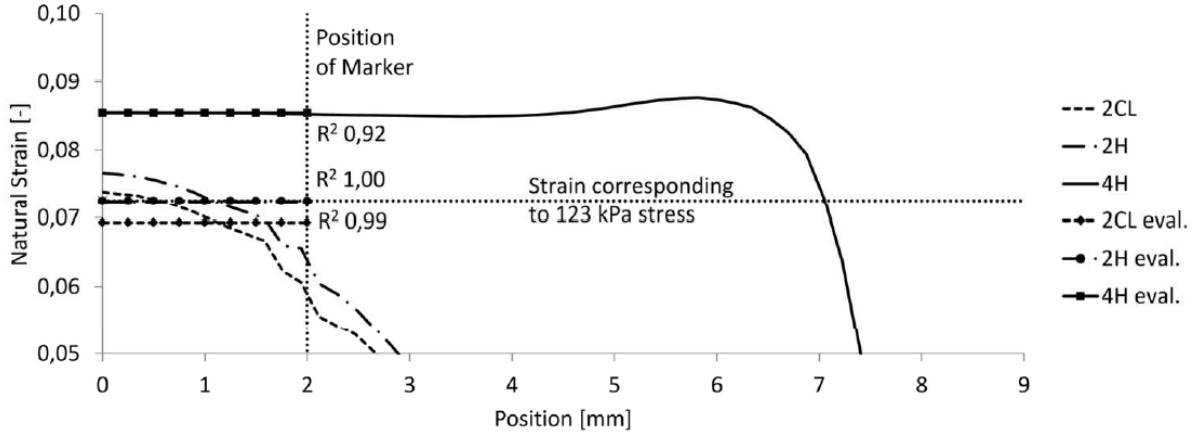


Figure 18 Distribution of strains across the half of the specimen for 2 clamps (2CL), 2 hooks (2H) and 4 hooks (4H) for material (iv).

Evaluation using comparison of resulting and input stress-strain curves

In my work I used comparison of resulting stress-strain curves obtained from the simulations with the corresponding theoretical responses of the original material models. The input (original, theoretical) stress-strain curve for each of the simulated tests was calculated analytically from the applied constitutive model by using the formula below for a chosen set of corresponding discrete strain values.

$$S_{ij} = \frac{\partial W}{\partial E_{ij}} = 2 \frac{\partial W}{\partial C_{ij}} \quad (4)$$

Where S_{ij} are components of 2. Piola-Kirchhoff stress tensor,

W is the strain energy density function related to unit undeformed volume,

E_{ij} are components of Green-Lagrange strain tensor,

C_{ij} are components of Cauchy-Green deformation tensor.

To obtain the resulting curve, all the quantities were calculated from the simulations in the same manner as in the experimental approach described in chapter 3.2. So the engineering stress was calculated from the total reaction force in the gripping elements and the undeformed specimen cross section area, while stretches were evaluated from displacements

of the mesh nodes located in the ROI similarly to the markers in real experiments. Due to the perfect symmetry and homogeneity of the 1/8 model and markers positioned in the symmetry planes, only one stretch component (representing average value for the ROI) was calculated from the corresponding displacement component of each of the markers, and no more recalculation (e.g. rigid body rotation) was needed as done in evaluation of real experiments. The R^2 value was calculated for each of the simulated tests separately by comparing the resulting stress-strain curve with the input (theoretical) one for the same loading protocol, and then the resulting R^2 for each specific setup of the test (type, number and size of gripping elements, material model, and specimen size) was calculated as average of all the applied loading protocols as follows:

$$R^2 = \frac{R_{1:1}^2 + R_{1:2}^2 + R_{2:1}^2 + R_{1:4}^2 + R_{4:1}^2}{5} \quad (5)$$

For isotropic materials it holds $R_{1:2}^2 = R_{2:1}^2$ and $R_{1:4}^2 = R_{4:1}^2$.

The R^2 value averaged for all the protocols was used in all analyses below with the exception of the analysis of influence of the loading protocol itself (par. 5.3). This approach was used for the specimen size 18x18 mm to estimate the best possible number and dimensions of the gripping elements and the effect of the material properties. Then we analysed also the effect of the specimen size under assumption of unchanged initial specimen thickness.

4.3 Evaluation of the parametric study

The quantitative evaluation of the individual cases was done as follows:

- 1) FE computational models (2-dimensional and 3-dimensional) were created for each of the evaluated assemblies in ANSYS software.
- 2) Resulting stresses and strains during the loading process were calculated in the same manner as in the experimental approach.
 - Engineering stresses (1st Piola-Kirchhoff) were calculated as total force in the given direction divided by the undeformed cross section area.
 - Stretches (principal components of deformation gradient tensor) or engineering strains were calculated from the positions of markers in the central region of the specimen in their undeformed and deformed configurations.

- 3) The corresponding theoretical curve was calculated for the set of chosen strain values using eq. (4).
- 4) The resulting stress-strain curve was compared with the theoretical one by means of coefficient of determination R^2 ($R^2=1$ for identity).

4.4 Limitations of the computational model

The created computational model represents a limited agreement with reality, so a number of simplifications and presumptions was made.

Simplifications

First, we simplified the process of penetration of the hook into the tissue by assuming the hole of the same diameter as the hook; so no stress is induced in the tissue before loading while in reality the penetration of the hook induces some stresses in the tissue which compress the hook. The effect of this simplification was not explored, it is assumed to be local only without any significant impact on the evaluated stress-strain curves. The straight shape of the hooks is not realistic either but they are placed in straight holes so that a full length contact (and better convergence) is ensured from the onset of loading; the differences against a curved hook in a curved hole are expected to be local only without any impact on the results.

Presumptions

Also all the numerical analyses assumed homogeneous materials while soft tissues are more or less heterogeneous which may affect primarily the results for large specimens which are naturally more heterogeneous. Next, perfectly symmetric and accurate positions of clamps and hooks were assumed in all the presented analyses. Naturally, the accuracy of the positioning of clamps or hooks represents another important operator-dependent factor influencing the accuracy of the experiment.

5 Sensitivity analysis of gripping method - Results

Simulation of one case took from 20 minutes to 2 hours on a 6CPU 16GB RAM computer. Overall more than 600 analyses were performed. The results of different parametric analyses are presented in the following subchapters.

5.1 Influence of 2D vs. 3D modelling

In Figure 19 a comparison of 2D and 3D simulations is shown. The graph represents the most differing case – material model 5 using clamps to grip the specimen. The R^2 differs significantly, indicating thus substantial differences in the results. Therefore it was concluded that 2D modelling is not acceptable and a full 3D approach has to be used instead.

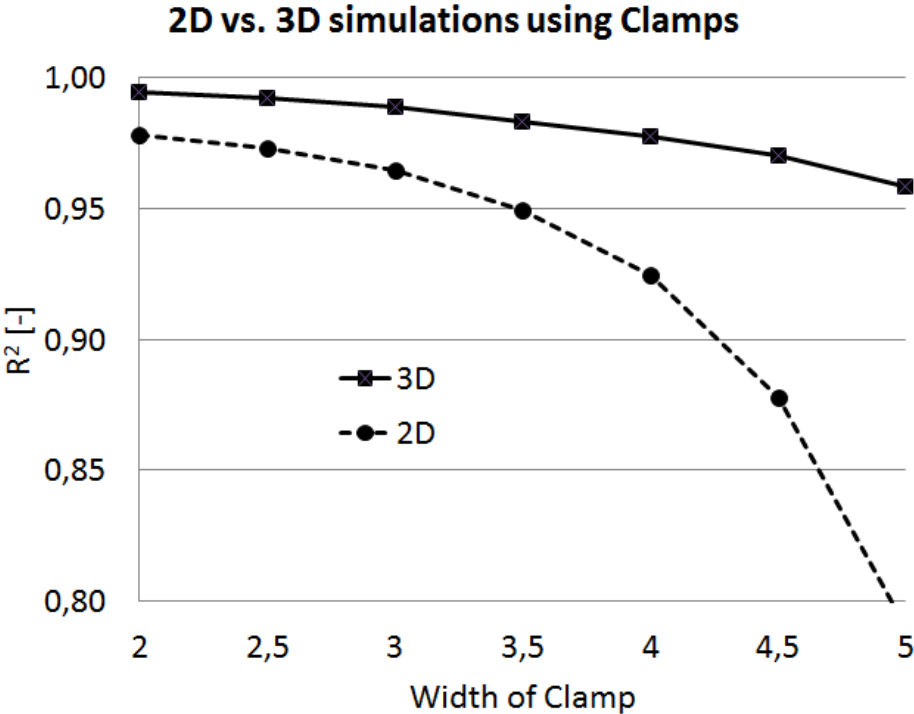


Figure 19 Comparison of resulting R^2 using 2D or 3D simulations.
Material model 5 was used.

The differing results are probably caused by some 3D effects in the vicinity of clamps and their simplifications in the 2D model, namely by not pressing the clamps into the specimen or by absent specimen material under the clamps.

5.2 Influence of dimensions and numbers of grips

Dependences of R^2 on the type of gripping elements, their number and size are shown in Figure 20 for various materials. It is shown that the most appropriate width of the clamps is between 2 and 3 mm independently of the analysed material, while the decrease of R^2 for clamps wider than 3 mm is highly material dependent. As the steep decrease of accuracy occurs for materials 1 and 3 which show pronounced strain stiffening, it can be concluded that this effect is probably related to material nonlinearity. However, as this effect is much less pronounced for the anisotropic material 2, its relation to the material anisotropy is also worth to be further investigated. On the contrary, the effect of hook diameter depends on the number of the applied hooks. Larger diameter is slightly better for two hooks for all materials, while it has a clear negative effect for 4 or 5 hooks, which becomes significant for material 4 with R^2 decreasing sometimes under 0,9. The effect of hook diameter is negligible for 3 hooks.

For a more detailed interpretation, the same results are depicted in Figure 21 in a different way, grouped by the experimental setup instead of material. This representation makes it possible to assess the expected accuracy of a specific experimental setup and material type.

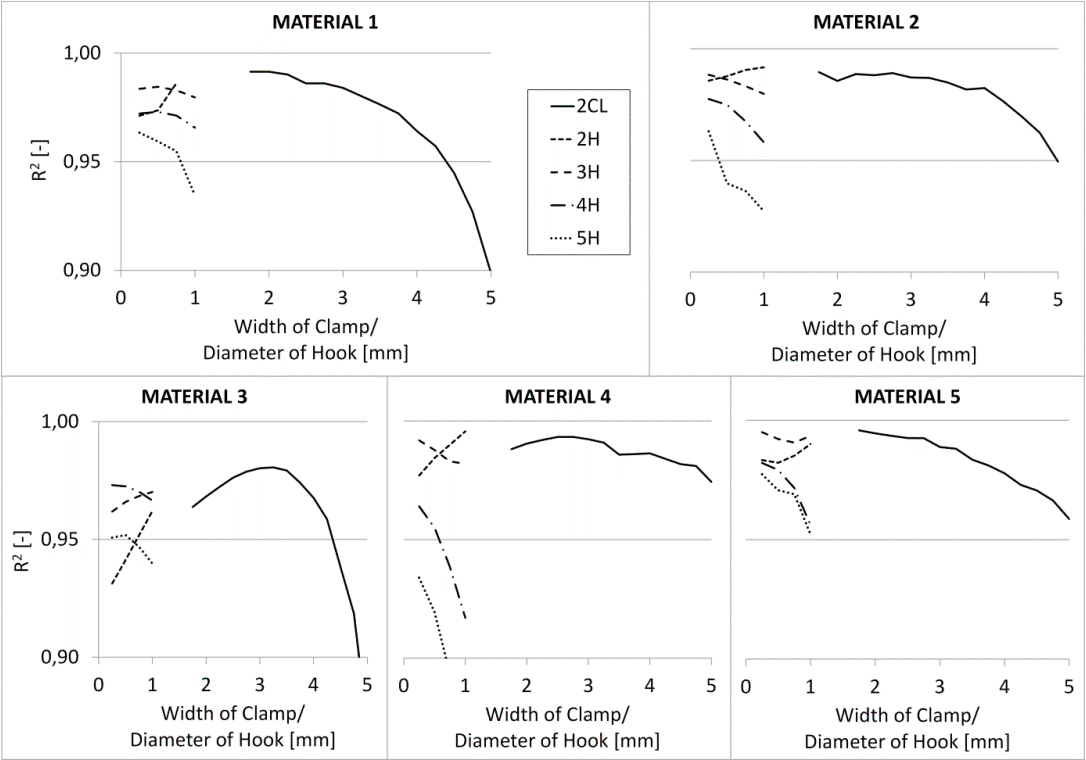


Figure 20 Influence of different gripping elements, their number and size on R^2 for various materials. In the legend CL and H denote clamps and hooks, respectively.

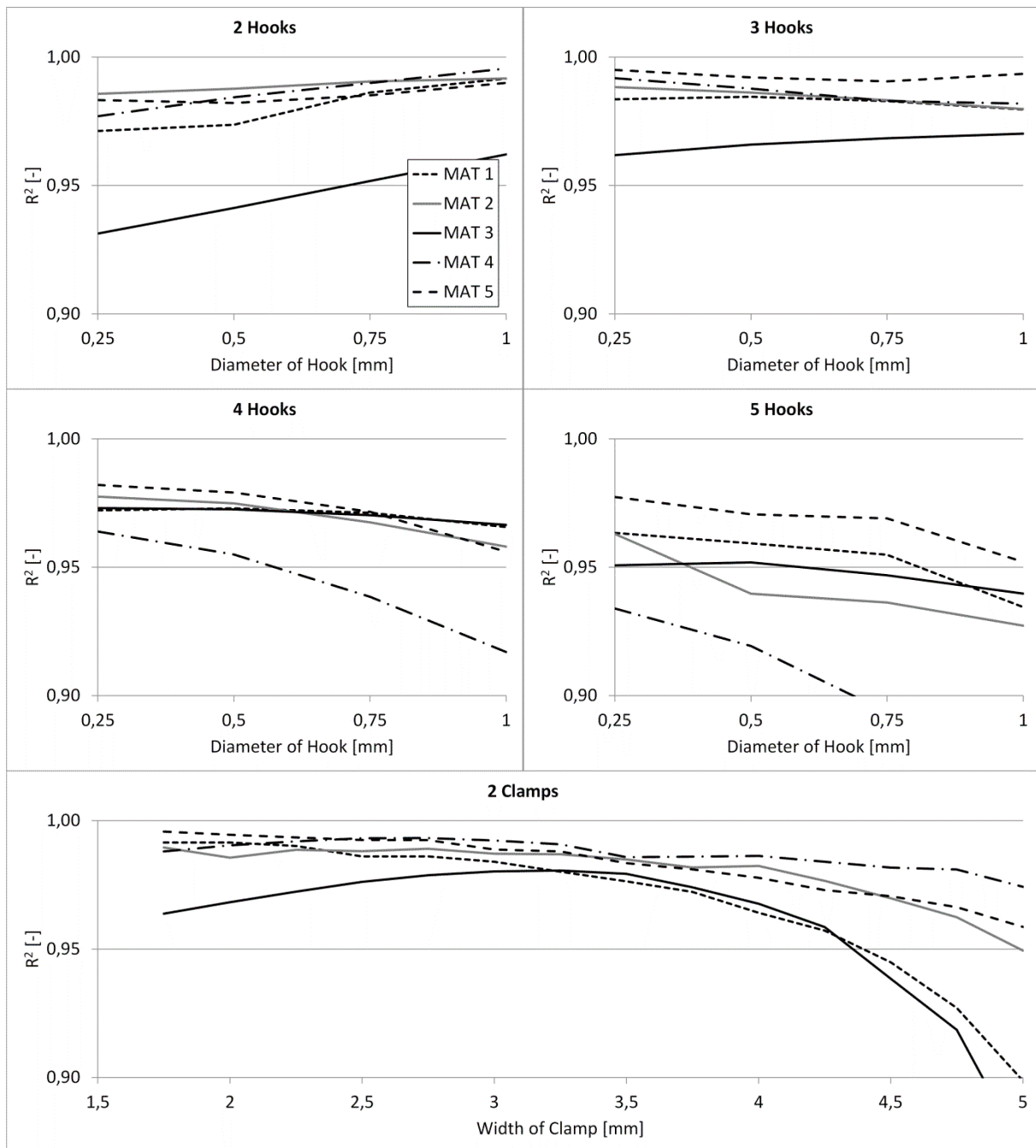


Figure 21 Impact of dimensions of gripping elements in the individual setups for different materials.

This comparison shows that the accuracy is always excellent with two clamps below 4 mm width, comparable with 2 or 3 hooks which give, however, a slightly worse accuracy for a highly non-linear material 3. The accuracy of setups with 4 or 5 hooks is slightly worse and, for some materials, decreases significantly for large diameters of the hooks.

Two clamps can also be used with adequate plausibility in a very wide range of sizes (1,75÷4,5 mm). These conclusions are valid for the basic specimen size of 18x18 mm and larger width of clamps is more suitable for large specimen sizes when it can partially compensate the deficit in number of gripping elements. On the other hand, use of wide clamps for small specimens cannot be recommended since they constrain the transversal deformation of the tissue too much which reduces the accuracy especially in non equibiaxial tests (see Figure 22).

5.3 Influence of the loading protocol

Figure 22 demonstrates a significant decrease in accuracy for non-symmetric loading protocols compared to the equibiaxial ones. This tendency occurs for both types and all numbers of gripping elements with isotropic materials, while for the anisotropic material it is less pronounced (it holds only if the load is higher in the softer material direction) and more dependent on the experimental setup. The increasing hook diameter improves the results for two hooks while it has an opposite effect for five hooks which is consistent with Figure 21.

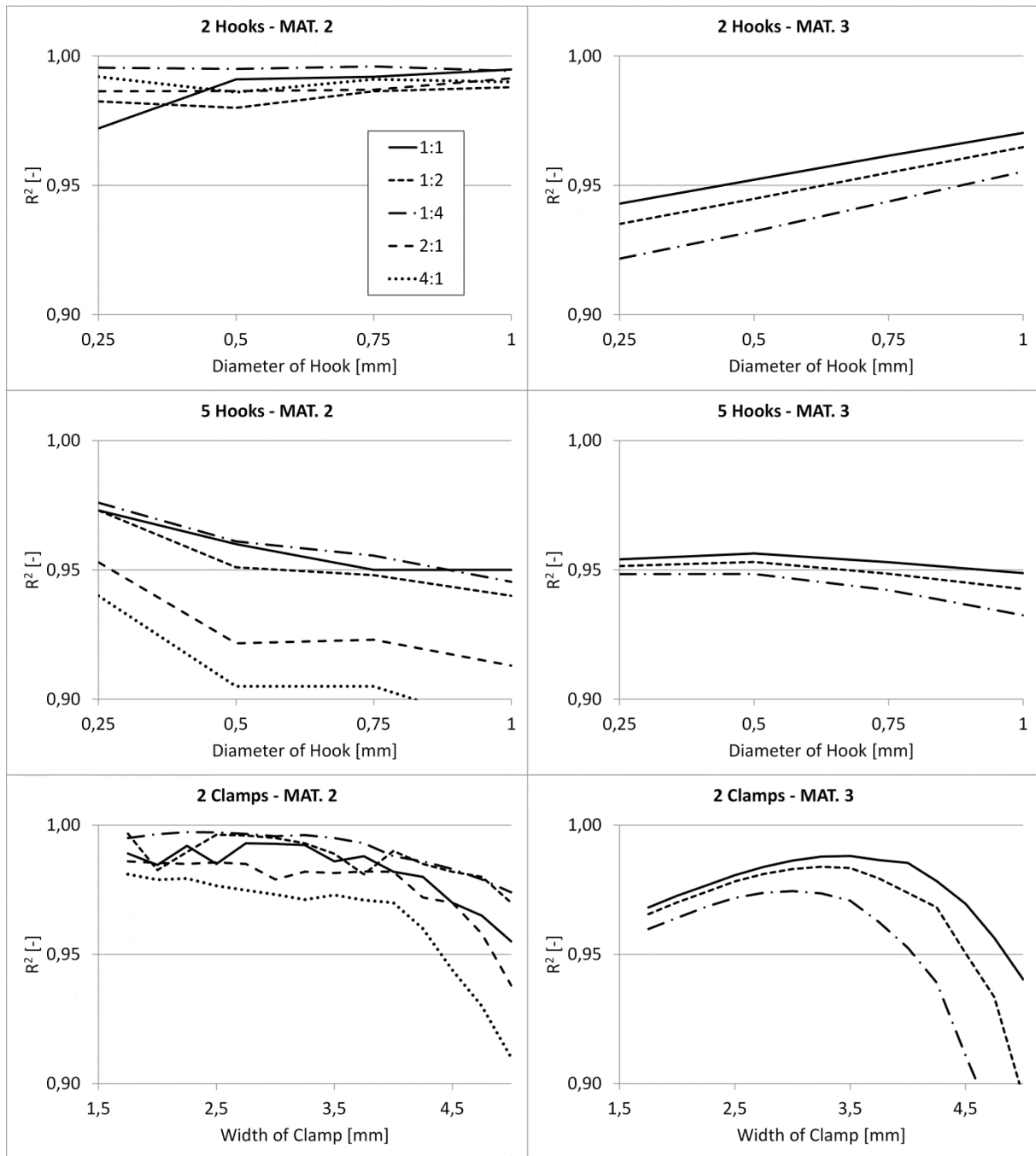


Figure 22 Influence of the different testing protocols for anisotropic (mat. 2) and the stiffest (mat. 3) materials evaluated for gripping via 2 or 5 hooks and 2 clamps.

The worst accuracy is always achieved for the most non-symmetric loading protocol.

5.4 Influence of the specimen size

The influence of the specimen size was investigated only for the hook diameter of 1 mm and for two clamps with 3,25 mm width. The results are presented in Figure 23. The accuracy

increases for all gripping setups with the increasing specimen size up to 30 mm representing the minimal specimen size needed for uniform load distribution via 5 hooks. Further increase of specimen size has negligible effect on the accuracy. This effect is most pronounced for the softening material model 4 (arterial elastin) and for the setup with 5 hooks.

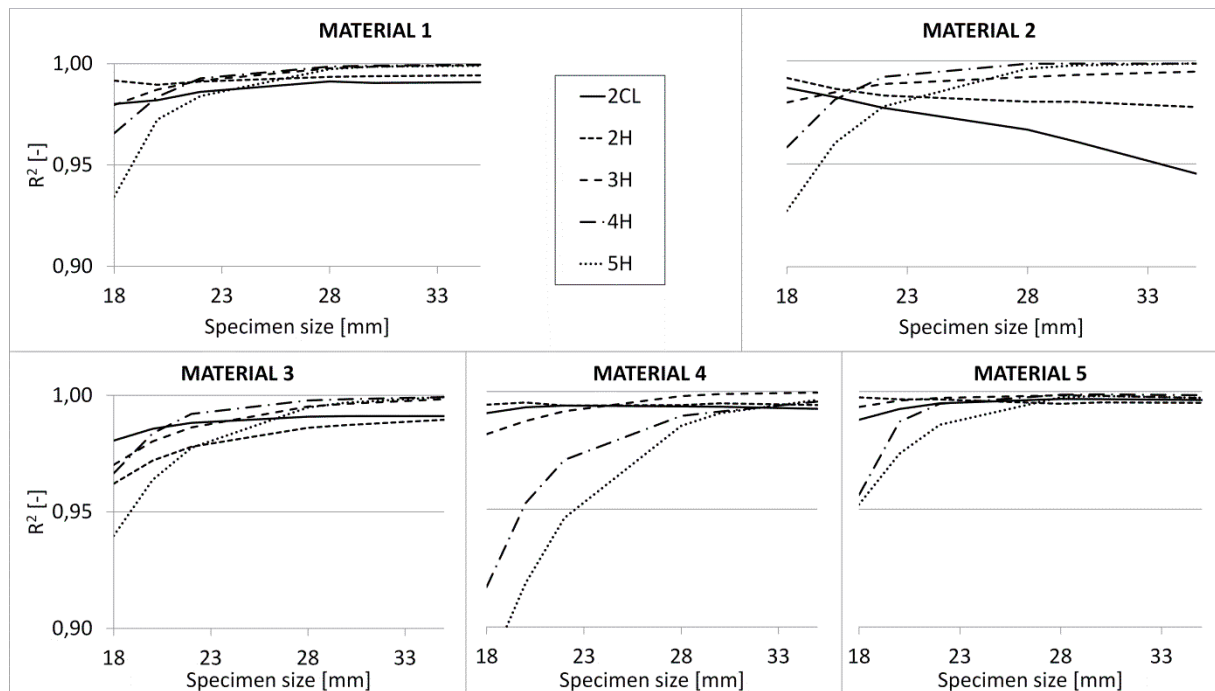


Figure 23 Influence of specimen size on accuracy for various types and numbers of gripping elements.

With small specimens I obtained worse accuracy for four and five hooks than for 2 hooks (consistent with Figure 20). This result can be explained by disruption of the uniform force distribution along the specimen edge because the gripping elements must be non-uniformly distributed to keep some minimal distance between them in the specimen corner. This is supported also by the observed significant increase of accuracy with increasing specimen size for 4 and 5 hooks (see Figure 23) because it gradually diminishes the non-uniform force distribution. When using small specimen with 18 mm edge, the obtained accuracy for 4 hooks is higher than for 5 hooks. This is because at small specimens, fewer hooks can be positioned more evenly than more hooks. Naturally this effect disappears for the largest specimens (above 30 mm) where a uniform distribution of hooks can be kept even for 5 hooks.

On the other hand, for some materials and the largest specimens the accuracy for 2 hooks or 2 clamps was significantly lower compared to 4 or 5 hooks setups. It means that 2 gripping elements are not capable to induce sufficient strains in the middle of the specimen (see Figure 16) due to their large distance from the symmetry plane of the specimen. As shown in Figure 16 and Figure 20 and explained in chapter 4.2, for the accuracy of the results accordance of the strain in the ROI with the average value throughout the whole specimen is more important than the size of the portion of the specimen with (nearly) homogeneous strain distribution. Therefore for small specimens the less homogeneous strain distribution for 2 gripping elements gives better results than for 4 hooks. For larger specimens the tendency is opposite because the overestimation of strains in the ROI decreases for 4 hooks and, on the contrary, 2 grips underestimate the strain in the ROI due to their increasing distance from the symmetry plane. Conclusively, a higher number of gripping elements should be avoided (regardless of the investigated material) if it could result in a non-uniform distribution of the load along the specimen edge, and 2 gripping elements should be avoided in tests of specimens larger than 30 mm.

5.5 Summary of results

A novel method of evaluation of the accuracy of biaxial tension tests was used which compares not the stress and strain distribution throughout the specimen but directly the simulated response with the theoretical material response based on input material models of the specimen (see chapters 4.2 and 4.3) by means of coefficient of determination R^2 . It was shown that this approach is superior to mere comparison of uniformity of strain (stress) distribution (see Figure 16).

The results are valid for a wide range of material stiffness occurring at soft tissues, from the very compliant ILT up to the stiffest wall of abdominal aortic aneurysm, and for a wide range of strains exceeding their physiological values. The only exception was the case of the anisotropic model which showed convergence problems well below physiological stresses as described in section Material models. This is the reason for having used the isotropic approximation of the same material for which the convergence was much better, and the resulting curves could be calculated up to strains of some 30%.

The analysis of influence of dimensions and numbers of grips shows that 2 or 3 hooks and 2 narrow clamps per edge give the best accuracy for small specimens. Larger hook diameter increases the accuracy for two hooks and decreases for a high number of hooks (4 - 5). Two clamps can be applied in a broad range of width (2 - 4 mm) independently of the analysed material.

Specimen size influences the accuracy of results significantly. If a relatively uniform load distribution is kept, the value of R^2 tends to the ideal value of 1 with increasing specimen size within the investigated range. In the case of a quite non-uniform load distribution using two clamps or hooks the R^2 value does not tend to 1, but to a slightly lower value (0,98), for the material 3 it even decreases with larger specimen size, but still with acceptable value of $R^2 = 0,95$ for 35 mm specimen edge. For large specimens the use of more (typically 4 or 5) hooks is recommended. 4 clamps may give similar results for large specimens but this case was not analysed.

All previous conclusions are relevant for different loading protocols. Non-equibiaxial protocols show worse accuracy than equibiaxial ones and are more dependent on the experimental setup as well as material properties.

The realized analyses are much more comprehensive than those presented in previous studies [8][9][10] and the results do not contradict any of them for comparable cases.

6 Predictive capabilities of different material models

A good computational model requires not only credible stress-strain experimental data but also their sufficiently accurate approximation by a mathematical function representing the chosen constitutive model. The ideal case is a material model accurately predicting a variety of stress-strain states on the basis of only minimum of needed experimental data. Uniaxial testing is less demanding in material preparation and size, measuring device and data post processing than biaxial testing. Thus many material models are fitted using uniaxial data only, predicting thus biaxial stress-strain states. Some of the used material models have better predictive capabilities than other models. Therefore validation of some constitutive models by assessing their capabilities in describing and predicting uniaxial and biaxial behaviour of porcine aortic tissue is the aim of another study done by the research group of my supervisor. The results were published in [95], the full text of which is attached as Appendix of this thesis. Here I present its basic concept and specify my individual contribution.

In short, specimens of porcine aorta were prepared and measured under uniaxial and biaxial testing protocols. Four constitutive models were chosen for comparison of their predictive capabilities: Holzapfel 2000 ([34], denoted as HGO model below), Gasser 2006 ([35], denoted as GST model below), Four fiber family [93, 94] and Microfiber [70] were fitted using uniaxial data and then used to predict the biaxial measured data and vice versa. Accuracy of the prediction was statistically evaluated and the models were ranked according to their predictive capability. The conclusion was that HGO and GST models were not capable to predict biaxial arterial behaviour while FFF model was the best of the investigated constitutive models. Knowledge of transversal strains in uniaxial tests improves predictive capability of the constitutive models.

The author's part in this study (see Figure 24) was the fitting of the measured data using different constitutive models followed by evaluating the accuracy of predictive capabilities. The result of the fitting and evaluating procedures is presented as a comprehensive overview of coefficients of determination R^2 and normalized root mean square error (NRMSE) for all predictive capabilities of all models.

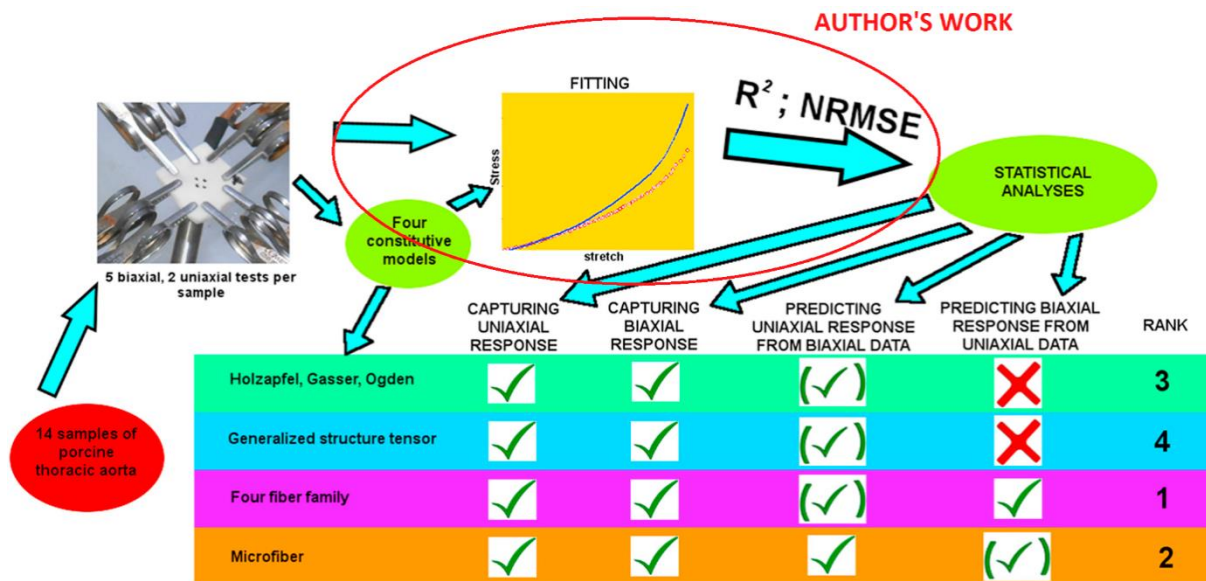


Figure 24 Schematic description of the process of evaluating the predictive capabilities of different material models [95]. The area of author's work is marked red.

A detailed description of author's work regarding this analysis is presented in the following part of the thesis and in the Appendix C. In the enclosed journal article the constitutive models, fitting process and results are presented. In this thesis these issues are not fully repeated but only shortly mentioned or completely left out. The aim of the appendix part is to show the detailed process of fitting of the measured data and obtaining the accuracy coefficients of their respective predicting capabilities and the following part shows some specifics of the fitting process and its dependencies. This procedure exploits the program Hyperfit (www.hyperfit.wz.cz) and was not yet presented.

6.1 Process of fitting the measured data using the program Hyperfit

Hyperfit, in contrast to ANSYS or other fitting programs, is capable to fit multiple data sets of the same type of test using a single constitutive model. This enables us to calculate response based on any number of measured specimens, e.g. a mean population response.

Firstly one specific feature of the analysis needs to be mentioned. The tested specimen was square shaped also when uniaxial tension test was applied instead of the usually used dog bone shape. The reason for this is explained in the journal article [95]:

“The uniaxial tests were performed by unclamping one of the axes.

It is also underlined that engineering strains in both principal directions ϵ_c and ϵ_a were recorded in all tests including the uniaxial ones. This was motivated by our effort to identify the effect of transversal strain on the predictive capability of the analyzed constitutive models since some of the analyzed constitutive models were shown previously not to estimate the transversal strain correctly (Skacel and Bursa, 2015). A secondary reason is in the use of square shape specimens which do not guarantee uniaxial state of stress during uniaxial testing. In this way we have obtained 7 data sets from 5 biaxial and 2 uniaxial tensile tests for each specimen.”

In short, the use of the square shaped specimen enables us to change the biaxial test into uniaxial one by simple unclamping one of the axes and, moreover, we can measure the transversal strain in the same manner as in biaxial tests. This enables us to evaluate the effect of transversal strain on the predictive capability of the analysed constitutive models.

The specimen is clamped into the testing device using multiple narrow clamps or hooks. These gripping elements cause a non-uniform deformation distribution along the edge of the specimen which may influence also the central part (ROI) of the specimen where strains are measured. Moreover, large deformations during the test cause rotation of the gripping elements inducing thus non-zero forces in the direction perpendicular to the direction of load.

These transversal forces influence the transversal strains and disturb the uniaxial state of stress. Therefore it is not an ideal uniaxial test but a test under biaxial stress state in which we are not able to measure the transversal stress. If the transversal strain derives from biaxial stress state, we prefer to fit the data using biaxial test mode and thus involve both strains of the specimen. Due to this additional information the predictive capability of the model may increase as a result.

More about starting parameters and their influence on the resulting coefficient of determination is analysed in the chapter 6.2 below. The whole fitting process is documented in Appendix C.

6.2 Dependence of coeff. of det. on starting and constrained parameters

6.2.1 Starting parameters

The quality of the fit, quantified by the resulting coefficient of determination R^2 , depends on the starting point, which is defined as a set of starting parameters, see Table 3, Table 4 and Figure 25 below.

The phenomenon was observed firstly when comparing the fit of the measured data using default starting points of the Hyperfit program and using parameters fitted previously from another measured data as a starting point. To examine the problem closely, only equibiaxial data sets (because of the rapid speed of fitting when using only one fifth of all datasets) were fitted using multiple starting points. Different starting points resulted in different coefficients of determination R^2 . The difference (distance) between the maximal and minimal R^2 can be explained as an uncertainty of the fitting process or the influence of different starting points on R^2 . The analysis has been extended back to all five testing protocols.

The phenomenon has been observed with all material models. The analysis is shown using the parallel Microfiber material model which is the best structural material model in regard of the prediction capabilities. The starting points are listed in the table below. The constraints are given by physical conditions only. The parameters are “free” to achieve any value, therefore it is called “All protocols, free” unlike the next chapter where the parameters are constrained.

Table 3 Starting points of the Microfiber material model.

Parameters		Starting point Number				Constraints	
Layer	Name	1	2	3	4	Min	Max
media	mu	1	5	500	50	0	-
	k	1	10	400	400	0	-
	l_min	1	1	1	1	1	-
	l_max	1,2	1,3	1,5	1,5	1	-
	b	0,1	0,5	1,5	1,5	0	-
adventitia	mu	0	0	0	0	Fix	Fix
	k	1	50	1,0E+07	1,0E+05	0	-
	l_min	1,1	1,2	1,1	1,3	1	-
	l_max	1,5	2	2	2	1	-
	b	0,1	0,5	0,5	0,5	0	-

Table 4 Coefficient of determination in dependence of starting point and data sets.

Starting point Number	Coefficient of Determination R ²	
	Equibiaxial only	All protoc., free
1	0,8525	0,9640
2	0,9772	0,9812
3	0,9972	0,9526
4	0,9974	0,9669
Min-Max distance	0,1449	0,0286

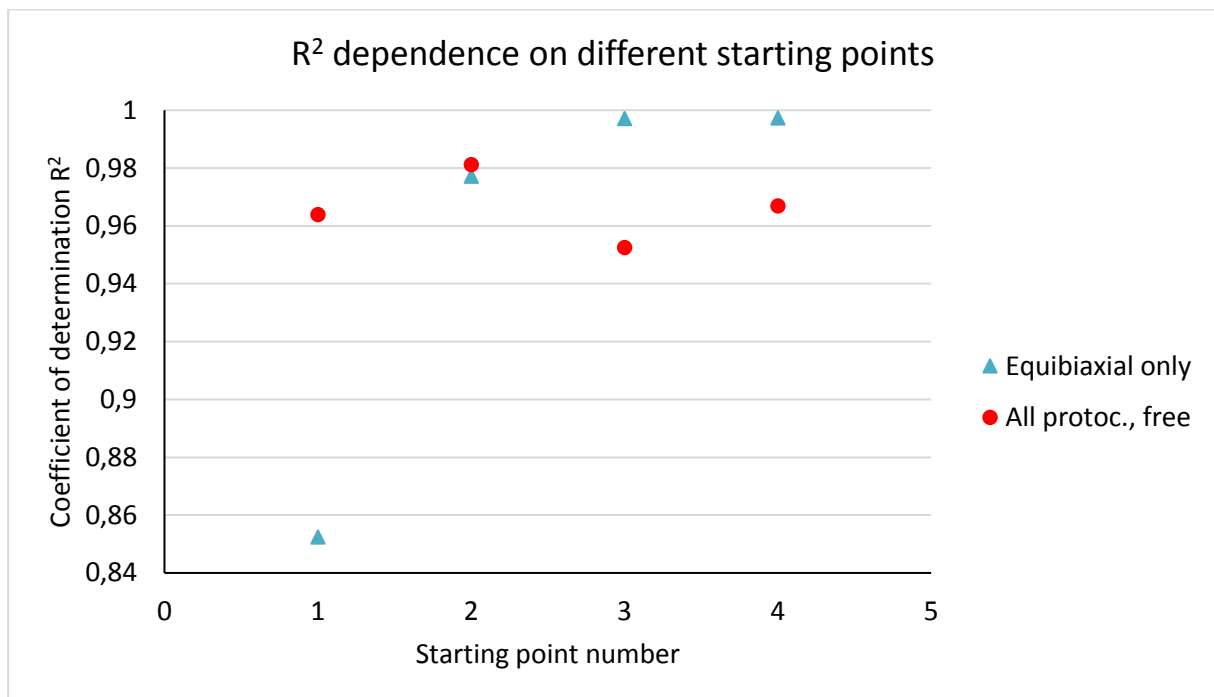


Figure 25 Coefficient of determination in dependence on different starting points for equibiaxial data set and for all data sets combined.

The greatest difference in the resulting R² was observed when using the most “soft” stress strain response, (starting point Nr.1) where most of the parameters were near the zero value. The R² values of the same starting points applied with different datasets differ not negligibly, therefore we can assume that there are no “ideal” starting points to be used when fitting experimental data.

The influence of starting points is unexpected because in most cases there exists only one residual maximum (or minimum) of the maximized (or minimalised) function. In case of

complex constitutive models multiple maxima can be found during the fitting process. When fitting, the program finds only one local maximum which needn't to be the global maximum. Therefore a restart of starting parameters is available in the program widening thus the area of search. Unfortunately we do not know the exact parameters of the material model which give the maximal and also unknown R^2 . Therefore we can never know the best starting points of the fitting process and it is recommended to use multiple starting points to increase the probability of the maximal achievable R^2 .

From the author's experience the most effective method how to achieve the best approximation of experimental data from many data sets is to select one group of the measured data sets and to fit this group using multiple starting points. The resulting set of parameters with the highest R^2 is then used as a starting point for all the other data sets. This approach combines the probability of finding the best approximation with minimization of the calculation time.

The fitted stress strain model curves are shown in the overview chapter below in comparison with the experimental data.

6.2.2 Constrained parameters

Some material models are structure based thus the parameters of the model should vary in a specific range of values. The value of R^2 will be influenced by restraining the possible values of parameters. The question remains, what criterion should be maximized – the R^2 which stands for the best fit of the measured data or that the parameters vary in a natural range of values? In [95] the authors have chosen to let the boundaries of the parameters free in order to obtain the best fit of the measured data.

The constraints of the more constrained material model were chosen on the basis of the structural data measured in [29].

Table 5 Starting points of the Microfiber material model, constrained and unconstrained.

Parameters		Starting point Number				Free		Constrained	
Layer	Name	1	2	3	4	Min	Max	Min	Max
media	mu	1	5	500	50	0	-	0	-
	k	1	10	400	400	0	-	0	-
	l_min	1	1	1	1	1	-	Fix	Fix
	l_max	1,2	1,3	1,5	1,5	1	-	1	2
	b	0,1	0,5	1,5	1,5	0	-	0	1,5
adventitia	mu	0	0	0	0	Fix	Fix	Fix	Fix
	k	1	50	1,0E+07	1,0E+05	0	-	0	-
	l_min	1,1	1,2	1,1	1,3	1	-	1	1,5
	l_max	1,5	2	2	2	1	-	Fix	Fix
	b	0,1	0,5	0,5	0,5	0	-	0	1,5

Table 6 Coefficient of determination in dependence of starting point and (un)constrained parameters.

Starting point Number	Coefficient of Determination R ²	
	All protoc., free	All protoc., constr.
1	0,9640	0,9640
2	0,9812	0,8796
3	0,9526	0,9671
4	0,9669	0,9669
Min-Max distance	0,0286	0,0875

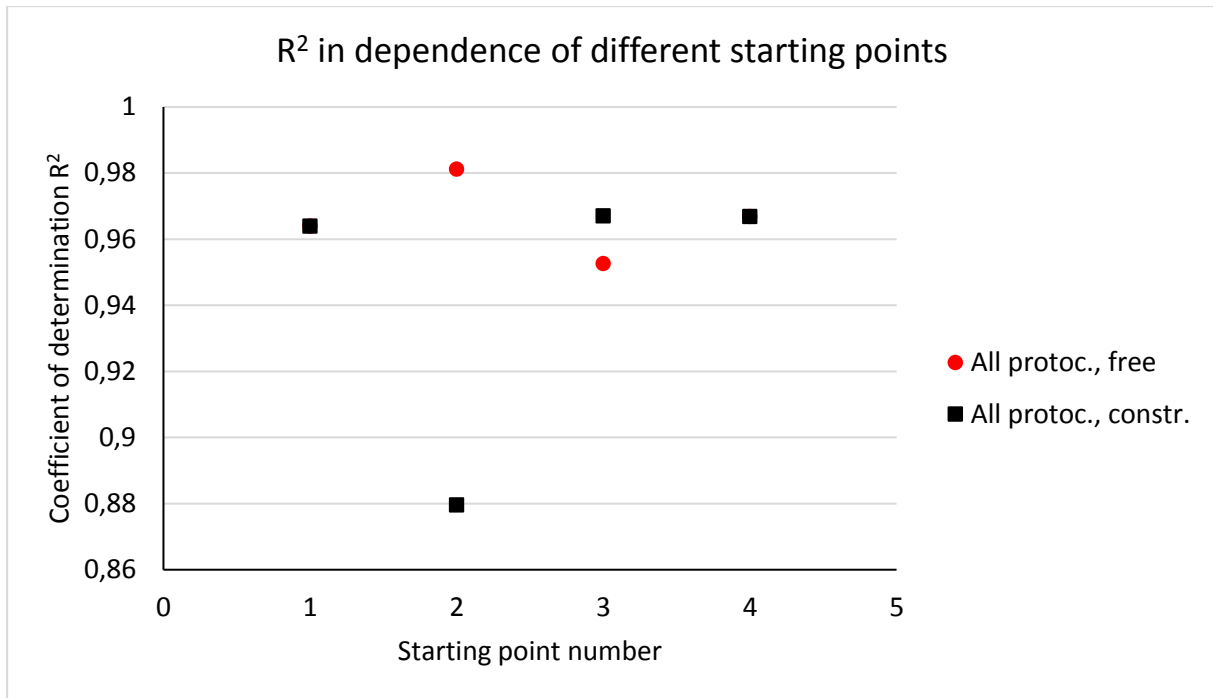


Figure 26 Coefficient of determination in dependence of different starting points for constrained and unconstrained parameters.

Constraint of the parameters results in influencing the R^2 of the fit unpredictably. In some cases the R^2 values are practically the same (starting points 1 and 4), in the case of SP 3 the difference is minimal and in the case of SP 2 the difference is large.

It cannot be said that in the analysed case constraint of the parameters influences the resulting fit negatively because there is no significant dependence.

The fitted stress strain model curves are shown in the overview chapter below in comparison with the experimental data.

6.2.3 Overview

To give an overview of all the analysed cases and dependencies a summary table, figure and graphs are shown below.

Table 7 Starting points of the Microfiber material model, constrained and unconstrained.

Parameters		Starting point Number				Free		Constrained	
Layer	Name	1	2	3	4	Min	Max	Min	Max
media	mu	1	5	500	50	0	-	0	-
	k	1	10	400	400	0	-	0	-
	l_min	1	1	1	1	1	-	Fix	Fix
	l_max	1,2	1,3	1,5	1,5	1	-	1	2
	b	0,1	0,5	1,5	1,5	0	-	0	1,5
adventitia	mu	0	0	0	0	Fix	Fix	Fix	Fix
	k	1	50	1,0E+07	1,0E+05	0	-	0	-
	l_min	1,1	1,2	1,1	1,3	1	-	1	1,5
	l_max	1,5	2	2	2	1	-	Fix	Fix
	b	0,1	0,5	0,5	0,5	0	-	0	1,5

Table 8 Coefficient of determination in dependence of starting point, (un)constrained parameters and datasets

Starting point Number	Coefficient of Determination R ²		
	Equibiaxial only	All protoc., free	All protoc., constr.
1	0,8525	0,9640	0,9640
2	0,9772	0,9812	0,8796
3	0,9972	0,9526	0,9671
4	0,9974	0,9669	0,9669
Min-Max distance	0,1449	0,0286	0,0875

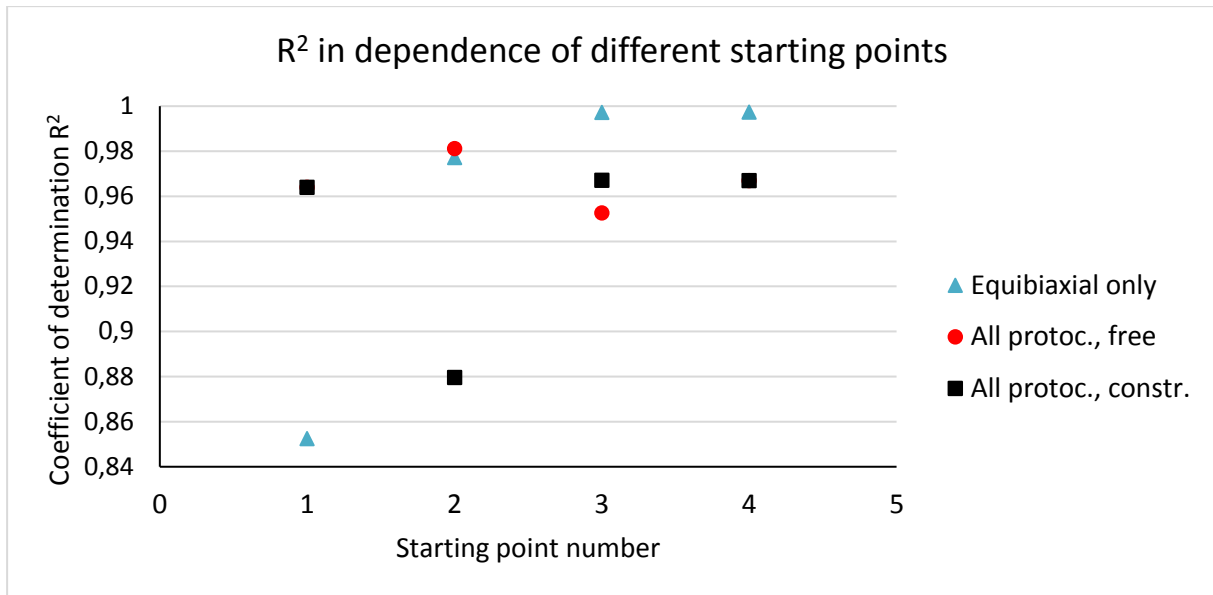


Figure 27 Coefficient of determination in dependence on different starting points for constrained and unconstrained parameters and for different datasets.

The resulting R^2 varies in a range of values between approximately 0,85 and 1,00 with the highest density between 0,95 and 1,00.

Every starting point generates a model curve which is fitted to the experimental data. All curves for each type of dataset or (un)constrained parameters are shown in Figures 28÷30 below.

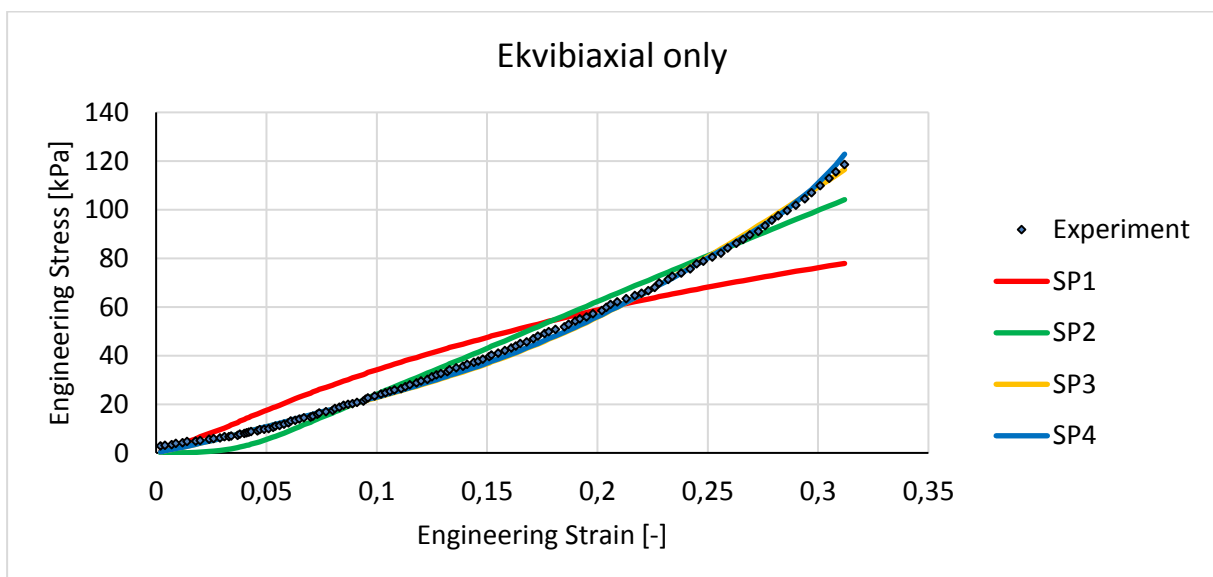


Figure 28 Stress strain model curves for different starting points for equibiaxial dataset in comparison with experimental data.

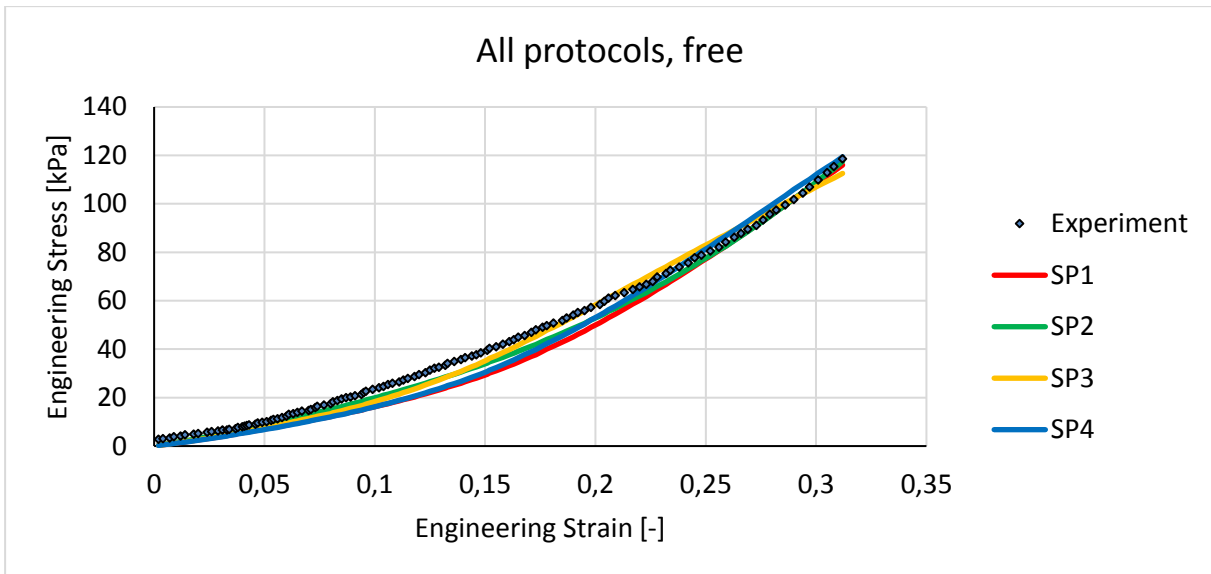


Figure 29 Stress strain model curves for different starting points for all datasets in comparison with experimental data, unconstrained (free) parameters.

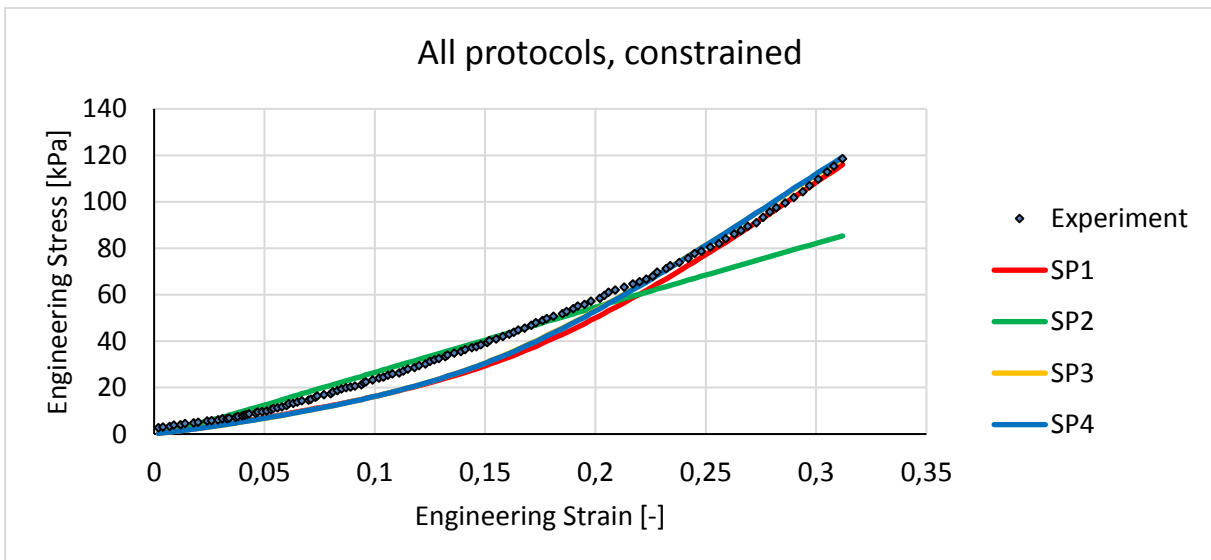


Figure 30 Stress strain model curves for different starting points for all datasets in comparison with experimental data, constrained parameters.

The table with all starting points, fitted parameters and residuals is in Appendix B.

6.3 Conclusion

The process of fitting the measured data with different constitutive models is a time and attention demanding activity for the operator. Therefore further automation of the process is advisable in order to prevent operator-based mistakes and to quicken the process significantly.

The resulting coefficient of determination R^2 depends on the starting point, which is defined as a set of starting parameters.

The greatest difference in resulting R^2 was observed when using the most “soft” stress-strain response where most of the parameters tended to the zero value. The R^2 values of the same starting points applied on different datasets differed significantly. Therefore we can conclude there are no “ideal” starting points to be used when fitting experimental data.

The most effective method how to achieve the best approximation of experimental data from many data sets is to select one group of the measured data sets and to fit this group using multiple starting points. The resulting set of parameters with the highest R^2 is then used as a starting point for all the other data sets. This approach combines the probability of finding the best approximation with minimization of the calculation time.

Constraint of the parameters results in unpredictable influencing the R^2 of the fit. In two cases the R^2 values were practically the same, in one case the difference was minimal and in one case the difference was large. It cannot be said that in the analysed case the constraint of the parameters influences the resulting fit negatively because there is no significant dependence.

7 The influence of affine deformation between matrix and fibres

7.1 Motivation

Constitutive models represent a challenging and important issue in biomechanical modelling. For description of mechanical behaviour of soft tissues different types of constitutive models have been used, from those formulated originally for rubber (e.g. Mooney-Rivlin model [97] and its simplified forms), through different types of isotropic or anisotropic phenomenological models proposed specifically for soft tissues (Demiray [98], Fung [99], Hayashi [100], and others), up to models reflecting at different levels the tissue structure (e.g. Lanir [101], Holzapfel [34], Gasser [35], Martufi [70]). A specific family of constitutive models reflecting active response of some soft tissues (e.g. Rachev [102,103], Stergiopoulos [104]) is not addressed in this study. Many of these models are capable to describe uniaxial or biaxial responses of arterial tissues with acceptable accuracy but most of them fail in prediction of biaxial response on the basis of uniaxial testing only. A similar problem occurs if stress-strain behaviour of arterial tissue under various types of biaxial stress or strain is to be predicted on the basis of equibiaxial tests only. Therefore biaxial testing under different ratios of displacements or forces in both directions is preferred. However, when we tried to capture five different biaxial testing protocols (with maximum displacement ratio 5:1) for abdominal aortic aneurysm wall, none of the known constitutive models, incl. those based on structure tensor, was capable to describe them reasonably. Thus our hypothesis came into existence on possible disruption of the assumption on affine deformation which is used intrinsically in all models.

7.2 Objective

To evaluate the possible impact of disruption of the assumption of affine deformation on the stress-strain response of the material. If this impact was large enough to explain the differences between experimental data and the constitutive models, the failure of all models in description of mechanical tests of abdominal aortic aneurysm wall might be explained by their common intrinsic assumption which was never substantiated experimentally.

7.3 Methods

In order to quantify the influence of possible non-affine deformation between matrix and collagen fibres, we have created a finite element model of a square-shaped specimen of soft tissue, with one family of collagen fibres oriented under varying angle to the direction of uniaxial load.

7.3.1 Geometry

The specimen consists of two layers of matrix (upper and lower) and many fibres aligned in one direction.

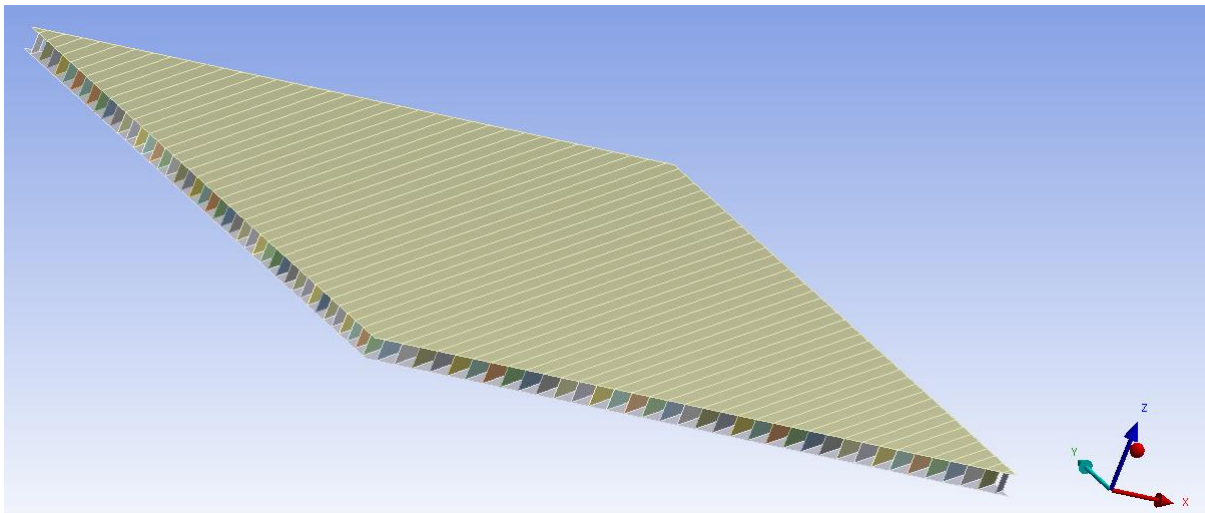


Figure 31 Geometry of the specimen. Two layers representing the matrix and the fibres between the layers.

Models with fibre angles from 0° up to 90° have been realized with the step of 5° . Examples of fibres under the angle of 10° and 25° are shown below.

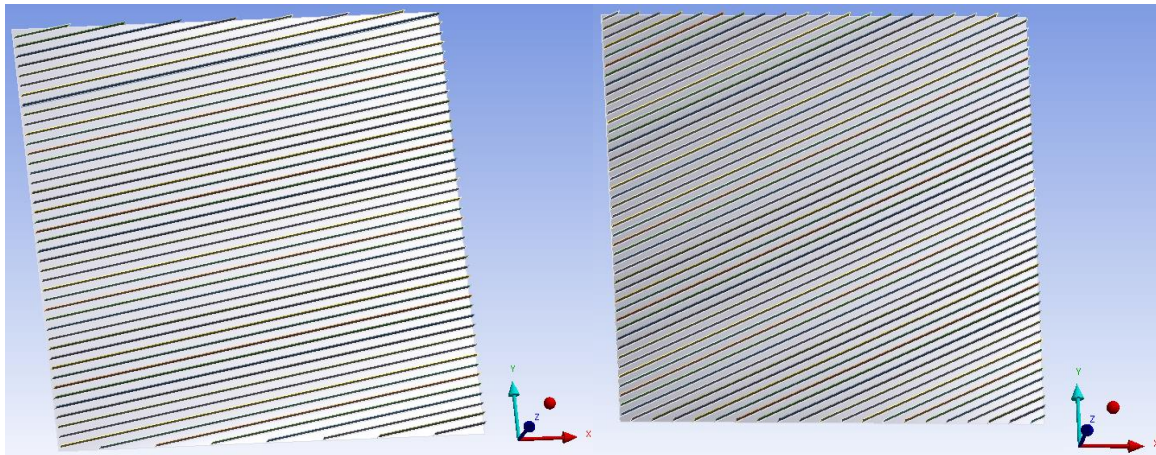


Figure 32 Models with fibre angles of 10° (left) and 25° (right).

7.3.2 Applied material models

The sample consists of fibres and matrix, Figure 33. Each type needs its own material model with relevant material constants.

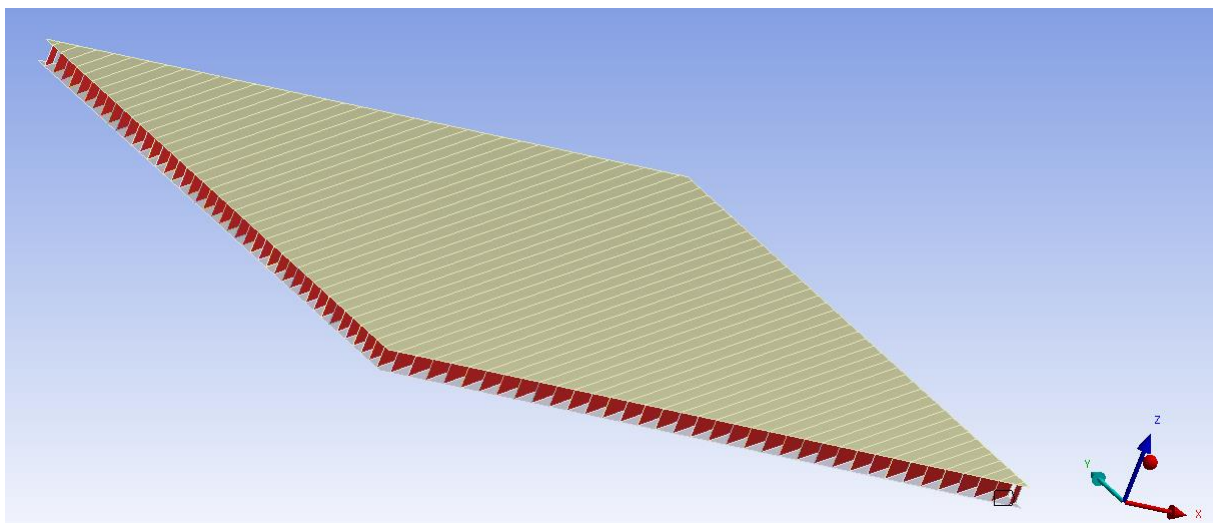


Figure 33 The matrix (grey) and the fibres (red). Matrix and fibres have different material properties.

Both material models are based on frequently used constitutive descriptions, such as Neo-Hooke and Yeoh material model, and experimentally acquired data. The presumption of incompressibility is active in both cases.

The matrix is very pliable under low stress. The constant for Neo-Hooke material model has the value $\mu = 20$ kPa.

The fibres are typically described using exponential stress strain curve. At first only small amount of stress is needed to gain large strain, after some 20 % strain the dependence becomes much stiffer and the stress can reach very high values. The parameters of 5-param. Yeoh material model are $c_{10} = 10$ Pa, $c_{20} = 8$ MPa, $c_{30} = c_{40} = 0$, $c_{50} = 200$ MPa based on a typical measured data of the relevant tissue.

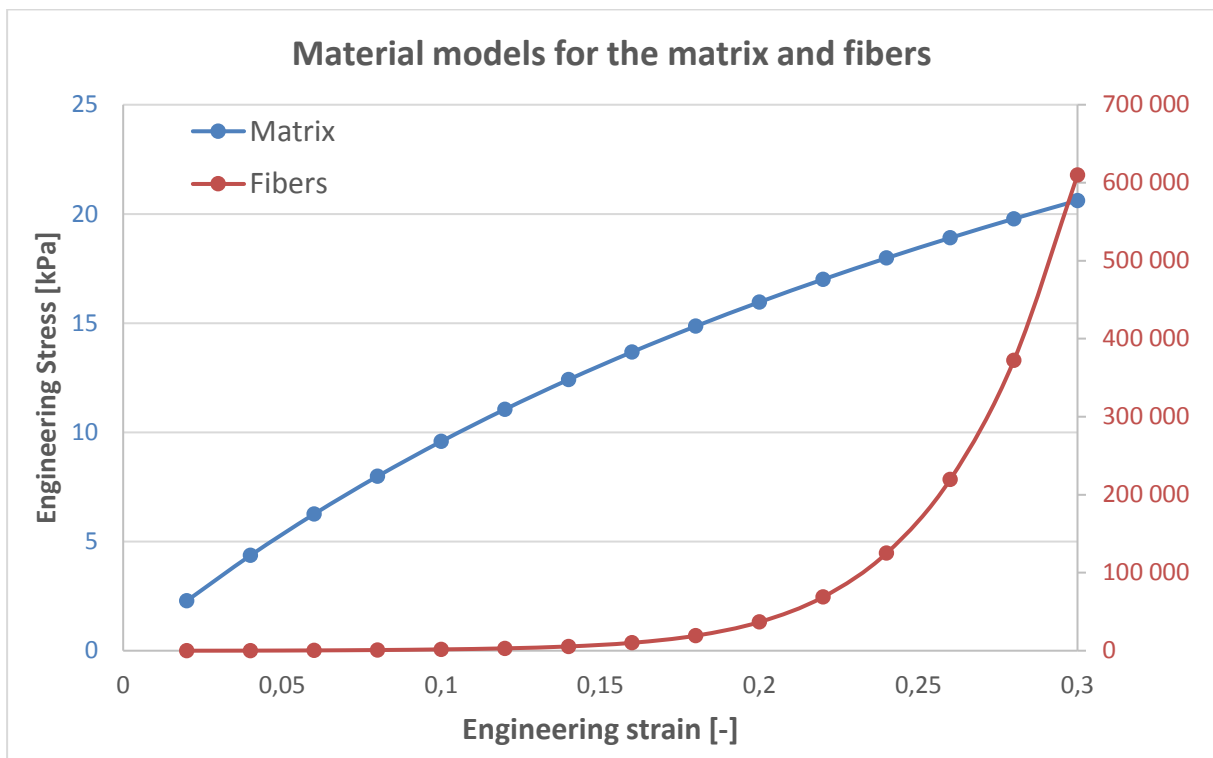


Figure 34 Stress strain curves of the matrix (blue, left) and fibre (red, right) material models.

The application of 5-param Yeoh material model in ANSYS Workbench user interface needs to be made by special Command in the solver section. The respective code is shown below.

```

/prep7

TB,HYPER,11,,5,YEOH           !Activate 5 term Yeoh data table
TBDATA,1,10,8000000,0,0,200000000 !Define C
!TBDATA,4,0,0,0,0,0           !Define D

esel,,,vlakna
emodif,all,MAT,11 !zmena materialu

nset,all
esel,all

/solv

```

Figure 35 ANSYS Command code to define and change the properties of fibres.

7.3.3 Mesh specifics, connections

The matrix was represented by 2D shell elements, while fibres were mimicked with shells perpendicular to the middle plane of the specimen and having the corresponding orientation with respect to the loading direction. The usage of 2D shell elements is explained in detail in the chapter 7.5. Each shell was divided into multiple elements along the fibre length and – for affine deformation – all the nodes were merged with the closest nodes of the matrix. In contrast, for non-affine deformation the displacements of nodes along the fibre length were independent of matrix deformation with exception of their end nodes.

A mesh density convergence was checked in order to secure mesh independent results of the finite element analysis.

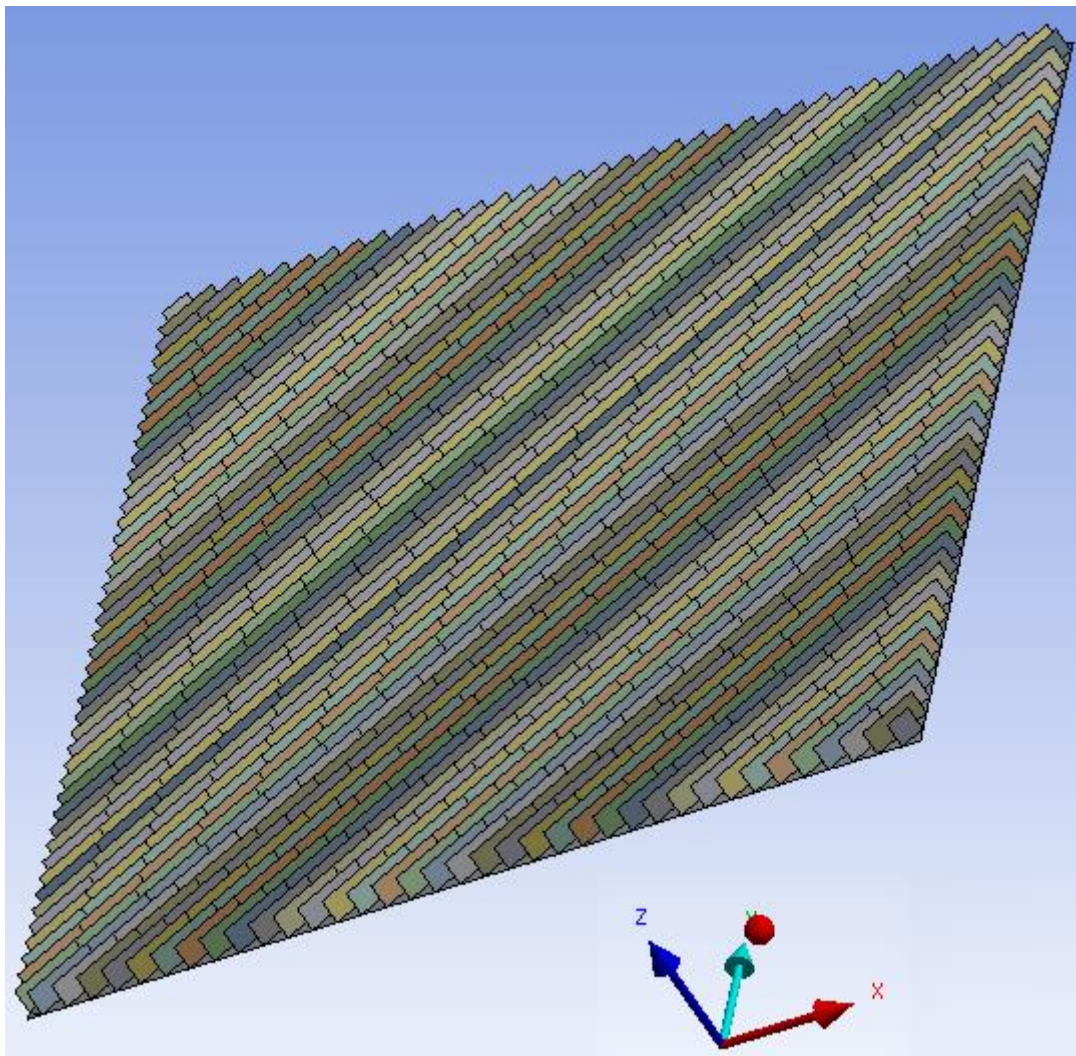


Figure 36 Mesh of the model (without upper layer to see the fibres). Each body is in different colour. The fibres consist of multiple elements in the length direction.

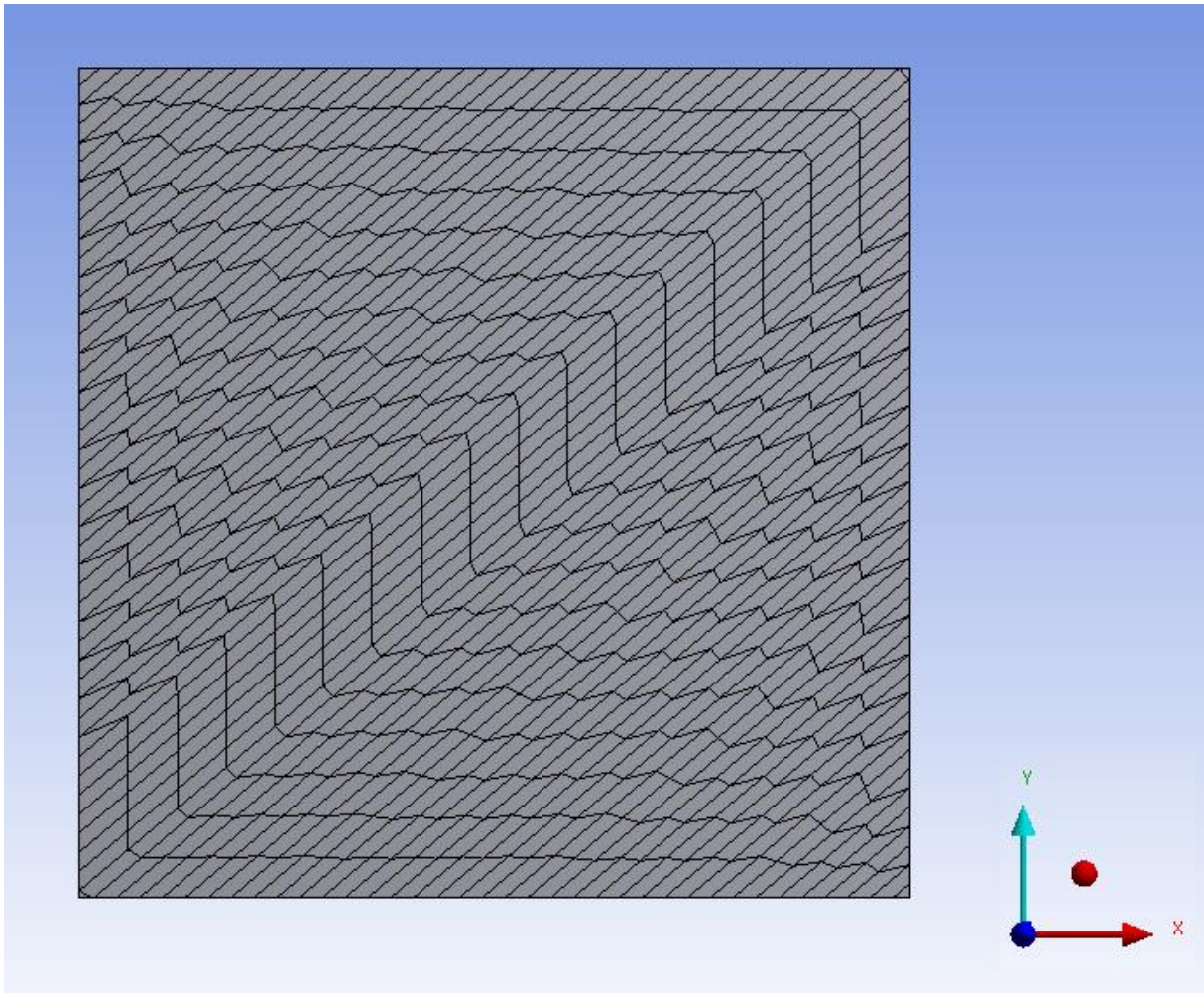


Figure 37 Mesh of the fibres. The element size was set constant if possible.

7.3.4 Loads and other boundary conditions, testing protocol

All loads and boundary conditions were applied ideally along the whole edge of the specimen. Symmetry (frictionless support) was used on the lower surface to save the calculation time.

Constraints (marked B and E in Figure 38 below) simulating symmetry were also applied on the relevant edges.

The deformation load of maximally 30 % of the starting specimen length was applied in the +x and +y direction (marked C and D on the Figure 38 below). In the case of proportional tests one of the loads was lowered in the relevant ratio. For example for the ratio of 2:1 the loads are 30 % in x axis and 15 % in y axis.

The testing protocol included uniaxial tension, planar tension, and biaxial tension with following displacement ratios: 1:1, 1:2, 2:1, 5:1, 1:5.

Note: As planar tension (plane strain tension) we denote the uniaxial tension test with constrained transversal deformation. If loaded in x direction with constrained displacement in y direction it is denoted as “ $dispY=0$ ” below.

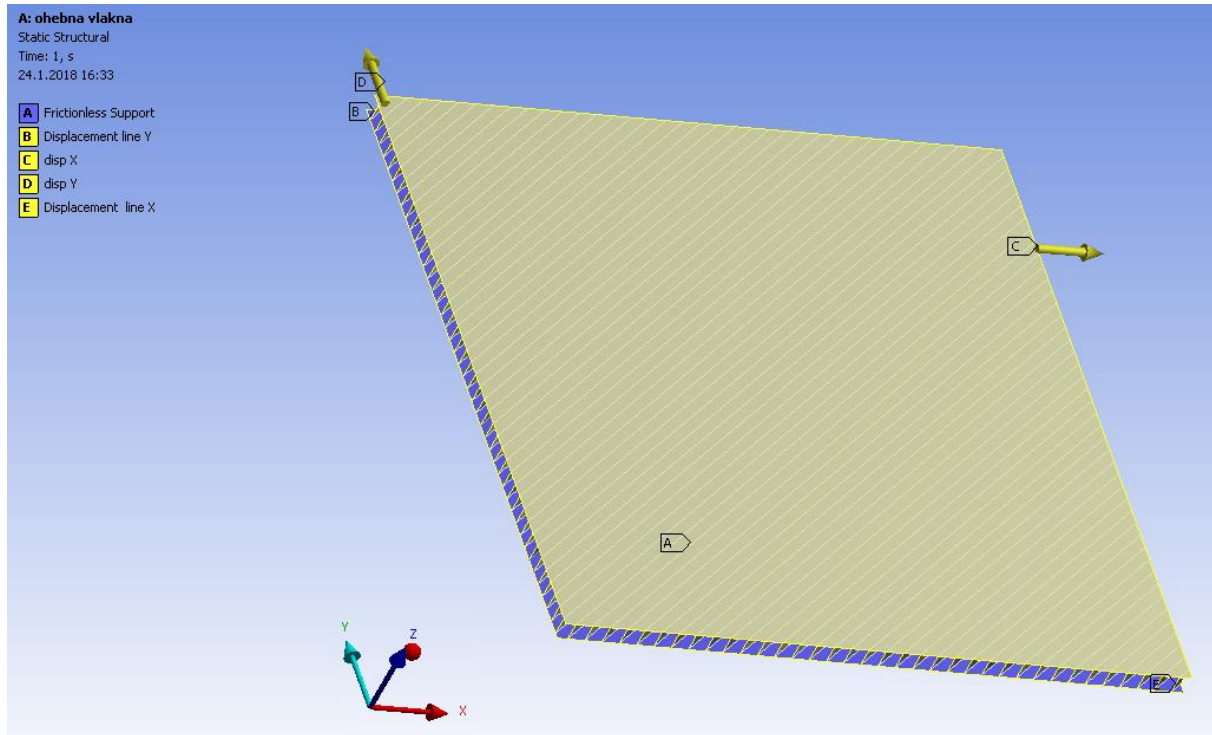


Figure 38 Boundary conditions of the model.

7.3.5 Parametric study

The parametric study consists of input parameters which we assume might be influential and of the output parameters which are observed. At the end, a possible connection between input and output parameters is analysed.

The input parameters are following:

- *The affinity of deformation:* Fibres either are or are not connected to the matrix along the whole length of the fibre. In any case the fibres are connected to the matrix at the edges of the specimen.
- *The fibre angle:* The fibres are oriented under different angles in the range from 5° to 90° with the steps of 5° .

The observed output parameter is the reaction force in relevant axis at the end of the loading process.

7.3.6 Examples of deformed state

A better idea of the results of the analysis can be provided by examples of deformed state of chosen specimens with different fibre angles and with affine or non-affine deformation.

In the pictures below, affine and non-affine deformations are presented on the left and right side, respectively. The testing protocol is equibiaxial.

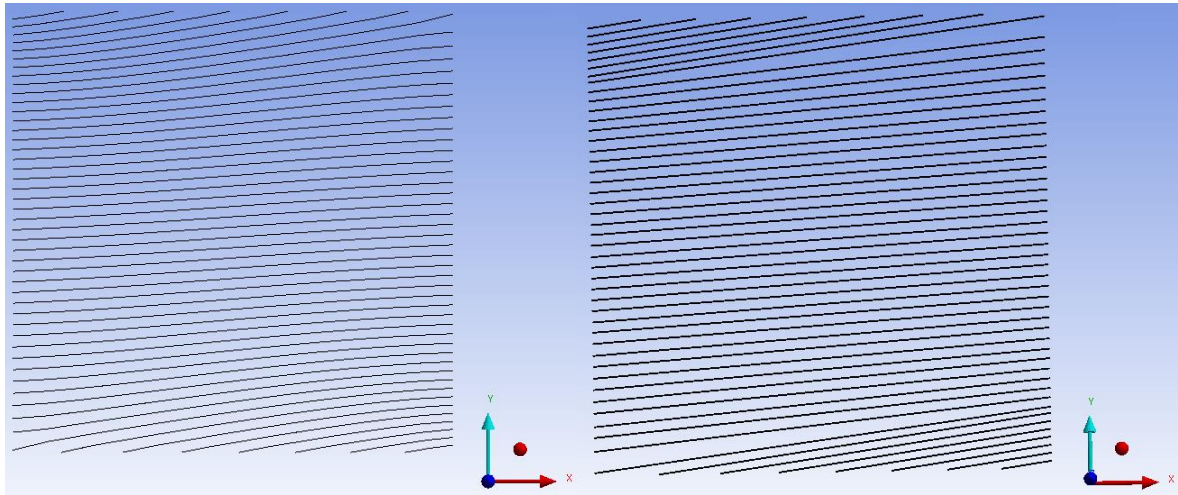


Figure 39 Example of affine (left - curved fibres) and non-affine (right - straight fibres) deformation, the fibre angle is 10° .

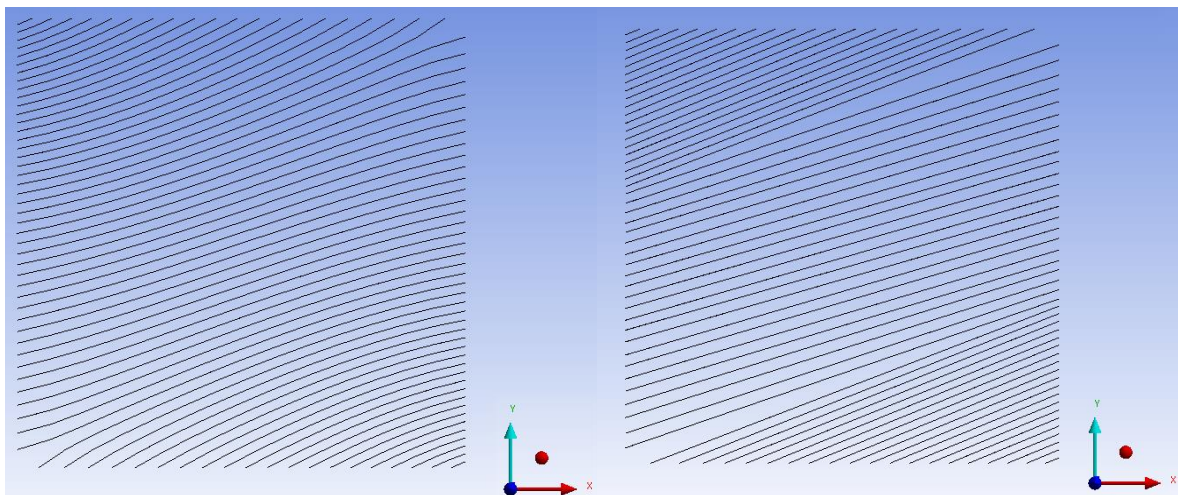


Figure 40 Example of affine (left - curved fibres) and non-affine (right - straight fibres) deformation, the fibre angle is 25° .

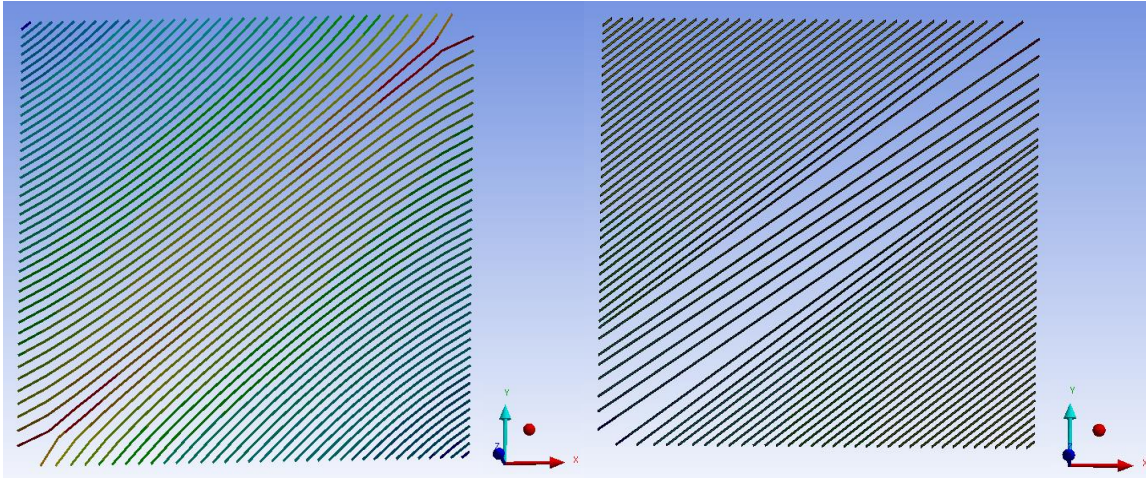


Figure 41 Example of affine (left - curved fibres) and non-affine (right -straight fibres) deformation, the fibre angle is 40° .

7.3.7 Evaluation of virtually measured data

From each FEA we acquire one dataset of strains (displacements) and stresses (forces) corresponding to the respective biaxial (or uniaxial) test. The comparison is performed between two corresponding datasets which differ only in their affine or non-affine deformation.

The simplest way of their comparison is done by calculating the difference (in %) of the force values at the end of the loading process where we assume the largest impact of affinity of deformation; affine and non-affine deformation cause different deformed shapes of fibres due to their interaction with the matrix.

The datasets could be also compared more rigorously using the coefficient of determination R^2 . In each step of the calculation, this method compares two stress values for one specific strain value, normalizes their difference, and summarizes the results along both functions.

The problem of the virtually measured datasets origins from the fact that the values of forces for both models are evaluated under different strains (although we prescribed the same displacement loads they may cause different strains).

Therefore one dataset needs to be altered to make it comparable with the other dataset. The alteration is done using material model function. The exact way of comparison is described in the following steps:

- 1) The first dataset is loaded into Hyperfit program.

- 2) A suitable material model is chosen and fitted on the data. The R^2 of the fit needs to be maximized in order to ensure that the model is a reliable representation of the measured data. In all the analysed cases the R^2 exceeded the value of 0,999.
- 3) After having obtained the model curve of the first dataset, the second dataset is loaded into the program.
- 4) The calculated R^2 of the second dataset and the model curve from the first dataset quantifies their accordance.

7.4 Results

As expected, the shape of the fibres was curved for the affine and straight for the non-affine deformation. The differences between both models were highly angle-dependent and ranged up to 10 percent regarding the force values at the end of the loading process. Such a difference might be significant for certain models but cannot explain the much larger contradictions between the structure-based constitutive models and the results of biaxial tests under different testing protocols. In addition, for the chosen constitutive model the coefficient of determination differs between both the respective stress strain curves by $\Delta R^2 = 0,01 \div 0,02$ which is an insignificant value in comparison with the larger contradictions described above.

Relative differences of maximal force values (with affine deformation model taken as basis) are shown for different loading protocols in dependence on the fibre angle in Figure 42 below.

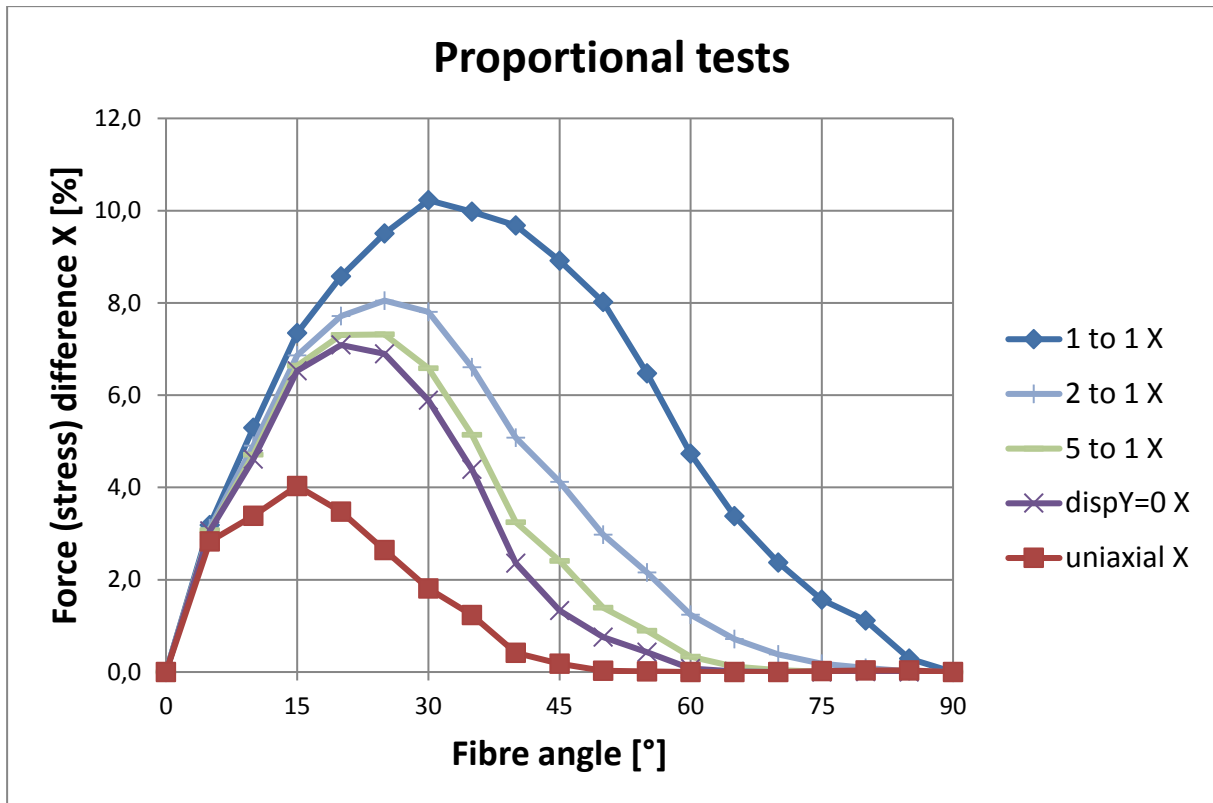


Figure 42 Relative differences of force values for different loading protocols in dependence on the fibre angle with preferred X direction.

The maximal relative difference 10,2 % was measured in the case of equibiaxial testing protocol. The difference decreases with decreasing transversal displacements (longitudinal displacements are kept constant in all the tests). The sequence of protocols according to the decreasing transversal displacement is as follows: 1:1 – 2:1 – 5:1 – dispY=0 – uniaxial test.

The maximal difference in regard to fibre angle occurs in the range between 15° and 30° depending on the testing protocol.

Table 9 Maximal force difference and its respective fibre angle for different testing protocols. The analyses have been performed with the fibre angle step of 5° which limits the accuracy of the evaluated angles.

Protocol	Difference [%]	Angle [°]
1 to 1	10,2	30
2 to1	8,1	25
5 to 1	7,3	25
dispY=0	7,1	20
uniax	4	15

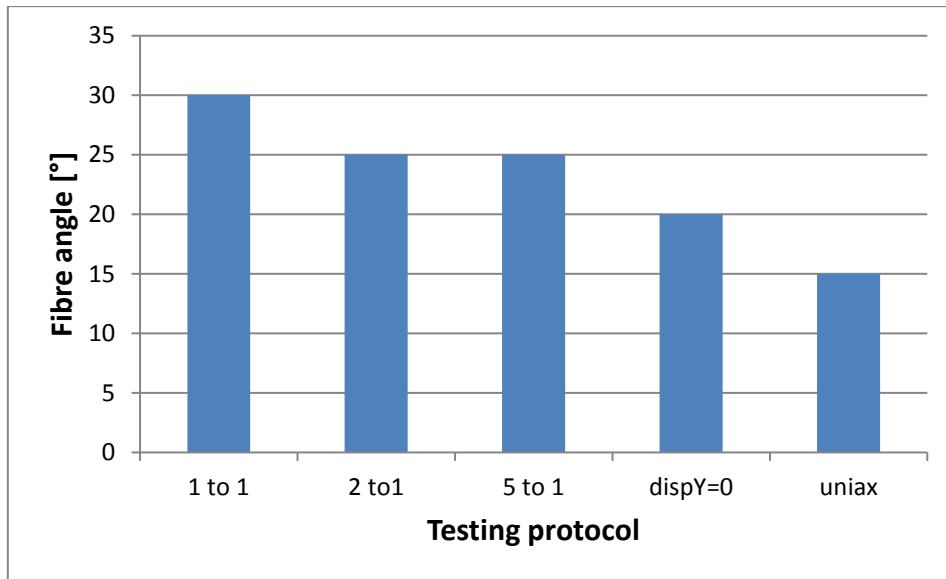


Figure 43 Graphical representation of the dependence of the fibre angle of the maximal force difference on the testing protocol.

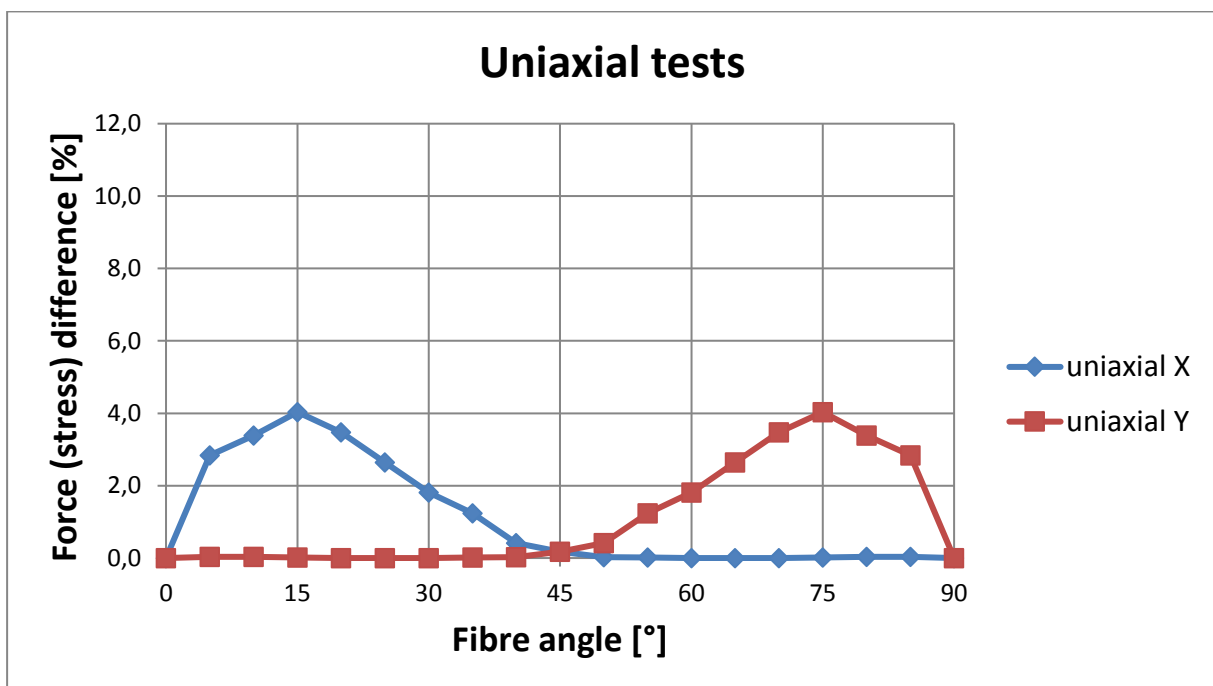


Figure 44 Maximal relative force difference as function of the fibre angle for uniaxial tests. The difference is highest for the angle of approximately 15° between the fibres and the axis of load and negligible for this angle being above 45°.

7.5 Discussion, limitations

The analysis is based on only one type of material model for matrix and fibres with one set of material parameters only. We presume that different material behaviour (other types of material models and sets of parameters) will affect the results quantitatively but not qualitatively. The aim of the study is primarily not to quantify the difference between affine and non-affine deformation but to analyse the problem qualitatively. Furthermore, the material model used in the analysis is commonly used in the field of artery wall FEA.

The usage of 2D elements instead of 3D or 1D was chosen for several reasons. If 3D elements would have been used, the FEM model would be very extensive as one can see in [96] and therefore unsuitable for sensitivity analyses. The specimen is thin, thus the stresses perpendicular to its midplane are negligible and the level of modelling in regard to the goals of the analysis admits 2D elements instead of 3D.

The focus is on the mechanical behaviour of the fibres and of the specimen in the x-y plane, the stress strain state across the thickness of the specimen is not important for the results of the analysis. The FEM program did not enable a proper connection of 2D shell and 1D link elements therefore the fibres were modelled using 2D shell elements where no problems regarding the mesh connections occurred. Furthermore, the shell elements may represent (from the perspective of mechanical behaviour) an infinite number of evenly distributed fibres (link elements) throughout the thickness of the specimen with evenly distributed stress throughout the thickness of the specimen.

The limitation of the model is its limited applicability. The structures (specimens) need to be thin walled because of the in plane (2D) stress state.

8 Conclusion

The dissertation thesis focuses on the plausibility of mechanical testing of soft biological tissues and on the predictive capabilities of different material models. Parameters of material models applied on these tissues are preferentially based on biaxial tension tests. The results of these tests can be significantly influenced by the choice of experimental setup which is chosen solely by the designer of the testing machine and the operator; there are no generally agreed standards for their execution.

Hooks are most commonly used but their application may bring some problems. Our research group uses two narrow clamps because of their easy, quick and practical use. This novel gripping method needs validation of its plausibility which is one of the major goals of this doctoral topic. Other goals represent analyses of various additional influencing parameters of the experimental setup and realisation. Validation of our novel gripping approach is done through comparison with the standard approach using hooks.

Computational modelling was used to examine all the named influencing parameters. A parametric FE model of biaxial tension test was created and different experimental setups were simulated. The accuracy of results was quantified by means of coefficient of determination R^2 comparing the virtually measured stress-strain data with the theoretical response of the input model of the specimen material. This novel approach is based on the way how stresses and strains are calculated in experiments and the applied comparison of input and output curves is superior to evaluation of uniformity of strains and stresses throughout the specimen applied in previous studies.

Present results have confirmed that two narrow clamps per edge as well as commonly used hooks are applicable for biaxial tension testing of different soft tissues using square shape specimens. Use of clamps is therefore a time efficient and reliable alternative not inferior to hooks. The analysis focused on recommendations for the choice of type, number and size of gripping elements for different specimen size was carried out in the thesis.

The process of fitting the measured data with different constitutive models is a time and attention demanding activity for the operator. Therefore further automation of the process is advisable in order to prevent operator-based mistakes and to quicken the process significantly.

The resulting coefficient of determination R^2 depends on the starting point, which is defined as a set of starting parameters, and there are no “ideal” starting points to be used when fitting experimental data. The most effective way of achieving the best approximation of experimental data from many data sets is based on the best fit of a selected data set and combines the probability of finding the best approximation with minimization of the calculation time.

Furthermore a constraint of the fitted parameters results in unpredictable influencing of the R^2 of the fit.

The differences between models simulating affine and non-affine deformation were highly angle-dependent and ranged up to 10 percent regarding the force values at the end of the loading process. Such a difference might be significant for certain models but cannot explain the much larger contradictions between the structure-based constitutive models and the results of biaxial tests under different testing protocols.

9 Future work

The analyses done in this doctoral thesis have shown some additional problems related to practical realization of experiments and their computational modelling. The solution to these problems could be provided by possible future work of the author or his continuator.

- The inaccuracy of positioning of gripping elements along the edge of the specimen may also influence the results of biaxial testing and make them operator-dependent. It was not yet analysed.
- Fitting of anisotropic constitutive models (without dispersion of fibre directions) to the experimental data from different biaxial tests resulted mostly in zero value of radial (isotropic) stiffness parameter. This disables a realistic simulation of compression of the tissue by clamps. A non-zero radial stiffness improves significantly the convergence of anisotropic material models, so application of other anisotropic material models could widen the validity of the study.
- The accuracy of the anisotropic material models of soft tissues based on results of biaxial tension tests could be further improved by adding experimental evaluation of radial stiffness of the tissue which is missing in the current analyses as well as in literature. A more detailed description of this possible future work is elaborated below.
- Hooks and clamps are widely used in biaxial testing. Nowadays also rakes are applied in some commercially available testing machines. Therefore further comparison between the named gripping elements could be useful.

9.1 Experimental estimation of radial stiffness

Radial stiffness of soft fibrous tissues has two major roles in this analysis. Firstly, in the case of using clamps when radial pressing is included, and secondly when fitting the experimental data with a material model. Radial stiffness of rabbit aorta and the influence of the stiffness on material model fitting were examined in an older study [69]. It proves a great difference in material parameters when only data from biaxial testing or also from radial stiffness testing are used. The material constant c_{10} can be directly connected with radial stiffness of the tissue (see eq. (1) and more details in chapter 4.1.2). This constant is often obtained with zero value from the fitting procedures although it cannot represent the physiological state and mechanical reality but only the best mathematical fit of the material model. A significant drawback of such value is very low initial radial stiffness which brings

difficulties in convergence of the FE simulations of compression in this direction. Addition of some experiment considering radial stiffness into the set of fitted data could bring a better validity of the resulting material models. The inclusion of experimental data from radial stiffness mechanical tests into the fitting process, where till now only tests under axial or circumferential loads were used, is one of the problems which could be solved somewhere in the future.

Standard tension test cannot be performed in radial direction because the maximum available length of specimen is about 2 mm which is far too small to grip via clamps or other gripping method. In case of inflation or radial compression tests the fibres are lengthened similarly as in case of biaxial tension test. Assuming relatively great specimen surface, on which the pressure would be applied, the radial compression test would tend to a volumetric test. On the basis of these problems a novel sophisticated experimental design is needed, possibly validated using FE simulations. The specimen size and shape and other experimental influencing parameters could have a major impact on experimental data, so a sensitivity analysis (experimental and computational) should be done to solve this issue.

After acquiring the needed data representing the radial stiffness of the artery, re-fitting of the anisotropic material models could give more realistic description of their mechanical response; then the previous FE models of biaxial tension tests could be recalculated and the range of validity of the presented analyses extended.

9.2 Using other anisotropic material models

Different mechanical behaviour of various soft tissues can be described by different material models, usually anisotropic, hyperelastic, polynomial or exponential, with fibre families and their dispersion etc. Previous results (Figure 20 and Figure 21) show the influence of material model and its parameters on the accuracy of biaxial tension tests, so a possible extension of the study with additional material models could be useful.

9.3 Analysis of gripping with rakes

In this study rakes were not analysed because they are not so broadly used as hooks. The goal of the study was to compare the most common gripping method (hooks) with the method applied in our research group (clamps). Rakes represent an interesting way to grip the

specimen because they are easier to apply than hooks but they distribute the force load unevenly due to their axial movement restriction. Thus they differ from hooks and clamps significantly and represent an interesting approach which is worth of analysis.

9.4 Inaccurate positioning of gripping elements

All analyses were set up with all gripping elements ideally positioned with no inaccuracy. This assumption cannot be met in real experiment; the operator can never place the clamps or hooks accurately to their required position. There will be always some deviation from the prescribed position, see Figure 45. These deviations or inaccuracies from ideal positioning can influence the results significantly.

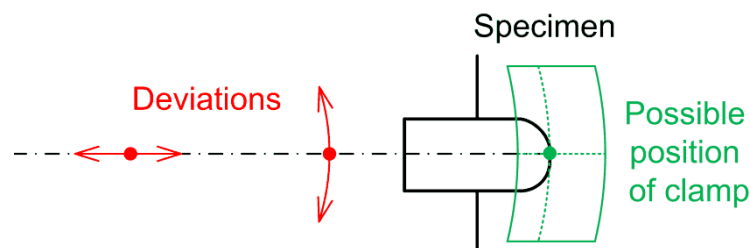


Figure 45 Schematic representation of possible positioning of a gripping element (clamp).

Red arrows show possible inaccuracy in positioning, green shows the possible area of gripping due to the inaccuracies.

The sensitivity analysis of inaccurate positioning of gripping elements was, according to the author's best knowledge, not yet accomplished.

Every gripping element should be positioned independently on the other elements. This requires modelling of the whole upper (or lower) part of the specimen with no more use of two of the symmetry planes. This fact and many possible (inaccurate) positions of the gripping elements determine the great amount of different combinations and consequently of computational time required for the analysis. Therefore the planning of these simulated experiments becomes a very important issue.

10 References

- [1] Deeken CR, Thompson DM, Castile RM, Lake SP. Biaxial analysis of synthetic scaffolds for hernia repair demonstrates variability in mechanical anisotropy, non-linearity and hysteresis. *J Mech Behav Biomed Mater.* 2014 Oct;38:6–16.
- [2] Sahoo S, DeLozier KR, Erdemir A, Derwin KA. Clinically relevant mechanical testing of hernia graft constructs. *J Mech Behav Biomed Mater.* 2015 Jan;41:177–88
- [3] Jhun C-S, Evans MC, Barocas VH, Tranquillo RT. Planar biaxial mechanical behavior of bioartificial tissues possessing prescribed fiber alignment. *J Biomech Eng.* 2009 Aug;131(8):081006
- [4] Quaglini V, Corazza C, Poggi C. Experimental characterization of orthotropic technical textiles under uniaxial and biaxial loading. *Compos Part A Appl Sci Manuf.* 2008 Aug;39(8):1331–42.
- [5] Payne T, Mitchell S, Bibb R, Waters M. The evaluation of new multi-material human soft tissue simulants for sports impact surrogates. *J Mech Behav Biomed Mater.* 2015 Jan;41:336–56.
- [6] Burša J., Zemánek M.: Evaluation of Biaxial Tension Tests of Soft Tissues. *Studies in health technology and informatics*, IOS Press, 2008, Vol. 133, pp. 45-55.
- [7] Virues Delgadillo JO, Delorme S, Diraddo R, Hatzikiriakos SG, Thibault F. Mechanical characterization of arterial wall: Should cruciform or square sample be used in biaxial testing? *J Biomech Eng.* 2006; pp.1-21.
- [8] Sun W, Sacks MS, Scott MJ: Effects of boundary conditions on the estimation of the planar biaxial mechanical properties of soft tissues. *J Biomech Eng* 127(4) 2005:709-15.

- [9] Waldman, Sacks, Lee: Boundary conditions during biaxial testing of planar connective tissues. *J. of Materials Science Letters* 21, 2002, 1215-1221.
- [10] Jacobs, Cortes, Vresilovic, Elliot: Biaxial Tension of Fibrous Tissue: Using Finite Element Methods to Address Experimental Challenges Arising From Boundary Conditions and Anisotropy. *J Biomech Eng*, 2013, 135 (2): 021004-1:10.
- [11] Bursa J, Zemanek M. Evaluation of Biaxial Tension Tests of Soft Tissues. *Studies in Health Technology and Informatics*, 2008, 133: 45-55.
- [12] Simón-Allué R, Cordero A, Peña E. Unraveling the effect of boundary conditions and strain monitoring on estimation of the constitutive parameters of elastic membranes by biaxial tests. *Mech Res Commun*. 2014; 57:82-89.
- [13] Bellini C, Glass, P, Sitti M, Di Martino ES. Biaxial modeling of the small intestine. *J Mech Behav Biomed Mater*. Elsevier Ltd; 2011 Nov; 4(8): 1727-40
- [14] Waldman SD, Sacks MS, Lee JM. Imposed state of deformation determines local collagen fibre orientation but not apparent mechanical properties. *Biomed Sci Instrum*. 1999 Jan 1;35:51–6.
- [15] Sommer G, Schriebl A, Zeindlinger G, Katzensteiner A, Ainödhofer H, Saxena A, et al. Multiaxial mechanical response and constitutive modeling of esophageal tissues: Impact on esophageal tissue engineering. *Acta Biomater*. 2013 Dec;9(12):9379–91.
- [16] Tong J, Cohnert T, Regitnig P, Holzapfel GA. Effects of age on the elastic properties of the intraluminal thrombus and the thrombus-covered wall in abdominal aortic aneurysms: biaxial extension behaviour and material modelling. *Eur J Vasc Endovasc Surg*. 2011 Aug;42(2):207–19.
- [17] Polzer S, Christian Gasser T, Bursa J, Staffa R, Vlachovsky R, Man V, et al. Importance of material model in wall stress prediction in abdominal aortic

- aneurysms. *Med Eng Phys. Institute of Physics and Engineering in Medicine*; 2013;35(9):1282–9.
- [18] Zhao X, Berwick ZC, Krieger JF, Chen H, Chambers S, Kassab GS. Novel Design of Cruciform Specimens for Planar Biaxial Testing of Soft Materials. *Exp Mech.* 2013 Sep 26;54(3):343–56.
- [19] Hu JJ, Chen GW, Liu YC, Hsu SS. Influence of Specimen Geometry on the Estimation of the Planar Biaxial Mechanical Properties of Cruciform Specimens. *Exp Mech.* 2013;54(4):615-631.
- [20] Kamenskiy A V., Pipinos II, Dzenis YA, Lomneth CS, Kazmi SAJ, Phillips NY, et al. Passive biaxial mechanical properties and in vivo axial pre-stretch of the diseased human femoropopliteal and tibial arteries. *Acta Biomater. Acta Materialia Inc.*; 2014 Mar;10(3):1301–13.
- [21] Cruz Perez B, Tang J, Morris HJ, Palko JR, Pan X, Hart RT, et al. Biaxial mechanical testing of posterior sclera using high-resolution ultrasound speckle tracking for strain measurements. *J Biomech.* 2014 Mar 21;47(5):1151–6.
- [22] Sommer G, Schriefl AJ, Andrä M, Sacherer M, Viertler C, Wolinski H, et al. Biomechanical Properties and Microstructure of Human Ventricular Myocardium. *Acta Biomater.* 2015, 24:172-192.
- [23] Pham T, Sun W. Comparison of biaxial mechanical properties of coronary sinus tissues from porcine, ovine and aged human species. *J Mech Behav Biomed Mater.* 2012 Feb;6:21–9.
- [24] Lyons M, Winter DC, Simms CK. Mechanical characterisation of porcine rectus sheath under uniaxial and biaxial tension. *J Biomech.* 2014 Jun 3;47(8):1876–84.

- [25] Kahlon A, Hurtig MB, Gordon KD. Regional and depth variability of porcine meniscal mechanical properties through biaxial testing. *J Mech Behav Biomed Mater.* 2015 Jan;41:108–14.
- [26] Cooney GM, Moerman KM, Takaza M, Winter DC, Simms CK. Uniaxial and biaxial mechanical properties of porcine linea alba. *J Mech Behav Biomed Mater.* 2015 Jan;41:68–82.
- [27] Azadani AN, Chitsaz S, Matthews PB, Jaussaud N, Leung J, Tsinman T, et al. Comparison of mechanical properties of human ascending aorta and aortic sinuses. *Ann Thorac Surg. Elsevier;* 2012 Jan 1;93(1):87–94.
- [28] Yeoh OH. Some forms of strain energy functions for rubber. *Rubber Chem Technol* 1993;66:754–71.
- [29] Polzer S., Gasser T.C., Novák K., Man V., Tichý M., Skácel P., Burša J. (2015): Structure based constitutive model can accurately predict planar biaxial mechanical properties of aorta wall tissue. *Acta Biomaterialia*, Vol. 14 (1) 133-145
- [30] Vande Geest JP, Sacks MS, Vorp DA. The effects of aneurysm on the biaxial mechanical behavior of human abdominal aorta. *J Biomech.* 2006 Jan;39(7):1324–34.
- [31] Raghavan ML, Vorp DA: Toward a biomechanical tool to evaluate rupture potential of abdominal aortic aneurysms: identification of a finite strain constitutive model and evaluation of its applicability. *J. Biomech*, 2000, 33:475-482.
- [32] Gundiah N, B Ratcliffe M, A Pruitt L. Determination of strain energy function for arterial elastin: Experiments using histology and mechanical tests. *J Biomech.* 2007, 40(3):586–94.

- [33] Gasser TG, Gorgulu G, Folkesson M, Swedenborg J. Failure properties of intraluminal thrombus in abdominal aortic aneurysm under static and pulsating mechanical loads. *J Vasc Surg* 2008;48:179-88.
- [34] Holzapfel GA, Gasser TC, Ogden RW. A new constitutive framework for arterial wall mechanics and a comparative study of material models. *J Elast.* 2000;61(1-3):1-48.
- [35] Gasser TC, Ogden RW, Holzapfel GA. Hyperelastic modelling of arterial layers with distributed collagen fibre orientations. *J R Soc Interface.* 2006 Feb 22; 3(6):15-35.
- [36] Kratzberg JA, Walker PJ, Rikkers E, Raghavan ML. The effect of proteolytic treatment on plastic deformation of porcine aortic tissue. *J Mech Behav Biomed Mater.* 2009 Jan;2(1):65-72.
- [37] Nolan DR, McGarry JP. On the correct interpretation of measured force and calculation of material stress in biaxial tests. *J Mech Behav Biomed Mater.* 2016 Jan;53:187-99.
- [38] Eilaghi A, Flanagan JG, Brodland GW, Ethier CR. Strain uniformity in biaxial specimens is highly sensitive to attachment details. *J Biomech Eng. American Society of Mechanical Engineers;* 2009 Sep 1;131(9):091003.
- [39] Lanir Y, Fung YC. Two-dimensional mechanical properties of rabbit skin—I. Experimental system. *J Biomech.* 1974;7:29-34.
- [40] Janíček P, Rosenberg J, Křen J. *Biomechanika.* 1. ed. Plzeň: Vydavatelství Západočeské univerzity, Fakulta aplikovaných věd; 1997.
- [41] Chomič D. Vliv mechanických vlastností cévních protéz na jejich klinické použití. Brno: Vysoké učení technické v Brně, Fakulta strojního inženýrství; 2010. p. 43. Vedoucí bak. práce prof. Ing. Jiří Burša, Ph.D.

- [42] Holubář O. Analýza šíření tlakové vlny v aortě. Brno: Vysoké učení technické v Brně, Fakulta strojního inženýrství; 2011. p. 73. Vedoucí dipl. práce prof. Ing. Jiří Burša, Ph.D.
- [43] Mucha P. Deformačně-napěťová analýza výdutí tepen. Brno: Vysoké učení technické v Brně, Fakulta strojního inženýrství; 2008. p. 59. Vedoucí dipl. práce prof. Ing. Jiří Burša, Ph.D.
- [44] Polzer S. Deformačně napěťová analýza aortálních aneuryzmat. Brno: Vysoké učení technické v Brně, Fakulta strojního inženýrství; 2012. p. 161. Vedoucí dizertační práce prof. Ing. Jiří Burša. Ph.D.
- [45] Burša J. Biomechanika III [Internet]. Biomechanika III. [cited 2014 Mar 29]. Available from: <http://www.umt.fme.vutbr.cz/cz/studium/studijni-materialy.html>
- [46] WikiSkripta [Internet]. [cited 2014 Mar 29]. Available from: <http://www.wikiskripta.eu/index.php/Home>
- [47] Gloeckner DC, Sacks MS, Fraser MO, Somogyi GT, de Groat WC, Chancellor MB. Passive biaxial mechanical properties of the rat bladder wall after spinal cord injury. *J Urol.* 2002 May;167(5):2247–52.
- [48] Szczesny SE, Peloquin JM, Cortes DH, Kadlowec JA, Soslowsky LJ, Elliott DM. Biaxial tensile testing and constitutive modeling of human supraspinatus tendon. *J Biomech Eng.* 2012 Mar;134(2):021004.
- [49] Engel N. Abdominal Aortic Aneurysm and Low Back Pain. *Dyn Chiropr.* 1996;14(16).
- [50] Ganong WF. *Review of Medical Physiology.* 22nd ed. McGraw-Hill Medical; 2005.
- [51] Timaran C, Rosero E, Clagett P, Lo H, Peshock R. Abdominal Aortic Wall-Thickness by Magnetic Resonance Imaging and Cardiovascular Disease in a Multi-ethnic Population-Based Study. *Circulation.* 2006;114.

- [52] Cleveland Clinic Web, Aorta Illustration [Internet]. [cited 2012 Mar 25]. Available from: http://my.clevelandclinic.org/heart/disorders/aorta_marfan/aortaillust.aspx
- [53] Gombala T. WikiSkripta: Cévy - Srovnání struktury arterie a vény při stejné tloušťce [Internet]. 2010 [cited 2014 Apr 26]. Available from: http://www.wikiskripta.eu/index.php/Soubor:Arterie_vena.png
- [54] Fratzl P. Collagen: Structure and Mechanics. Boston, MA: Springer US; 2008.
- [55] Timmins LH, Wu Q, Yeh AT, Moore JE, Greenwald SE. Structural inhomogeneity and fiber orientation in the inner arterial media. *Am J Physiol Heart Circ Physiol*. 2010 May;298(5):H1537–45.
- [56] O’Connell MK, Murthy S, Phan S, Xu C, Buchanan J, Spilker R, et al. The three-dimensional micro- and nanostructure of the aortic medial lamellar unit measured using 3D confocal and electron microscopy imaging. *Matrix Biol*. 2008 Apr;27(3):171–81.
- [57] Alexander JJ. The pathobiology of aortic aneurysms. *J Surg Res*. Elsevier; 2004 Mar 1;117(1):163–75.
- [58] Řez aortou [Internet]. [cited 2014 Apr 26]. Available from: http://anatomy.kmu.edu.tw/BlockHis/Block3/slides/block4_20.html
- [59] WikiSkripta: Pojiva [Internet]. [cited 2014 Apr 26]. Available from: http://www.wikiskripta.eu/index.php/Pojivová_tkáň
- [60] WikiSkripta: Hladké svalstvo [Internet]. [cited 2014 Apr 26]. Available from: http://www.wikiskripta.eu/index.php/Hladké_svalstvo
- [61] Mortality results for randomised controlled trial of early elective surgery or ultrasonographic surveillance for small abdominal aortic aneurysms. The UK Small Aneurysm Trial Participants. *Lancet*. 1998 Nov 21;352(9141):1649–55.

- [62] Gundiah N, Ratcliffe MB, Pruitt LA. The biomechanics of arterial elastin. *J Mech Behav Biomed Mater*. Elsevier Ltd; 2009;2(3):288–96.
- [63] Fratzl P. *Collagen: Structure and Mechanics*. Fratzl P, editor. Boston, MA: Springer US; 2008.
- [64] Carlisle CR, Coulais C, Guthold M. The mechanical stress-strain properties of single electrospun collagen type I nanofibers. *Acta Biomater*. 2010 Aug;6(8):2997–3003.
- [65] YC. *Biomechanics: Mechanical Properties of Living Tissues*. Springer; 1993.
- [66] Fung YC. Elasticity of soft tissues in simple elongation. *Am J Physiol*. 1968;213(6):1532 – 44.
- [67] Novák K. *Analýza zbytkových napětí ve stěně tepny*. Brno: Vysoké učení technické v Brně, Fakulta strojního inženýrství; 2013. p. 95. Vedoucí dipl. práce prof. Ing. Jiří Burša, Ph.D.
- [68] Sacks MS. Biaxial mechanical evaluation of planar biological materials. *J Elast Phys Sci solids*. Springer; 2000;61(1):199–246.
- [69] Chuong CJ, Fung YC. Compressibility and constitutive equation of arterial wall in radial compression experiments. *J Biomech [Internet]*. 1984 Jan [cited 2014 Aug 13];17(1):35–40.
- [70] Martufi G, Gasser TC. A constitutive model for vascular tissue that integrates fibril, fiber and continuum levels with application to the isotropic and passive properties of the infrarenal aorta. *J Biomech*. 2011 Sep 23; 44(14):2544–50.
- [71] Holzapfel GA, Sommer G, Gasser CT, Regitnig P. Determination of layer-specific mechanical properties of human coronary arteries with nonatherosclerotic intimal thickening and related constitutive modeling. *Am J Physiol Heart Circ Physiol*. 2005 Nov; 289(5):H2048–58.

- [72] Fung YC. What are the residual stresses doing in our blood vessels? *Ann Biomed Eng.* Kluwer Academic Publishers; 1991 May; 19(3):237–49.
- [73] Carew TE, Vaishnav RN, Patel DJ. Compressibility of the Arterial Wall. *Circ Res.* 1968 Jul 1; 23(1):61–8.
- [74] Skacel P, Bursa J. Poisson's ratio of arterial wall – Inconsistency of constitutive models with experimental data. *J Mech Behav Biomed Mater.* 2016;54:316–27.
- [75] Volokh KY. Compressibility of arterial wall in ring-cutting experiments. *Mol Cell Biomech.* 2006 Mar; 3(1):35–42.
- [76] Yosibash Z, Manor I, Gilad I, Willentz U. Experimental evidence of the compressibility of arteries. *J Mech Behav Biomed Mater.* 2014;39:339–54.
- [77] Peña JA, Martínez MA, Peña E. Layer-specific residual deformations and uniaxial and biaxial mechanical properties of thoracic porcine aorta. *J Mech Behav Biomed Mater.* 2015 Jun 4; 50:55–69.
- [78] Karimi A, Navidbakhsh M, Shojaei A. A combination of histological analyses and uniaxial tensile tests to determine the material coefficients of the healthy and atherosclerotic human coronary arteries. *Tissue Cell.* 2015 Apr; 47(2):152–8.
- [79] Sokolis DP, Boudoulas H, Karayannacos PE. Assessment of the aortic stress–strain relation in uniaxial tension. *J Biomech.* 2002;35(9):1213–23.
- [80] Pham T, Martin C, Elefteriades J, Sun W. Biomechanical characterization of ascending aortic aneurysm with concomitant bicuspid aortic valve and bovine aortic arch. *Acta Biomater.* 2013 Aug; 9(8):7927–36.
- [81] Lawton RW. The Thermoelastic Behavior of Isolated Aortic Strips of the Dog. *Circ Res* [Internet]. Lippincott Williams & Wilkins; 1954 Jul 1;2(4):344–53.
- [82] Carew TE, Vaishnav RN, Patel DJ. Compressibility of the Arterial Wall. *Circ Res.* 1968 Jul 1;23(1):61–8.

- [83] Tickner EG, Sacks AH. A theory for the static elastic behavior of blood vessels. *Biorheology*. 1967 Sep;4(4):151–68.
- [84] Chuong CJ, Fung YC. Compressibility and constitutive equation of arterial wall in radial compression experiments. *J Biomech*. Elsevier; 1984 Jan;17(1):35–40.
- [85] Dobrin, Rovick. Static elastic properties of the dog carotid arterial wall. *Fed Proc*. 1967;26:1021.
- [86] Faury G, Maher GM, Li DY, Keating MT, Mecham RP, Boyle WA. Relation between outer and luminal diameter in cannulated arteries. *Am J Physiol*. 1999 Nov;277(5 Pt 2):H1745–53.
- [87] Girerg X, Acar C, Mourad J, Boutouyrie P, Safar M, S. L. Incompressibility of the human arterial wall: an in vitro ultrasound study. *J Hypertens*. 1992;10(Suppl. (6)):S111–5.
- [88] Boutouyrie P, Germain DP, Tropeano A-I, Laloux B, Carezni F, Zidi M, et al. Compressibility of the Carotid Artery in Patients With Pseudoxanthoma Elasticum. *Hypertension* [Internet]. Lippincott Williams & Wilkins; 2001 Nov 1;38(5):1181–4.
- [89] Chesler NC, Thompson-Figueroa J, Millburne K. Measurements of Mouse Pulmonary Artery Biomechanics. *J Biomech Eng*. American Society of Mechanical Engineers; 2004;126(2):309.
- [90] Di Puccio F, Celi S, Forte P. Review of Experimental Investigations on Compressibility of Arteries and Introduction of a New Apparatus. 2012. p. 895–902.
- [91] Aaron BB, Gosline JM. Optical properties of single elastin fibres indicate random protein conformation. *Nature*. Nature Publishing Group; 1980 Oct 30; 287(5785):865–7.

- [92] Horný L, Netušil M, Voňavková T. Axial prestretch and circumferential distensibility in biomechanics of abdominal aorta. *Biomech Model Mechanobiol.* Springer Berlin Heidelberg; 2014 Aug 18; 13(4):783–99.
- [93] Ferruzzi J., Vorp D. A., Humphrey J. D. On constitutive descriptors of the biaxial mechanical behaviour of human abdominal aorta and aneurysms. *J. R. Soc. Interface*, Mar. 2011, vol. 8, no. 56, pp. 435–50.
- [94] Baek S., Gleason R. L., Rajagopal K. R., Humphrey J. D. Theory of small on large: Potential utility in computations of fluid–solid interactions in arteries. Jun. 2007, *Comput. Methods Appl. Mech. Eng.*, vol. 196, no. 31–32, pp. 3070–3078.
- [95] Schroeder F., Polzer S., Slažanský M., Man V., Skácel P. Predictive capabilities of various constitutive models for arterial tissue. Feb. 2018, *J. Mech. Behav. Biomed. Mater.* vol. 78, pp. 369–380.
- [96] Lasota T., Computational modelling of mechanical behaviour of “elastomer – steel fibre” composite. 2013. Doctoral thesis, Brno University of Technology.
- [97] Mooney, M. "A Theory of Large Elastic Deformation", *J. of Appl. Physics*, pp. 582-592, 1940.
- [98] Demiray, H. "A note on the elasticity of soft biological tissues", *Journal of Biomechanics* 5, pp. 309-311, 1972.
- [99] Chuong, C. J., Fung, Y. C. "Three-dimensional stress distribution in arteries", *J. Biomech. Eng.* 105, pp. 268–274, 1983.
- [100] K. Takamizawa and K. Hayashi, “Strain energy density function and uniform strain hypothesis for arterial mechanics.” *J. Biomech.*, vol. 20, no. 1, pp. 7–17, 1987.
- [101] Lanir Y. Constitutive equations for fibrous connective tissues. *J Biomech.* 1983;16(1):1–12.

- [102] A. Rachev., Theoretical study of the effect of stress-dependent remodeling on arterial geometry under hypertensive conditions. *Journal of Biomechanics*, 30:819–827, 1997.
- [103] Rachev A., Hayashi K.: Theoretical study of the effects of vascular smooth muscle contraction on strain and stress distributions in arteries. *Ann. Biomed. Engr.*, Vol. 27, 1999, pp. 459-468.
- [104] Zulliger M.A., Rachev A., Stergiopoulos N.: A constitutive formulation of arterial mechanics including vascular smooth muscle tone. *Am J Physiol Heart Circ Physiol*, Vol. 287, 2004, pp. H1335-H1343.

11 List of Figures

Figure 1 The microstructure of the tunica media including tunica intima. Coordinates r , z , and θ represent radial, axial, and circumferential directions, respectively. Dimensions of the specimen $\theta \times z \times r$ are $80 \mu\text{m} \times 60 \mu\text{m} \times 45 \mu\text{m}$. Elastin (white letters EL, IEF, ES and EP), smooth muscle cells (blue nucleus, cytoplasm white) and collagen (indicated by the black arrows) can be seen [56]..... 13

Figure 2 Acquiring of the specimen of the human aorta from a surgery (left) and from a porcine aorta (middle). Specimens are cut according to axial and circumferential directions (right)..... 16

Figure 3 Gripped specimen with contrast points (markers) in the centre of the specimen. 17

Figure 4 Different gripping methods and specimen shapes [8]. 19

Figure 5 Different gripping methods using sutures or one wide clamp on square or cruciform specimen [9][10]. 20

Figure 6 Example of gripped specimen using hooks (left [13], right [16]) and markers..... 21

Figure 7 Specimen gripping using rakes (left [25], right [37]). 22

Figure 8 Real specimen of young porcine aortic tissue gripped using two clamps (A) or four hooks (B) per edge. 22

Figure 9 Geometry of emplacement of hooks and clamps according to their numbers. The solid lines represent the largest and the dotted lines the smallest investigated size of the gripping element..... 28

Figure 10 Geometry of 1/8 of the analysed experimental setup showing gripping via four hooks (left) and two clamps (right) per edge. The system of levers with knuckle joints ensures an even distribution of the load induced by the displacements U_x and U_y prescribed to the model as indicated by the red arrows in both figures..... 29

Figure 11 Equibiaxial stress-strain curves of all the investigated materials demonstrate fundamental differences in their behaviour..... 31

Figure 12 Different mesh sizing in the region of interest and in the contact region..... 34

Figure 13 Pillar-like elements in the contact region under clamps..... 34

Figure 14 Long-shaped elements in the contact region under the clamp, before and after compression..... 35

Figure 15 Long-shaped elements in the contact region with hooks..... 35

Figure 16 Distribution of natural strain ϵ_x for various gripping setups and two materials (isotropic and anisotropic) at the same load of 0,1 N during equibiaxial tensile test. Two

hooks and two clamps provide similar strain distributions for each material while four hooks provide more uniformly distributed strains in most of the specimen.....	37
Figure 17 Von Mises stress distribution from the centre of the specimen (normalized distance = 0) to grippers (normalized distance = ± 0.5)[8]. Square specimen was gripped via 4 (SA4), 6 (SA6) and 8 (SA8) hooks. Normalized distance was used because of specimen size varied with different gripping methods.....	38
Figure 18 Distribution of strains across the half of the specimen for 2 clamps (2CL), 2 hooks (2H) and 4 hooks (4H) for material (iv).....	39
Figure 19 Comparison of resulting R^2 using 2D or 3D simulations. Material model 5 was used.....	42
Figure 20 Influence of different gripping elements, their number and size on R^2 for various materials. In the legend CL and H denote clamps and hooks, respectively.....	43
Figure 21 Impact of dimensions of gripping elements in the individual setups for different materials.....	44
Figure 22 Influence of the different testing protocols for anisotropic (mat. 2) and the stiffest (mat. 3) materials evaluated for gripping via 2 or 5 hooks and 2 clamps. The worst accuracy is always achieved for the most non-symmetric loading protocol.....	46
Figure 23 Influence of specimen size on accuracy for various types and numbers of gripping elements.....	47
Figure 24 Schematic description of the process of evaluating the predictive capabilities of different material models [95]. The area of author's work is marked red.....	51
Figure 25 Coefficient of determination in dependence on different starting points for equibiaxial data set and for all data sets combined.....	55
Figure 26 Coefficient of determination in dependence of different starting points for constrained and unconstrained parameters.....	58
Figure 27 Coefficient of determination in dependence on different starting points for constrained and unconstrained parameters and for different datasets.....	60
Figure 28 Stress strain model curves for different starting points for equibiaxial dataset in comparison with experimental data.....	60
Figure 29 Stress strain model curves for different starting points for all datasets in comparison with experimental data, unconstrained (free) parameters.....	61
Figure 30 Stress strain model curves for different starting points for all datasets in comparison with experimental data, constrained parameters.....	61

Figure 31 Geometry of the specimen. Two layers representing the matrix and the fibres between the layers.	64
Figure 32 Models with fibre angles of 10° (left) and 25° (right).	65
Figure 33 The matrix (grey) and the fibres (red). Matrix and fibres have different material properties.	65
Figure 34 Stress strain curves of the matrix (blue, left) and fibre (red, right) material models.	66
Figure 35 ANSYS Command code to define and change the properties of fibres.	66
Figure 36 Mesh of the model (without upper layer to see the fibres). Each body is in different colour. The fibres consist of multiple elements in the length direction.	67
Figure 37 Mesh of the fibres. The element size was set constant if possible.	68
Figure 38 Boundary conditions of the model.	69
Figure 39 Example of affine (left - curved fibres) and non-affine (right - straight fibres) deformation, the fibre angle is 10°.	70
Figure 40 Example of affine (left - curved fibres) and non-affine (right -straight fibres) deformation, the fibre angle is 25°.	70
Figure 41 Example of affine (left - curved fibres) and non-affine (right -straight fibres) deformation, the fibre angle is 40°.	71
Figure 42 Relative differences of force values for different loading protocols in dependence on the fibre angle with preferred X direction.	73
Figure 43 Graphical representation of the dependence of the fibre angle of the maximal force difference on the testing protocol.	74
Figure 44 Maximal relative force difference as function of the fibre angle for uniaxial tests. The difference is highest for the angle of approximately 15° between the fibres and the axis of load and negligible for this angle being above 45°.	74
Figure 45 Schematic representation of possible positioning of a gripping element (clamp). Red arrows show possible inaccuracy in positioning, green shows the possible area of gripping due to the inaccuracies.	80
Figure 46 Adding data sets into the Hyperfit program.	104
Figure 47 Loaded data sets. Underlined testing protocols.	105
Figure 48 Sorted data sets.	105
Figure 49 The two uniaxial data sets will be set up.	106
Figure 50 Changing X and Y axis to show the desired data.	107

Figure 51 Setting the weight of chosen stress values to zero, first window.	108
Figure 52 Setting the weight of chosen stress values to zero, second window.....	108
Figure 53 Setting the weight of chosen stress values to zero, second data set.....	109
Figure 54 Deactivating of the uniaxial data sets.	110
Figure 55 Setting the Coeff. of Determination as the objective function.	111
Figure 56 Setting the numerical method.	112
Figure 57 Choosing the material model.	112
Figure 58 Detailed way how to set up the first chosen material model.	113
Figure 59 Choosing the second material model.	114
Figure 60 Detailed way how to set up the second chosen material model.....	114
Figure 61 Table of parameters for chosen material model. Default values.	115
Figure 62 Constraining one matrix stiffness parameter.	116
Figure 63 Start of the fitting proces.	117
Figure 64 During the fitting proces the model curves (blue) are getting closer to the experimental data.	117
Figure 65 After the fitting process is finished, the values of R^2 and NRMSE are written down.	118
Figure 66 Also the model parameters are written down.	118
Figure 67 Switching the data sets. Writing down the R^2 and NRMSE.....	119
Figure 68 Fitting the other data sets (uniaxial).	120
Figure 69 During the fitting process the model curves (blue) are getting closer to the experimental data (uniaxial).....	120
Figure 70 The fitting process is complete for all data sets. R^2 and NRMSE are written down.	121
Figure 71 The model parameters are also written down.	121
Figure 72 The data sets are switched again and the R^2 and NRMSE are written down.	122

12 List of Tables

Table 1 Summary of experimental data from past studies on incompressibility of arterial wall [76]. NS – not specified, US - ultrasound	23
Table 2 Overview of parameters of experimental setups published in literature.	27
Table 3 Starting points of the Microfiber material model.....	54
Table 4 Coefficient of determination in dependence of starting point and data sets.	55
Table 5 Starting points of the Microfiber material model, constrained and unconstrained.	57
Table 6 Coefficient of determination in dependence of starting point and (un)constrained parameters.	57
Table 7 Starting points of the Microfiber material model, constrained and unconstrained.	59
Table 8 Coefficient of determination in dependence of starting point, (un)constrained parameters and datasets	59
Table 9 Maximal force difference and its respective fibre angle for different testing protocols. The analyses have been performed with the fibre angle step of 5° which limits the accuracy of the evaluated angles.	73
Table 10 Starting points of the Microfiber material model, constrained and unconstrained.	101
Table 11 Starting points of the Microfiber material model with resulting fitted parameters and residuals R^2 and NRMSE for equibiaxial dataset.....	102
Table 12 Starting points of the Microfiber material model with resulting fitted parameters and residuals R^2 and NRMSE for all datasets combined, unconstrained (free).....	102
Table 13 Starting points of the Microfiber material model with resulting fitted parameters and residuals R^2 and NRMSE for all datasets combined, constrained.....	103

13 Authors publications

Conference papers:

SLAŽANSKÝ, M.; BURŠA, J., POLZER, S. FINITE ELEMENT MODELLING OF BIAXIAL TENSION TESTS OF SOFT TISSUES WITH CLAMPS AND HOOKS. In WCCM 2014, *11th World Congress on Computational Mechanics*. Barcelona, Spain, 2014.

SLAŽANSKÝ, M.; BURŠA, J., POLZER, S. INFLUENCE OF GRIPPING METHOD IN BIAXIAL TESTING OF SOFT BIOLOGICAL TISSUES. In CM Špičák 2014, *30th Conference on Computational Mechanics*. Špičák, Czech Republic, 2014.

SLAŽANSKÝ, M.; POLZER, S.; BURŠA, J. FINITE ELEMENT BASED PARAMETRIC STUDY OF INACCURACIES IN MECHANICAL TESTING OF SOFT TISSUE. In ESB Prague 2015, *21st Congress of the European Society of Biomechanics*. Prague, Czech Republic, 2015.

SLAŽANSKÝ, M.; POLZER, S.; BURŠA, J. ANALYSIS OF ACCURACY OF BIAXIAL TESTS BASED ON COMPUTATIONAL SIMULATIONS. In CMBE15, *4th International Conference on Computational & Mathematical, Biomedical Engineering*. Swansea, United-Kingdom: CMBE, Zeta Computational Resources Ltd.Swansea, United- Kingdom, 2015. s. 168-171. ISBN: 978-0-9562914-3- 1.

SLAŽANSKÝ, M.; POLZER, S.; BURŠA, J. IMPACT OF ASSUMPTION OF AFFINE DEFORMATION ON CONSTITUTIVE MODELS OF ARTERIAL TISSUE. In WCB-ESB, *8th World Congress of Biomechanics, European Society of Biomechanics*. Dublin, Ireland, 2018.

Journal articles:

SLAŽANSKÝ M.; POLZER S.; MAN V., BURŠA J.

ANALYSIS OF ACCURACY OF BIAXIAL TESTS BASED ON THEIR COMPUTATIONAL SIMULATIONS. Strain, 52(5), 2016, pp. 424-435. (IF = 1.694, 71 percentile).

Authors' participation on the article:

Literature research, FE simulations, and resulting data processing were done exclusively by M. Slažanský; experimental part of the article was done exclusively by V. Man. The other parts (results interpretation, discussion, formulation of conclusions, stylistic and language form) were done in cooperation with the other co-authors.

SCHROEDER F., POLZER S., SLAŽANSKÝ M., MAN V., SKÁCEL P.

PREDICTIVE CAPABILITIES OF VARIOUS CONSTITUTIVE MODELS FOR TISSUE.

Journal of the Mechanical Behavior of Biomedical Materials, 78, 2018, pp. 369-380.

(IF = 3.110, 92 percentile).

Authors' participation on the article:

Fitting of the measured data, evaluation of predictive capabilities, overview of coefficients of determination R^2 and normalized root mean square errors (NRMSE) for all predictive capabilities of all models.

14 Appendix A

SCHROEDER F., POLZER S., SLAŽANSKÝ M., MAN V., SKÁCEL P.

PREDICTIVE CAPABILITIES OF VARIOUS CONSTITUTIVE MODELS FOR TISSUE.

Journal of the Mechanical Behavior of Biomedical Materials, 78, 2018, pp. 369-380.

(IF = 3.110, 92 percentile).

Authors' participation on the article:

Fitting of the measured data, evaluation of predictive capabilities, overview of coefficients of determination R^2 and normalized root mean square errors (NRMSE) for all predictive capabilities of all models.



Contents lists available at ScienceDirect

Journal of the Mechanical Behavior of Biomedical Materials

journal homepage: www.elsevier.com/locate/jmbbm

Predictive capabilities of various constitutive models for arterial tissue

 Florian Schroeder^{a,b,1}, Stanislav Polzer^{c,d,*}, Martin Slažanský^{c,1}, Vojtěch Man^{c,1}, Pavel Skácel^{c,1}
^a Department of Biofluid Mechanics, Technical University of Applied Sciences (OTH), Regensburg, Germany^b Regensburg Center of Biomedical Engineering (RCBE), OTH and Universität Regensburg, Josef Engert Strasse 9, Biopark 1, 93053 Regensburg, Germany^c Institute of Solid Mechanics, Mechatronics and Biomechanics, Brno University of Technology, Technická 2896/2, 616 69 Brno, Czech Republic^d Department of Applied Mechanics, VSB-Technical University Ostrava, 17.listopadu 15/2172, 708 33 Ostrava-Poruba, Czech Republic

ARTICLE INFO

Keywords:

Mechanical testing
 Uniaxial – biaxial tension
 Constitutive modeling, Arterial biomechanics

ABSTRACT

Introduction: Aim of this study is to validate some constitutive models by assessing their capabilities in describing and predicting uniaxial and biaxial behavior of porcine aortic tissue.

Methods: 14 samples from porcine aortas were used to perform 2 uniaxial and 5 biaxial tensile tests. Transversal strains were furthermore stored for uniaxial data. The experimental data were fitted by four constitutive models: Holzapfel-Gasser-Ogden model (HGO), model based on generalized structure tensor (GST), Four-Fiber-Family model (FFF) and Microfiber model. Fitting was performed to uniaxial and biaxial data sets separately and descriptive capabilities of the models were compared. Their predictive capabilities were assessed in two ways. Firstly each model was fitted to biaxial data and its accuracy (in term of R^2 and NRMSE) in prediction of both uniaxial responses was evaluated. Then this procedure was performed conversely: each model was fitted to both uniaxial tests and its accuracy in prediction of 5 biaxial responses was observed.

Results: Descriptive capabilities of all models were excellent. In predicting uniaxial response from biaxial data, microfiber model was the most accurate while the other models showed also reasonable accuracy. Microfiber and FFF models were capable to reasonably predict biaxial responses from uniaxial data while HGO and GST models failed completely in this task.

Conclusions: HGO and GST models are not capable to predict biaxial arterial wall behavior while FFF model is the most robust of the investigated constitutive models. Knowledge of transversal strains in uniaxial tests improves robustness of constitutive models.

1. Introduction

Numerical modeling of mechanical behavior of arterial tissue can help us in understanding design, function and pathology of arteries. There are hundreds of studies where numerical simulations of arteries are used for better understanding of many events occurring in arterial tree such as rupture of abdominal aortic aneurysms (Erhart et al., 2014; Khosla et al., 2014), or atherosclerotic plaques (Cheng et al., 1993; Holzapfel et al., 2014), effects of angioplasty (Holzapfel et al.) or arterial clamping (Gasser et al., 2002) on arterial wall, or effect of stents on stresses in arterial wall (Lally et al., 2005). Constitutive models of arterial wall establishing a mathematical relationship between deformations and stresses represent a vital part of such studies. In last few decades a great development of these models has been in progress. While early studies relied on linear models (Mower and Gambhir, 1997), there are tens of more or less sophisticated models at this time

[see reviews Vito and Dixon, 2003; Holzapfel et al., 2010 and references therein]. Their proposing tends clearly from phenomenological models with the only aim to describe accurately a mechanical response of artery measured experimentally (Yeoh, 1993; Demiray, 1972; Raghavan and Vorp, 2000) towards structure-based constitutive models (Gasser et al., 2006; Martufi and Gasser, 2011; Weisbecker et al., 2015; Chen et al., 2011) the individual parameters of which have a clear physical meaning related to individual structural constituents of the arterial wall such as elastin or collagen. These models also allow more sophisticated analyses of stresses in the modeled arteries. Moreover, they are also considered to be more robust (to have better predictive capability) compared to phenomenological models. This means they should be able to predict the mechanical response of arterial wall with high accuracy even outside the range of experimental data. In fact this capability is crucial for performing reliable numerical analyses of wall stresses in arteries in vivo where the state of stress differs significantly from the

* Corresponding author at: Department of Applied Mechanics, VSB-Technical University Ostrava, 17.listopadu 15/2172, 708 33 Ostrava-Poruba, Czech Republic

E-mail addresses: florian.schroeder@st.oth-regensburg.de (F. Schroeder), polzer@seznam.cz (S. Polzer), slazanskym@seznam.cz (M. Slažanský), xmanv@seznam.cz (V. Man), skacy@email.cz (P. Skácel).

¹ Co-authors.

conditions in the test. This is most pronounced in case of small (e.g. coronary) arteries or parts of arteries (e.g. extracted atherosclerotic plaque (Holzapfel et al., 2004)) which do not allow preparation of specimens sufficiently large for planar biaxial testing and thus can be tested only uniaxially.

Surprisingly the predictive capabilities of individual constitutive models are tested rarely (Polzer et al., 2015; Hollander et al., 2011). Instead the effort is focused on analyses of validity of claimed physical meaning of structural parameters of individual models. Therefore it has been shown that the response of model proposed by Holzapfel, Gasser, Ogden (Holzapfel et al., 2000) (denoted as HGO below) differs significantly from the response of fibrous tissue modeled with the same structure as prescribed into model (Chen et al., 2011). The same was shown for models based on generalized structure tensor (GST) (Gasser et al., 2006) which were also shown not correctly capture the response of materials modeled with widely dispersed fibers (Cortes et al., 2010; Skacel and Bursa, 2014; Yoram Lanir, 2015). Moreover both models were shown unable to capture the transversal strains of arterial tissue (Skacel and Bursa, 2015). Nevertheless, it is not known how much these limitations truly limit the predictive capability of mentioned models since these models are known to accurately capture biaxial behavior of various soft tissues if their parameters are not constrained according to assumed tissue structure (or by other words if they are treated as phenomenological models) (Holzapfel et al.; Zhang et al., 2011; Alastrué et al., 2008). If the error in predicting uniaxial or biaxial behavior was acceptable (Hollander et al., 2011) the mentioned models could still be used as phenomenological despite the mentioned limitations. More generally, the predictive capability is unknown for most of other currently used constitutive models; this lack of information motivated our study. We analyzed descriptive and predictive capabilities of four well known constitutive models by means of testing their accuracy in capturing the experimental uniaxial and biaxial data and in predicting the biaxial response of the specimen when fitted only to uniaxial data (and vice versa).

2. Methods

2.1. Mechanical testing

Experimental data were obtained from tensile testing of porcine thoracic aorta harvested at a local slaughterhouse and stored frozen at $-18\text{ }^{\circ}\text{C}$ till the testing. 14 aortas were thawed at room temperature and square sized specimens $18 \times 18\text{ mm}$ were cut out from the same straight anterior part of each aorta. Excessive tissue was removed using scalpel and tweezers. The circumferential specimen axis was marked for later alignment in the testing device to avoid interchange of both principal material directions (Polzer et al., 2015). Then markers were drawn on each specimen edge to ensure repeatable mounting. It is noted the repeated mounting was enabled due to application of narrow clamps (two per specimen edge) instead of hooks. Acceptable accuracy of this gripping method was confirmed elsewhere (Slazansky et al., 2016). Before and after the test, the specimens were placed in 0.9% saline solution heated to the temperature of testing ($37\text{ }^{\circ}\text{C}$).

Displacement controlled tensile tests were performed (see Fig. 1) using a custom made planar bi-axial testing device (Camea s.r.o, Czech Republic) with fixed values of circumferential (u_c) and axial (u_a) displacements of the clamps. The testing system is equipped with two 20 N load cells PW4MC3 (HBM GmbH, Germany) and an optical strain measurement system. More details regarding the testing device and data acquisition can be looked up in (Erhart et al., 2014; Khosla et al., 2014). Each specimen was clamped in the testing rig and 10 equibiaxial preconditioning cycles were performed at the maximum deformation of 6.3 mm with deformation rate of 0.333 mm/s. Afterwards

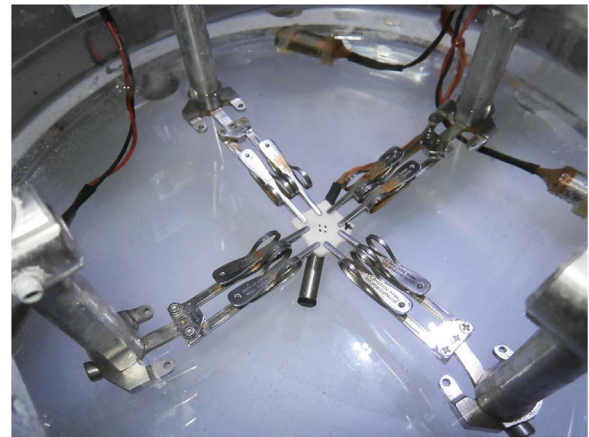


Fig. 1. Detail of the experimental rig with the tested specimen gripped by 8 narrow clamps. Clamps are mounted using pin supports on the leverage system balancing the forces transmitted by the clamps in their longitudinal direction and minimizing the perpendicular forces.

the specimen was unclamped, placed between two glass slides and its thickness T was measured under specimen compression of $1 \pm 0.1\text{ kPa}$ using a thickness gauge. For a contactless measurement of in-plane deformation four markers were created on the specimen surface. Then the specimen was mounted into the testing rig again.

A pre-tension of 0.1 N was applied and five biaxial tests under various loading protocols ($u_c: u_a = 1: 5/1: 2/1: 1/2: 1/5: 1$) were performed by prescribing individual clamp displacements. In order to precondition the specimen correctly for different mechanical tests, 5 loading cycles were repeated before each test using its loading protocol. Circumferential L_c and axial L_a dimensions of the specimen were determined using the first image acquired of the equi-biaxial protocol (by measuring the pixel values and converting them by means of the known pixel size). Afterwards the uniaxial tests were performed by unclamping one of the axes, applying first the pretension of 0.1 N and then 5 preconditioning cycles followed by the testing cycle. The same protocol was used for the other axis. Seven specimens were first tested axially and then circumferentially, while the other seven specimens were tested in the opposite order. During the test evaluation the shear stresses and specimen rotation were also calculated to make sure the rotation was negligible and shear stresses two orders lower than normal stresses. Finally, the axial P_a and circumferential P_c First Piola-Kirchhoff (FPK) stresses were calculated from the recorded forces and the measured specimen dimensions as follows:

$$P_a = \frac{F_a}{L_c T}; \quad P_c = \frac{F_c}{L_a T} \quad (1)$$

It is also underlined that engineering strains in both principal directions ε_c and ε_a were recorded in all tests including the uniaxial ones. This was motivated by our effort to identify the effect of transversal strain on the predictive capability of the analyzed constitutive models since some of the analyzed constitutive models were shown previously not to estimate the transversal strain correctly (Skacel and Bursa, 2015). A secondary reason is in the use of square shape specimens which do not guarantee uniaxial state of stress during uniaxial testing. In this way we have obtained 7 data sets from 5 biaxial and 2 uniaxial tensile tests for each specimen.

2.2. Constitutive models

For further analysis we have chosen four well known and widely used constitutive models, all of them in their incompressible form. All

parameters of all considered models are listed in the Appendix A (see Table A.1) together with their units. First we used the constitutive model proposed by Holzapfel et al. (2000) which will be further denoted as HGO model. We used its two-layer version to respect different mechanical properties of aortic media and adventitia. This model describes the strain energy density by the following function (SEDF):

$$\psi = \psi_{iso,M} + \psi_{aniso,M} + \psi_{aniso,A} = \frac{c}{2}(I_1 - 3) + \sum_{j=M,A} \sum_{i=1,2} \frac{k_{ij}}{2 \cdot k_{2j}} (e^{k_{2j}(I_{4ij}-1)^2} - 1) \quad (2)$$

where c is a stress-like material constant describing the isotropic response of elastin in the media, k_{1j} is a stress-like constant defining the layer specific stiffness of collagen fibers, and k_{2j} refers to collagen-based stiffening of each layer during deformation. I_1 is the first invariant of the right Cauchy-Green deformation tensor \mathbf{C} , $I_{41j} = \mathbf{a}_{1j} \cdot \mathbf{C} \mathbf{a}_{1j}$ and $I_{42j} = \mathbf{a}_{2j} \cdot \mathbf{C} \mathbf{a}_{2j}$ are invariants related to two families of fibers in each layer; for direction vectors of fiber families 1 and 2 it holds $\mathbf{a}_{1j} = (\cos \varphi_j, \sin \varphi_j, 0)^T$ and $\mathbf{a}_{2j} = (-\cos \varphi_j, \sin \varphi_j, 0)^T$, with φ_j representing the angle between each fiber family and the circumferential direction in the undeformed state. Subscripts $j = M, A$ relate to the media and adventitia layers, respectively.

The second constitutive model was proposed by Gasser et al. (2006). It is based on generalized structure tensor approach and will be further denoted as GST model. SEDF for its two-layer version reads:

$$\psi = \psi_{iso,M} + \psi_{aniso,M} + \psi_{aniso,A} = \frac{c}{2}(I_1 - 3) + \sum_{j=M,A} \sum_{i=1,2} \frac{k_{ij}}{2 \cdot k_{2j}} (e^{k_{2j}E_{ij}^2} - 1) \quad (3)$$

where the newly introduced parameter $E_{ij} = \mathbf{H}_{ij} : \mathbf{C} - 1$ represents average strain measure of fibers for the layer j . Here the generalized structure tensor $\mathbf{H}_{ij} = \kappa \mathbf{I} + (1 - 3\kappa)(\mathbf{a}_{ij} \otimes \mathbf{a}_{ij})$ contains the κ parameter describing dispersion of each fiber family around its mean direction φ_j , and \mathbf{a}_{ij} as well as the other parameters hold the same meaning as in the above HGO model.

The third analyzed model was proposed by Baek et al. (2007), Ferruzzi et al. (2011) and will be further referred to as four fiber family (FFF) model. It is a variation of the HGO model with two orthogonal and two arbitrary (but symmetric) diagonal families of fibers. Its SEDF is:

$$\psi = \psi_{iso} + \psi_{aniso} = \frac{c}{2}(I_1 - 3) + \sum_{i=1,4} \frac{k_{4i}}{2 \cdot k_{2i}} (e^{k_{2i}(I_{4i}-1)^2} - 1) \quad (4)$$

where 4 families of fibers are introduced. Invariants $I_{4i} = \mathbf{a}_i \cdot \mathbf{C} \mathbf{a}_i$ related to each family of fibers are defined here similarly to the HGO model while directions of the individual families of fibers are specified as $\mathbf{a}_1 = (0, 1, 0)^T$ and, $\mathbf{a}_2 = (1, 0, 0)^T$, $\mathbf{a}_3 = (\cos \varphi, \sin \varphi, 0)^T$ and $\mathbf{a}_4 = (-\cos \varphi, \sin \varphi, 0)^T$, with φ representing the angle between each diagonal fiber family and the circumferential direction. It is further assumed the diagonal families of fibers show the same mechanical properties (see Ferruzzi et al., 2011), thus $k_{14} = k_{13}$ and $k_{24} = k_{23}$.

Finally, the fourth analyzed constitutive model was proposed by Martufi and Gasser (2011), follows the work of Lanir (1983) and will be further referred as Microfiber model to underline that it uses integration of the fiber stresses over a unit sphere instead of exploitation of the generalized structure tensor such as in the GST model (see Eq. (3)). The two layer version of the Microfiber model is defined by the following SEDF:

$$\psi = \psi_{iso} + \psi_{aniso} = \frac{c}{2}(I_1 - 3) + \sum_{j=M,A} \int_{\omega_j} \rho_{dj} \psi_{fj}^a(\mathbf{C}, \mathbf{a}_j) d\omega \quad (5)$$

where ψ_{fj}^a represents the contribution of the fibers oriented in \mathbf{a}_j

direction and ω_j is the domain of all possible fiber directions in the individual layer (a unit circle in our case of in plane fiber distributions). The FPK stress P in the given direction is determined as:

$$\frac{\partial \psi_{fj}^a}{\partial I_4} = \frac{1}{2\lambda^2} P(\lambda(\mathbf{a}_j)) \quad (6)$$

where λ is the fiber stretch in the specific direction. The specific constitutive model assumes the following uniaxial responses of fibers (Martufi and Gasser, 2011):

$$P(\lambda) = \begin{cases} 0, & 0 < \lambda < \lambda_{\min j} \\ \frac{2k_j}{3\Delta\lambda^2} \lambda (\lambda - \lambda_{\min j})^3, & \lambda_{\min j} < \lambda \leq \bar{\lambda} \\ k_j \lambda \left[\lambda - \frac{2(\lambda - \lambda_{\max j})^3}{3\Delta\lambda^2} - \bar{\lambda} \right], & \bar{\lambda} < \lambda \leq \lambda_{\max j} \\ k_j \lambda (\lambda - \bar{\lambda}), & \lambda_{\max j} < \lambda < \infty \end{cases} \quad (7)$$

with $\Delta\lambda = \lambda_{\max j} - \lambda_{\min j}$, $\bar{\lambda} = (\lambda_{\max j} + \lambda_{\min j})/2$, and k_j referring to the stiffness of the collagen fibril – proteoglycan complexes in the j layer. This constitutive model is based on a triangular distribution of fiber waviness with its lower and upper stretch limits being $\lambda_{\min j}$ and $\lambda_{\max j}$ for the j -th layer, respectively.

This model was further adjusted on the basis of previous experiments. Firstly, there is a good evidence for assuming a negligible portion of fibers heading out of the axial circumferential plane (Gasser et al., 2012; Tsamis et al., 2013), and secondly, on the basis of our previous experiments (Polzer et al., 2015) the collagen distribution in both media and adventitia can be described by planar von Mises distributions as follows:

$$\rho_j(\alpha) = \frac{\exp \left[b_j \cos \left(\frac{\pi(\alpha - \varphi_j)}{180} \right) \right]}{\frac{1}{180\pi} \int_0^\pi \exp [b_j \cos(\beta)] d\beta} \quad (8)$$

where the angle φ_j denotes the mean fiber orientation, while the fiber concentration parameter b_j quantifies the anisotropy in the j layer. Isotropic and unidirectional (Dirac Delta) fiber distributions are defined by $b_j = 0$ and $b_j \rightarrow \infty$, respectively. On the basis of the experiments (Polzer et al., 2015) we have aligned φ_j with the circumferential direction and constrained the concentration parameter to $b_{media} \in \langle 0.5, 1.55 \rangle$ and $b_{adventitia} \in \langle 0, 0.5 \rangle$. Further we have set $\lambda_{\min media} = 1$, ($\lambda_{\max media}$ was kept free), $\lambda_{\min adventitia} > 1.2$ and $\lambda_{\max adventitia} = 2$.

2.3. Fitting procedure

The above constitutive models were fitted to the experimental data by means of Least square optimization using HYPERFIT software (<http://www.hyperfit.wz.cz>, Brno University of Technology, Czech Republic). Nelder-Mead (Gasser et al., 2008) iterative procedure was used for the regression analysis. First, each model was fitted to biaxial data (5 protocols) to confirm the capability of each model to capture the measured biaxial responses of arterial tissue. Each fitting procedure was repeated 3 times using different sets of starting parameters; the first one giving much more compliant response with respect to experimental data, the second producing a similar stiffness (in very rough sense), and the third one being significantly stiffer. Unlike most available studies we have not used the sum of squared differences as an error function for the fitting procedure. Instead the fitting procedure was set to maximize the coefficient of determination R^2 which is a more robust choice according to our experience and the obtained results are much less dependent on the starting points compared to the sum of squared

differences. Since more tests are fitted at once the resulting R^2 is calculated as an unweighted average of the R^2 values from the individual tests. This ensures the weight of each test is the same regardless of the number of experimental points stored in the individual test. The lowest admissible change of parameters between iterations was set to 0.01 and the fitting procedure was stopped when R^2 did not change by more than 10^{-5} between two consecutive iterations. The parameters representing the best fit among the above three starting points were stored together with their R^2 . Similar to another study (Hollander et al., 2011), the value of normalized root mean square error (NRMSE) was also stored to provide alternative error metric for a better analysis of quality of the fit. NRMSE is defined as follows:

$$NRMSE = \frac{\sqrt{\frac{1}{n} \sum_{i=1}^n (y_{ei} - y_{mi})^2}}{\frac{1}{n} \sum_{i=1}^n y_{ei}}, \quad (9)$$

where n denotes the number of experimental points while y_{ei} and y_{mi} are individual experimental and model values, respectively. Unlike R^2 , the NRMSE has a clear physical meaning of mean deviation between experiment and model.

The same procedure was then applied to analyze the capability of each model to capture both uniaxial tests. However, the fitting procedure was repeated twice. In the first run we fitted the uniaxial tests in a standard way, i.e. we did not include the transversal strain although they were measured in our experiments. This test is further referred as “uniaxial-one strain” test. In the second run of the fitting procedure, the measured transversal strain was also included; thus we assumed a biaxial state of stress with the transversal stress being unknown. This condition also led to necessity of assigning zero weight to the stresses in the second axis since they were not measured. Consequently, in this case we used only one FPK stress which is a function of two strains. This test is further referred as “uniaxial-two strain” test. Since the transversal stress is unknown, we can estimate only qualitatively whether the values predicted by the individual models are reasonable which can be quantified that we expect this stress to be positive but at least by order lower than the maximal longitudinal stress.

The predictive capability of the individual models was tested in both sequences. First, the parameters associated with the best fit of biaxial responses were prescribed and their uniaxial-two strain response was calculated for the same sets of strain values as in the measured uniaxial-one strain responses. R^2 and NRMSE were then calculated as a metrics of the predictive capability of each model. The same procedure was applied also vice versa, i.e. the best fit values from the model fitted to either both uniaxial one-strain tests or both uniaxial-two strain responses were used to predict all the 5 measured biaxial tensile tests. Finally, descriptive capability of each model and predictive capability of each of their pairs were analyzed statistically using non-parametric Man-Whitney test. Here a null hypothesis was used stating there is no difference in descriptive/predictive capability of both models (in terms of R^2 values). The alternative hypothesis states that one of the models has a better descriptive/predictive capability than the other. Statistical testing was carried in Minitab 15.0 (Minitab Inc.). Finally, the sensitivity of all constants to the different type of test (biaxial, two strain uniaxial and one strain uniaxial) was tested by calculating the $X_{\text{biaxial}}/X_{\text{two-strain uniaxial}}$ and $X_{\text{biaxial}}/X_{\text{one-strain uniaxial}}$ ratios of individual constants of all models. The obtained values were then statistically tested using non-parametric Wilcoxon test with null hypothesis stating the median of each ratio equals to 1 and alternative hypothesis the median differs from 1.

Overall 98 tensile tests of 14 specimens of porcine aortic tissue were performed in order to test the descriptive and predictive capabilities of the four chosen constitutive models of arterial tissue. 9 fitting procedures were performed with the recorded data set of each specimen (5

biaxial, 2 uniaxial-one strain and 2 uniaxial-two strain test) to analyze the descriptive capability of each of the 4 analyzed constitutive models which gives 504 fits in total. Moreover, the predictive capability of each model was tested in three directions (from biaxial to uniaxial-two strain, from uniaxial-one strain to biaxial and from uniaxial-two strain to biaxial) for each specimen and constitutive model resulting in additional 168 analyses.

3. Results

3.1. Experimental testing

The performed experimental testing was capable to describe the analyzed tissue in a wide range of stretch ratios covering the values expected in the analyzed artery “in vivo”, as shown in Fig. 2. All rough experimental data can be found in the electronic Supplementary files. This provides a robust basis for testing the descriptive and predictive capabilities of the chosen constitutive models.

Statistical descriptions of all constants of all the considered models fitted to all the three types of test are provided in Table A.1. Here it was observed that uniaxial types of test lead always to a significant increase of c constant describing the initial isotropic response of each model. This was further confirmed by calculating the biaxial/two strain uniaxial and biaxial/one strain uniaxial ratios of each constant as presented in Table A.2. Statistical testing revealed which constants were significantly dependent on the type of the test. For HGO model, c and k_{1M} constants were dependent for biaxial/two strain uniaxial ratios and c only for biaxial/one strain uniaxial ratios. For GST model it was c only for the biaxial/two-strain uniaxial ratios and c , k_{2M} , κ_A for biaxial/one-strain uniaxial ratios. For FFF model it was c , k_{11} , k_{13} for biaxial/two-strain uniaxial ratios and c , k_{11} , ϕ for biaxial/one-strain uniaxial ratios. Finally for the Microfiber model it was c , k_M , b_M , $\lambda_{\min A}$, b_A for biaxial/two-strain uniaxial ratios and c , $\lambda_{\max M}$, b_M , $\lambda_{\min A}$ for biaxial/one-strain uniaxial ratios. All the ratios and p-values from the statistical testing are presented in Table A.2 in the Appendix A.

3.2. Descriptive capability

The descriptive capability of all the considered models was very good in both types of tests as shown in Fig. 3, Table 1 and Table A.3 provided in the Appendix A. All models captured the biaxial behavior slightly worse than the uniaxial response. Testing of the above hypotheses revealed that FFF model performed statistically better than HGO model in capturing the uniaxial-two strain response, while comparisons of the other models have not reached the level of significance. On the other hand, the Microfiber model performed significantly worse in capturing the biaxial responses compared to all the other models as shown by both the lower values of R^2 and the NRMSE of about 18% being almost twice worse compared to the other models (see Table A.3).

Quality of capturing the uniaxial-two strain data was also described by maximal perpendicular stress estimated by the individual models. Their values presented in Table 1 should be negligible compared to the maximal longitudinal stresses in the samples (130 ± 25 kPa). The results show the HGO and GST models estimate the transversal stresses as high as 30%, while the Microfiber model predicts their magnitude to be 21% of the longitudinal stress. The best performance is shown by the FFF model which predicts the transversal stress to be as low as 12% of the longitudinal stress.

3.3. Predictive capability

In all models the prediction of uniaxial-two strain response on the basis of the model parameters fitted to biaxial data resulted in a

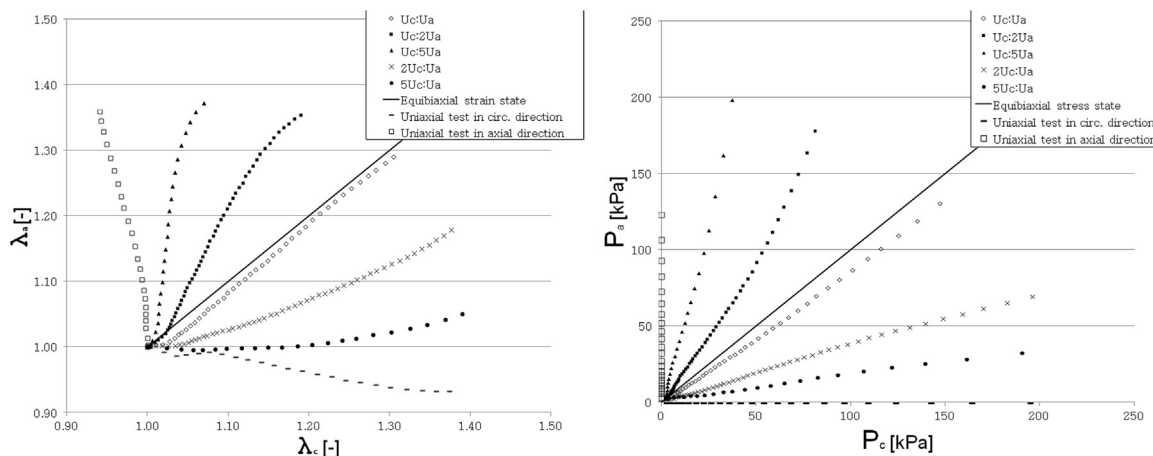


Fig. 2. Experimentally covered ranges of stretches (left) and 1st PK stresses (right) of a typical sample. For sake of visibility, only every 3rd experimental point is shown.

significantly worse performance compared to their descriptive capability, as shown in Fig. 5A, Table 2 and Table A.4. The Microfiber model showed the best predictive capability in this test with median R^2 still above 0.9 and NRMSE of about 22% while the other models were statistically equal having the median of R^2 about 0.8 and NRMSE about 30%.

All the models showed the worst performance in prediction of biaxial response from the parameters estimated on the basis of uniaxial-two strain or uniaxial-one strain tests as demonstrated in Fig. 4, Fig. 5B,C, Table 2 and also Table A.4 in the Appendix A. Here, the GST and HGO models failed completely, while the FFF and Microfiber models were still capable to provide fairly accurate biaxial response when fitted to uniaxial-two strain tests (Fig. 5B) having median of R^2 about 0.8 and NRMSE about 30%. The FFF model gave a similar accuracy even if fitted to uniaxial-one strain tests (Fig. 5C) while Microfiber model showed already considerable error (median of R^2 about 0.5 and NRMSE about 45%.

4. Discussion

Knowledge of both descriptive and predictive capabilities of constitutive models represents a crucial information for researchers when

choosing a proper model for their simulations. It is most critical in cases of deformation driven problems in which different deformation modes occur than the tissue was tested in. Typical examples are all simulations respecting the axial pre-stretch of arteries or simulations based on closing an opened artery to induce residual stresses in it. If deformation is prescribed in these simulations, the stress calculations depend critically on accuracy of the constitutive models used. Surprisingly, the authors seldom show predictive power of the proposed constitutive models (Gasser et al., 2006; Martufi and Gasser, 2011; Holzapfel et al., 2000; Ferruzzi et al., 2011; Zeinali-Davarani et al., 2011) which encourages doubts about their robustness. Out of the models analyzed here, the predictive capability of HGO model was investigated (Hollander et al., 2011) showing one can expect about twice higher error compared to micro structurally motivated constitutive model in predicting torsion-pressure-elongation response of coronary arterial media. Besides that the predictive power of the Microfiber model was recently tested by our group which confirmed it is capable to predict other biaxial responses when fitted to a single non-equibiaxial test (Polzer et al., 2015). In the actual study, however, we used more challenging combinations of experimental tests to verify both descriptive and predictive powers of the chosen constitutive models.

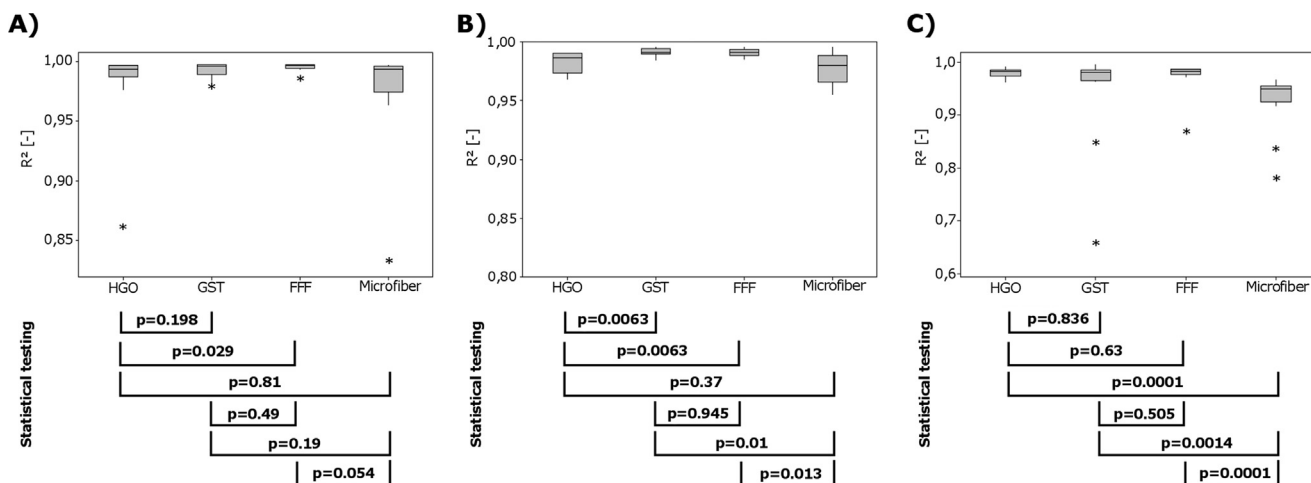


Fig. 3. Descriptive capability of the analyzed constitutive models. All the models were capable to accurately capture both uniaxial-two strain (A), uniaxial-one strain (B), and biaxial (C) behavior of arterial tissue. Statistical testing revealed the GST and FFF models to be the most accurate models in description of uniaxial tests. On the contrary, all the models performed equally well in capturing the biaxial tests, with exception of the Microfiber model showing a significantly worse (although still very good) performance.

Table 1

Descriptive capabilities of the investigated constitutive models. All the models can accurately capture all types of experimental tests.

Model	Capturing of uniaxial-two strain tests		Capturing of uniaxial-one strain tests Median R ² [-] (interquartil range)	Capturing of biaxial tests Median R ² [-] (interquartil range)
	Median R ² [-] (interquartil range)	Estimated transversal stress (Mean ± Standard deviation [kPa])		
HGO	0.993 (0.987 ÷ 0.996)	38 ± 20	0.987 (0.977 ÷ 0.99)	0.983 (0.974 ÷ 0.986)
GST	0.996 (0.989 ÷ 0.996)	38 ± 13	0.991 (0.989 ÷ 0.993)	0.982 (0.966 ÷ 0.997)
FFF	0.996 (0.994 ÷ 0.997)	15 ± 7	0.991 (0.989 ÷ 0.993)	0.984 (0.978 ÷ 0.987)
Microfiber	0.993 (0.974 ÷ 0.996)	27 ± 9	0.98 (0.970 ÷ 0.987)	0.950 (0.926 ÷ 0.956)

Table 2

Predictive capabilities of the investigated constitutive models. All the models were much better in predicting uniaxial response when calibrated on biaxial data than vice versa.

Model	Predicting uniaxial-two strain tests when fitted on biaxial tests	Predicting biaxial tests when fitted on uniaxial-two strain tests	Predicting biaxial tests when fitted on uniaxial-one strain tests
	Median of R ² [-] (interquartil range)	Median of R ² [-] (interquartil range)	Median of R ² [-] (interquartil range)
HGO	0.828 (0.641 ÷ 0.912)	0.4 (-6.4 ÷ 0.8)	-14 (-36 ÷ -3.7)
GST	0.826 (0.696 ÷ 0.893)	-54 (-1787 ÷ -15)	-4e7 (-2e8 ÷ -6e6)
FFF	0.797 (0.667 ÷ 0.916)	0.829 (0.805 ÷ 0.894)	0.845 (0.747 ÷ 0.899)
Microfiber	0.915 (0.887 ÷ 0.940)	0.789 (0.673 ÷ 0.853)	0.529 (0.371 ÷ 0.57)

4.1. Description of arterial behavior is model-independent

As expected, all the investigated models were capable to capture uniaxial-two strain, uniaxial-one strain and biaxial behavior very accurately. The worst (although still very good) performance was observed for Microfiber model; this can be explained by (complete or partial) constraint applied on majority of its parameters so that this model did not have so much freedom to fit the experimental data as the

other models. This result was confirmed by other studies as well (Gasser et al., 2006; Polzer et al., 2015; Hill et al., 2012; Tong et al., 2013). On the other hand, these constrains resulted in the lowest sensitivity (or highest robustness) of model constants to the underlying experiment. The very narrow interquartile ranges of individual constant ratios for the Microfiber model shown in Table A.2 confirm that the effect of underlying experiment is small, although measurable (as confirmed by p-values being often below 0.05). For the other models the picture is blurred by larger interquartile ranges resulting mostly in statistical non-significance (except for the case of constant *c* as discussed below).

Other models captured both uniaxial and biaxial behavior of arterial wall better. However here it must be mentioned that observed values of mean fiber family orientation ϕ_i and fiber dispersion κ_i does not correspond to independently obtained values (see Table A.1) (Polzer et al., 2015; Schriefel et al., 2012a, 2012b). In conclusion, HGO and GST models can be also used for capturing the arterial behavior as long as they are treated as phenomenological models similarly as the FFF model.

A global conclusion can be drawn that the choice of a material model is not important if one can guarantee that the range and ratio of the deformation components occurring in the simulations lay inside the range of the experiments on which the parameters were estimated. Unfortunately, this verification is often omitted in current studies dealing with numerical simulations (Ohayon et al., 2005; Polzer et al., 2013; Cilla et al., 2012).

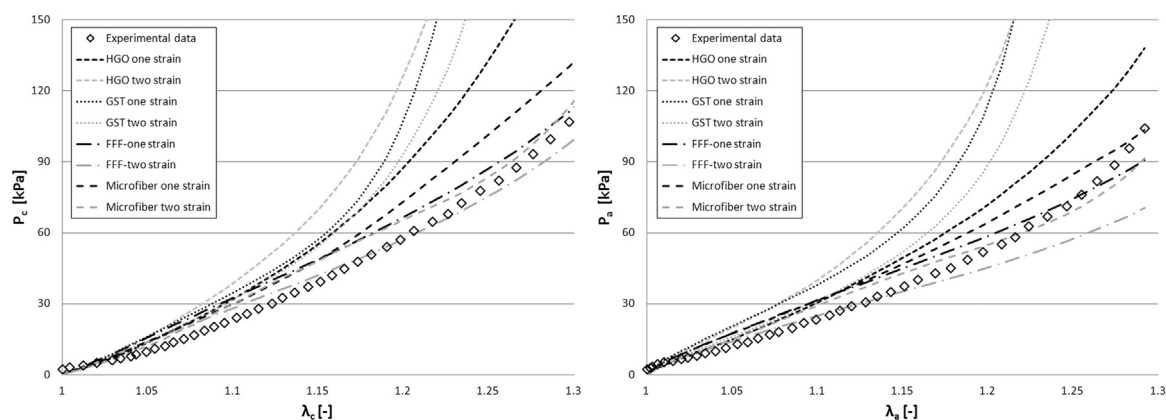


Fig. 4. Visualization of predictive capability of the analyzed constitutive models for a typical specimen. All the models were fitted to either uniaxial one-strain (black lines) or uniaxial two-strain data (grey lines) and then their predicted biaxial response of 5 different loading protocols was compared with experimental data. Only equibiaxial (in terms of displacements) response in both circumferential (left) and axial (right) directions is shown. It is evident that HGO and GST models fail completely in these predictions while FFF and Microfiber models give reasonably accurate predictions being even better when uniaxial two-strain data are used for the model calibration. Quality of the prediction of the HGO model from uniaxial two-strain and one-strain data was $R^2 = -14$; $NRMSE = 266\%$ and $R^2 = -0.2$; $NRMSE = 77\%$, respectively. For GST model it was $R^2 = -5$; $NRMSE = 178\%$ and $R^2 = -7 \cdot 10^7$; $NRMSE = 10^5\%$. For FFF model it was $R^2 = 0.91$; $NRMSE = 21\%$ and $R^2 = 0.74$; $NRMSE = 33\%$. For Microfiber model it was $R^2 = 0.78$; $NRMSE = 30\%$ and $R^2 = 0.54$; $NRMSE = 45\%$.

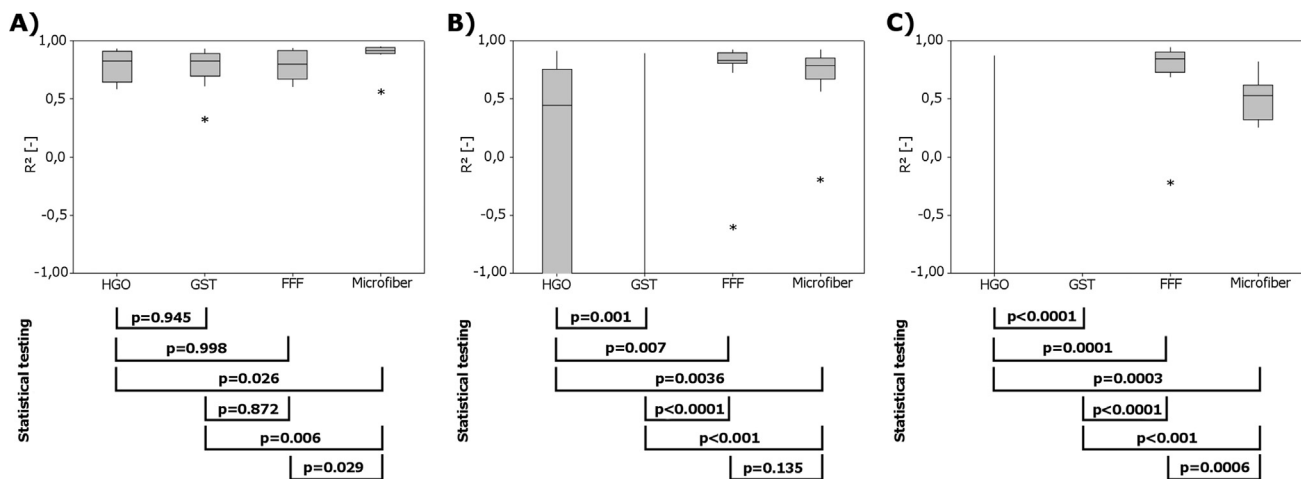


Fig. 5. Predictive capability of the analyzed constitutive models. Uniaxial-two strain response predicted from biaxial data (A) is performed best by the Microfiber model, both Microfiber and FFF models can predict the biaxial response rather accurately on the basis of uniaxial-two strain data (B) while FFF model is the most accurate in predicting the biaxial response on the basis of uniaxial-one strain data (C). HGO and GST models fail completely in prediction of the biaxial response.

4.2. Uniaxial response is initially stiffer than biaxial

Our results show a significant effect of the type of experimental test on the constant c which represents the initial isotropic stiffness of the tissue in all the models. Regardless of the chosen model, c was consistently 2–10 times higher (see Table A.1 and A.2) when the model was fitted on uniaxial data as confirmed in Table A.2. Similar effect can be also observed in the literature. For instance, the models fitted on uniaxial tests of aneurysmal tissue (Raghavan and Vorp, 2000; Reeps et al., 2013) show consistently several times higher initial stiffness compared to the models fitted on biaxial tests of the same tissue (Tong et al., 2013; Vande Geest et al., 2006). However, explanation of this phenomenon is still unknown. It is underlined that the referenced studies use different testing machines, experimental protocols, sample sizes and fitting procedures so that a systematic error in the experiments or fitting procedure is very unlikely. Therefore we hypothesize the explanation may be in some basic assumptions used commonly in definitions of constitutive models such as assumption on affine deformation or local incompressibility. Consequently more research on this topic is needed.

4.3. Predictive power is highly model-dependent

A completely different situation occurred when the predictive power of the investigated models was analyzed. Here the Microfiber model performed best when being able to predict very accurately the uniaxial-two strain response when fitted to biaxial tests; its median R^2 was still above 0.9 and most of the predictions were not worse than $R^2 = 0.887$. In contrast, the other models predicted the uniaxial-two strain response with a considerable error ($R^2 \in \langle 0.64; 0.92 \rangle$). It is worth to underline that none of the models failed completely in predicting uniaxial response; although not presented here, one strain response prediction was never worse than the respective two strain prediction. This predictive power of all the models can be explained by the wide range of biaxial tests used in our prediction when strains in some of them are rather close to uniaxial testing (see Fig. 2).

Predictions of biaxial responses from uniaxial data were not only the most challenging issues in this study but they have also the highest practical relevance representing the indigenous motivation of our work. It is because tissue specimens harvested from most arteries (except for the largest ones such as aorta or iliac arteries) are nearly always too

small for biaxial mechanical testing (Holzapfel et al., 2004, 2005; Cunnane et al., 2016); sometimes uniaxial testing may be chosen due to the available testing equipment, or the tests may focus also on ultimate stress (Reeps et al., 2013; Gasser et al., 2008; Raghavan et al., 1996, 2011). Our results show the choice of constitutive model is critical in these cases. HGO model predicted biaxial response with large error while GST model failed completely in these tests. In contrast, Microfiber and surprisingly also FFF model provide reasonable predictions (although not perfect). Especially the predictive power of the FFF model was very good regardless of the type of uniaxial tests used in its calibration; its predictions have mostly shown values of $R^2 > 0.8$ and NRMSE about 30%. This is a surprising result when considering the fact the FFF model is solely phenomenological, i.e. collagen waviness is included only implicitly in the collagen response function, and its four families of fibers without any dispersion do not correlate with histological findings. Despite these limitations the FFF model was able to predict the biaxial response more accurately (especially in term of NRMSE, see Table A.4 in the Appendix A) than the Microfiber model. In this structure based model a majority of parameters were constrained according to the actual knowledge on the tissue structure, thus it was expected to be more robust. This expectation was not confirmed for predictions of biaxial tests, especially when the model calibration was done on the basis of uniaxial-one strain data (in these cases interquartile ranges were $R^2 \in \langle 0.37; 0.57 \rangle$, $NRMSE \in \langle 25\%; 52\% \rangle$, respectively); this failure indicates either possible oversimplifications in the definition of Microfiber model (i.e. assumption of planar fiber distribution) and/or improper ranges of the structural parameters. From this point of view it is suspicious that the values of fiber dispersion obtained in media reach almost exclusively its lowest allowable value (see values of b_M in Table A.1). This suggests the fitting algorithm could prescribe even smaller values than measured separately (Polzer et al., 2015) which was also observed before (Polzer et al., 2015). Reasons for that should be analyzed in future works.

Similarly, the performance of HGO and GST models was surprisingly bad in the prediction mode regardless of the type of uniaxial tests used for their calibration. The GST model predicts a very low fiber dispersion especially for the adventitia (see Table A.1) which does not correspond to the histological data (Polzer et al., 2015; Schriefel et al., 2012a) from which we have extracted the applied range of dispersion parameters $\kappa_M \in \langle 0.19; 0.28 \rangle$, $\kappa_A \in \langle 0.29; 0.33 \rangle$. We tried to use also another fit of

the GST model where the fiber dispersion parameters κ were constrained on the basis of the known fiber dispersion (Polzer et al., 2015) in porcine aorta but no improvement of results was observed. This is in accordance with other studies (Chen et al., 2011; Cortes et al., 2010; Skacel and Bursa, 2014; Yoram Lanir, 2015) where robustness of the models based on generalized structure tensor (i.e. GST model) was impeached. Our analyses confirmed that GST as well as HGO models showed the worst predictive performance in this direction. Thus they are not applicable for simulating biaxial states of stress when fitted to uniaxial tests only.

4.4. Uniaxial-one strain vs. uniaxial-two strain data

Interestingly, the predictive capability of the Microfiber model was relatively good when the biaxial responses were predicted from uniaxial-two strain data while the error raised significantly when uniaxial-one strain data was used for calibration (see Table 2 and Table A.4). We can offer two possible explanations for that. Firstly, the stress in the samples may be biaxial (with some transversal component) due to directions of the used narrow clamps changing with specimen deformation and due to friction in the leverage system reducing the transversal deformation of the specimen. In such case the performance of the Microfiber model cannot be impeached because no constitutive model could predict biaxial response correctly if calibrated under wrong assumptions (of true uniaxial stress state in this case). On the other hand the calibration of the Microfiber model on the uniaxial-two strain data led to estimation of maximal perpendicular force of $(1,0 \text{ N} \pm 0,3 \text{ N})$ when loaded by the maximum force of $(4,4 \pm 0,7 \text{ N})$ which we believe is not a realistic value since the perpendicular force can be carried only due to friction between clamps and leverage system. For comparison the FFF model which showed a similar accuracy predicted a more realistic maximal perpendicular force of $(0,5 \pm 0,3 \text{ N})$ when loaded by the maximum force of $(4,7 \pm 0,6 \text{ N})$. Therefore, we prefer another explanation stating the Microfiber model is oversimplified and does not calculate the transversal strain correctly; this was shown for this model already (and for HGO and GST models as well) (Skacel and Bursa, 2015), especially for strains above 30% (in our uniaxial experiments the strains were up to 40%). Exploitation of transversal strain data evidently improves the predictive capability in such case. However, this hypothesis requires further investigation.

4.5. Large samples satisfy better the incompressibility assumption

All the results must be regarded with respect to features of the performed test. Especially uniaxial tests are performed rarely with square shape specimens of arteries (Reeps et al., 2010). This kind of tests was motivated by two reasons. First, we wanted to ensure analyzing the same specimen in all the tests to avoid bias due to the known inter specimen variability. This would be violated by cutting some material away to obtain a narrower sample (with larger aspect ratio) ensuring uniaxial stress state during uniaxial test. Second, our effort aimed at minimization of problems with tissue compressibility. All the analyzed models are used in their incompressible form as commonly assumed (Gasser et al., 2002; Lally et al., 2005; Erhart et al., 2016, 2015). Although this can be a reasonable assumption for analysis of a whole artery (Carew et al., 1968), it was shown that radial compression (which is equivalent to biaxial tension) of specimens cut out of an artery results in a fluid outflow causing violation of the incompressibility assumption (Chuong and Fung, 1984). That study revealed the initial bulk modulus of an arterial sample cut out of the artery was not more than

300 kPa. This value is definitely comparable with the stiffness values exhibited during biaxial tests, thus the incompressibility assumption is highly questionable in such kind of tests, as well as in pressure-extension tests when only a small piece of artery is used (Di Puccio et al., 2012). As investigation of impact of sample compressibility on the robustness of constitutive models is beyond the scope of this study, we tried to minimize the ratio of the cut surfaces of the specimen to its volume and consequently also the effect of the fluid outflow. Therefore we used a relatively large specimen size in this analysis, and it should be kept in mind that a uniaxial state of stress might not be guaranteed as discussed in chapter 4.3. However it is stressed out that even this setup does not guarantee local incompressibility (Skacel and Bursa, 2015; Volokh, 2006) although it is assumed in all the analyzed constitutive models.

4.6. Limitations

Besides the limitations discussed above, another one may lie in the same deformation range used in both types of tests (biaxial and uniaxial) which leads to significantly lower stresses in uniaxial tests (see Fig. 2); this may deteriorate the prediction of biaxial responses from uniaxial tests. Nevertheless we expect a similar impact on all models thus it should not change the presented conclusions.

5. Conclusions

In this study we compare the descriptive and predictive capabilities of four chosen constitutive models commonly used for simulations of mechanical behavior of arterial tissue. Our results show that all the models can be recommended if the simulated deformation range is covered completely by experiments. The best predictive capability was observed for the phenomenological FFF model which was the only one capable to reasonably predict biaxial response when calibrated only on uniaxial tests, regardless of their type. The structure based Microfiber model performed comparably well if the transversal strains were measured in uniaxial tests and used for calibration. However, it requires structural information on the analyzed tissue as an additional input. Consequently the FFF model can be recommended as the first choice if the simulated deformations or their ratio lie out of the tested range. If the detailed structure of the tissue is known and uniaxial experimental data are available including transversal strains, the Microfiber model is similarly robust. HGO and GST models are not capable to predict mechanical responses outside of the tested range and should not be used in simulations in which the stress and/or strain ranges and ratios of their components lay outside of the experimentally covered area.

Acknowledgement

This work is an output of project NETME CENTRE PLUS (LO1202), created with financial support from the Ministry of Education, Youth and Sports under the National Sustainability Programme I. This work was also supported by the project No. 8E15B008 “New approaches in structural analysis of soft biological tissues” as part of the program of Czech-Bavarian cooperation in research and innovations provided by Ministry of Education, Youth and Sports Czech Republic and BAYHOST.

Conflict of interest

The authors declare they have no conflict of interest.

Appendix A

See appendix Tables A1-A4 here.

Table A.1
Statistical description of individual constants of all constitutive models obtained by fitting under various loading conditions-.

HGO model constant	Units	Biaxial tests Median [-] (interquartile range)	Uniaxial two strain tests Median [-] (interquartile range)	Uniaxial one strain tests Median [-] (interquartile range)
<i>c</i>	kPa	8.3(2.45 ÷ 12.8)	22(16.6 ÷ 34)	21.5(12.4 ÷ 29.4)
<i>k</i> _{1M}	kPa	23.14(13.75 ÷ 25.92)	15(11.2 ÷ 20.6)	25.9(19.4 ÷ 43.4)
<i>k</i> _{2M}	–	0.69(0.55 ÷ 0.9)	1.46(0.93 ÷ 3.78)	1.14(0.33 ÷ 2.13)
<i>ϕ</i> _M	rad	0.99(0.43 ÷ 1.35)	0.79(0.36 ÷ 1.15)	1.1(0.93 ÷ 1.16)
<i>k</i> _{1A}	kPa	0.82(0.6 ÷ 1.2)	21.3(5.8 ÷ 29.9)	1.03(0.46 ÷ 2.47)
<i>k</i> _{2A}	–	0.1(0.09 ÷ 0.11)	1.33(0.56 ÷ 2.04)	0.52(0.48 ÷ 0.58)
<i>ϕ</i> _A	rad	0.983(0.976 ÷ 0.985)	0.58(0.23 ÷ 0.95)	0.09(0.074 ÷ 0.12)
GST model constant		Biaxial tests Median [-] (interquartile range)	Uniaxial two strain tests Median [-] (interquartile range)	Uniaxial one strain tests Median [-] (interquartile range)
<i>c</i>	kPa	9.41(8.24 ÷ 13.44)	22.6(19.4 ÷ 24.95)	28.2(24.5 ÷ 30.1)
<i>k</i> _{1M}	kPa	21.89(14.65 ÷ 36.43)	20.42(12.94 ÷ 60.4)	19.68(17.95 ÷ 21.36)
<i>k</i> _{2M}	–	1.51(0.95 ÷ 2.28)	2.32(1.5 ÷ 9.97)	18.61(16.17 ÷ 19.98)
<i>ϕ</i> _M	rad	0.3(0.11 ÷ 1.11)	0.42(0.03 ÷ 0.77)	0.77(0.65 ÷ 0.81)
<i>κ</i> _M	–	0.07(0.02 ÷ 0.14)	0.14(0.02 ÷ 0.28)	0.2(0.18 ÷ 0.2)
<i>k</i> _{1A}	kPa	18.86(10.88 ÷ 23.22)	19.11(13.68 ÷ 41.09)	22.5(19.6 ÷ 26.2)
<i>k</i> _{2A}	–	1.28(1.06 ÷ 1.54)	7.84(3.54 ÷ 29.33)	20.5(18.04 ÷ 21.88)
<i>ϕ</i> _A	rad	0.99(0.06 ÷ 1.58)	0.73(0.25 ÷ 1.02)	0.73(0.67 ÷ 0.77)
<i>κ</i> _A	–	0.07(0.02 ÷ 0.12)	0.1(0.04 ÷ 0.08)	0.07(0.06 ÷ 0.08)
FFF model constant		Biaxial tests Median [-] (interquartile range)	Uniaxial two strain tests Median [-] (interquartile range)	Uniaxial one strain tests Median [-] (interquartile range)
<i>c</i>	kPa	3.82(1.31 ÷ 10.54)	41.72(34.24 ÷ 48.76)	33.7(26.24 ÷ 42)
<i>k</i> ₁₁	kPa	49.21(42.27 ÷ 55.81)	14.29(8.66 ÷ 22.74)	24.8(18.7 ÷ 29)
<i>k</i> ₂₁	–	0.99(0.69 ÷ 1.16)	1.3(1.16 ÷ 1.74)	0.9(0.64 ÷ 1.13)
<i>k</i> ₁₂	kPa	38.92(19.05 ÷ 49.6)	21.84(7.33 ÷ 32.23)	29(24.2 ÷ 37.1)
<i>k</i> ₂₂	–	0.55(0.36 ÷ 1.18)	1.08(0.77 ÷ 1.86)	0.97(0.65 ÷ 1.34)
<i>k</i> ₁₃ = <i>k</i> ₁₄	kPa	34.39(25.11 ÷ 50.55)	1.58(0.26 ÷ 5.61)	22.1(18.5 ÷ 28.8)
<i>k</i> ₂₃ = <i>k</i> ₂₄	–	0.89(0.52 ÷ 1.19)	1.97(0.24 ÷ 4.98)	0.74(0.32 ÷ 1.11)
<i>ϕ</i>	rad	0.66(0.57 ÷ 0.71)	0.68(0.23 ÷ 1.24)	0.52(0.51 ÷ 0.62)
Microfiber model constant		Biaxial tests Median [-] (interquartile range)	Uniaxial two strain tests Median [-] (interquartile range)	Uniaxial one strain tests Median [-] (interquartile range)
<i>c</i>	kPa	27.2(25.3 ÷ 27.8)	46.3(39.8 ÷ 51)	57.9(51 ÷ 66.3)
<i>k</i> _M	kPa	236(210 ÷ 257)	162(142 ÷ 237)	314(189 ÷ 376)
<i>λ</i> _{max ,M}	–	1.15(1.12 ÷ 1.2)	1.14(1.1 ÷ 1.29)	1.3(1.26 ÷ 1.3)
<i>b</i> _M	–	0.5(0.5 ÷ 0.501)	0.52(0.5 ÷ 1)	0.56(0.51 ÷ 0.93)
<i>k</i> _A	kPa	20191(16695 ÷ 31339)	26918(17626 ÷ 35554)	23637(16448 ÷ 41453)
<i>λ</i> _{min ,A}	–	1.2(1.2 ÷ 1.2008)	1.23(1.2 ÷ 1.27)	1.26(1.25 ÷ 1.31)
<i>b</i> _A	–	0.002(0.0001 ÷ 0.03)	0.23(0.16 ÷ 0.45)	0.13(0.1 ÷ 0.3)

Table A.2
Sensitivity of individual constants of all models to individual tests. Ideally they should be 1 and the interquartile range should be very narrow. Results are completed by providing p-values from testing whether the median of each ratio of the constants equals to 1.

HGO model constant	Biaxial to two-strain uniaxial ratios		Biaxial to one-strain uniaxial ratios	
	Median [-] (interquartile range)	p-value	Median [-] (interquartile range)	p-value
<i>c</i>	0.3(0.07 ÷ 0.5)	0.024	0.29(0.15 ÷ 0.63)	0.017
<i>k</i> _{1M}	1.55(0.79 ÷ 2.34)	0.045	0.78(0.39 ÷ 1.18)	0.49
<i>k</i> _{2M}	0.75(0.48 ÷ 0.98)	0.167	1.22(0.71 ÷ 1.51)	0.900
<i>ϕ</i> _M	1.44(0.74 ÷ 2.85)	0.149	1.06(0.38 ÷ 1.28)	0.754
<i>k</i> _{1A}	1.09(0.63 ÷ 3.01)	0.286	0.64(0.365 ÷ 0.88)	0.346
<i>k</i> _{2A}	0.69(0.37 ÷ 1.95)	0.999	0.66(0.33 ÷ 2.08)	0.9
<i>ϕ</i> _A	1.36(0.62 ÷ 2.14)	0.187	1.71(0.61 ÷ 2.52)	0.069

(continued on next page)

Table A.2 (continued)

HGO model		Biaxial to two-strain uniaxial ratios		Biaxial to one-strain uniaxial ratios	
constant	Median [-] (interquartile range)	p-value		Median [-] (interquartile range)	p-value
GST model		Biaxial to two-strain uniaxial ratios		Biaxial to one-strain uniaxial ratios	
constant	Median [-] (interquartile range)	p-value		Median [-] (interquartile range)	p-value
<i>c</i>	0.36(0.34 ÷ 0.67)	0.028		0.37(0.29 ÷ 0.49)	0.001
<i>k</i> _{1M}	0.97(0.21 ÷ 3.24)	0.49		1.1(0.74 ÷ 1.64)	0.379
<i>k</i> _{2M}	0.57(0.18 ÷ 8.9)	1		0.08(0.05 ÷ 1.64)	0.001
<i>γ</i> _M	0.36(0.12 ÷ 2.373)	0.379		0.39(0.16 ÷ 1.03)	0.379
<i>κ</i> _M	0.46(0.13 ÷ 3.61)	0.9		0.38(0.1 ÷ 0.84)	0.149
<i>k</i> _{1A}	0.69(0.42 ÷ 1.28)	0.414		0.85(0.45 ÷ 1)	0.209
<i>k</i> _{2A}	0.2(0.03 ÷ 0.28)	0.233		0.08(0.05 ÷ 0.12)	0.117
<i>γ</i> _A	0.51(0.23 ÷ 1.94)	0.802		1.39(0.07 ÷ 2.31)	0.286
<i>κ</i> _A	0.52(0.2 ÷ 1.97)	0.727		0.29(0.11 ÷ 0.6)	0.001
FFF model		Biaxial to two-strain uniaxial ratios		Biaxial to one-strain uniaxial ratios	
constant	Median [-] (interquartile range)	p-value		Median [-] (interquartile range)	p-value
<i>c</i>	0.10(0.02 ÷ 0.24)	0.001		0.10(0.03 ÷ 0.43)	0.001
<i>k</i> ₁₁	3.30(2.2 ÷ 6.36)	0.001		1.81(1.47 ÷ 2.74)	0.003
<i>k</i> ₂₁	0.75(0.48 ÷ 0.98)	0.167		1.22(0.71 ÷ 1.51)	0.379
<i>k</i> ₁₂	1.57(0.95 ÷ 7.26)	0.06		1.29(0.73 ÷ 2.03)	0.233
<i>k</i> ₂₂	0.49(0.25 ÷ 1.12)	0.295		0.92(0.48 ÷ 1.23)	0.66
<i>k</i> ₁₃ = <i>k</i> ₁₄	21.32(7.31 ÷ 886)	0.001		1.24(0.8 ÷ 2.24)	0.13
<i>k</i> ₂₃ = <i>k</i> ₂₄	0.75(0.13 ÷ 5.34)	0.315		1.41(0.97 ÷ 2.19)	0.06
<i>φ</i>	1.55(0.58 ÷ 2.87)	0.09		1.14(1.00 ÷ 1.44)	0.028
Microfiber model		Biaxial to two-strain uniaxial ratios		Biaxial to one-strain uniaxial ratios	
constant	Median [-] (interquartile range)	p-value		Median [-] (interquartile range)	p-value
<i>c</i>	0.58(0.48 ÷ 0.72)	0.001		0.43(0.41 ÷ 0.47)	0.001
<i>k</i> _M	1.37(0.97 ÷ 1.58)	0.017		0.78(0.6 ÷ 1.2)	0.616
<i>λ</i> _{max ,M}	1(0.94 ÷ 1.04)	0.398		0.89(0.88 ÷ 0.93)	0.002
<i>b</i> _M	1(0.61 ÷ 1)	0.045		0.92(0.61 ÷ 1)	0.005
<i>k</i> _A	1.1(0.62 ÷ 1.34)	1		0.77(0.51 ÷ 1.35)	0.754
<i>λ</i> _{min ,A}	0.98(0.95 ÷ 1)	0.009		0.96(0.92 ÷ 0.97)	0.002
<i>b</i> _A	0.04(0.0 ÷ 0.3)	0.002		0.05(0.001 ÷ 1.01)	0.576

Table A.3

Descriptive capabilities of the investigated constitutive models assessed via NRMSE metric. All models except for Microfiber were able to capture measured data with median of NRMSE≤10%.

Model	Capturing of uniaxial- two strain tests Median NRMSE [%] (interquartil range)	Capturing of uniaxial- one strain tests Median NRMSE [%] (interquartil range)	Capturing of biaxial tests Median of NRMSE [%] (interquartil range)
HGO	6.3 (4.8 ÷ 7.8)	8.7 (7.4 ÷ 11.9)	9.9 (8.8 ÷ 11.3)
GST	4.7 (4.1 ÷ 7.6)	7.3 (6.2 ÷ 7.8)	10 (8.5 ÷ 12.7)
FFF	4.5 (4 ÷ 5.9)	7.2 (6.3 ÷ 8)	9.6 (8.5 ÷ 10.8)
Microfiber	6.3 (5 ÷ 11.3)	10.7 (8.9 ÷ 13.5)	18.1 (15.6 ÷ 21.3)

Table A.4

Predictive capabilities of the investigated constitutive models assessed via NRMSE metric. FFF model performed best in all the three tests while HGO and GST models failed completely in predicting biaxial response; Microfiber model was able to predict biaxial response comparably to FFF model only when fitted on uniaxial two-strain data.

Model	Predicting uniaxial-two strain tests when fitted on biaxial tests	Predicting biaxial tests when fitted on uniaxial-two strain tests	Predicting biaxial tests when fitted on uniaxial-one strain tests
	Median NRMSE [%] (interquartile range)	Median NRMSE [%] (interquartile range)	Median of NRMSE [%] (interquartile range)
HGO	31 (22 ÷ 37)	45 (36 ÷ 158)	238 (151 ÷ 443)
GST	29 (24 ÷ 34)	454 (255 ÷ 1705)	3e5 (1e5 ÷ 9e5)
FFF	33 (22 ÷ 36)	29 (24 ÷ 31)	27 (24 ÷ 33)
Microfiber	22 (19 ÷ 24)	30 (25 ÷ 38)	45 (40 ÷ 52)

Appendix A. Supporting information

Supplementary data associated with this article can be found in the online version at <http://dx.doi.org/10.1016/j.jmbbm.2017.11.035>.

References

- Alastrué, V., Peña, E., Martínez, M.A., Doblaré, M., 2008. Experimental study and constitutive modelling of the passive mechanical properties of the ovine infrarenal vena cava tissue. *J. Biomech.* 41, 3038–3045.
- Baek, S., Gleason, R.L., Rajagopal, K.R., Humphrey, J.D., 2007. Theory of small on large: potential utility in computations of fluid-solid interactions in arteries. *Comput. Methods Appl. Mech. Eng.* 196, 3070–3078.
- Carew, T.E., Vaishnav, R.N., Patel, D.J., 1968. Compressibility of the arterial wall. *Circ. Res.* 23.
- Chen, H., Liu, Y., Zhao, X., Lanir, Y., Kassab, G.S., 2011. A micromechanics finite-strain constitutive model of fibrous tissue. *J. Mech. Phys. Solids* 59, 1823–1837.
- Cheng, G.C., Loree, H.M., Kamm, R.D., Fishbein, M.C., Lee, R.T., 1993. Distribution of circumferential stress in ruptured and stable atherosclerotic lesions. A structural analysis with histopathological correlation. *Circulation* 87, 1179–1187.
- Chuong, C.J., Fung, Y.C., 1984. Compressibility and constitutive equation of arterial wall in radial compression experiments. *J. Biomech.* 17, 35–40.
- Cilla, M., Peña, E., Martínez, M.A., 2012. 3D computational parametric analysis of eccentric atheroma plaque: influence of axial and circumferential residual stresses. *Biomech. Model. Mechanobiol.* 11, 1001–1013.
- Cortes, D.H., Lake, S.P., Kadlowec, J.A., Soslowky, L.J., Elliott, D.M., 2010. Characterizing the mechanical contribution of fiber angular distribution in connective tissue: comparison of two modeling approaches. *Biomech. Model. Mechanobiol.* 9, 651–658.
- Cunnane, E.M., Mulvihill, J.J.E., Barrett, H.E., Hennessy, M.M., Kavanagh, E.G., Walsh, M.T., 2016. Mechanical properties and composition of carotid and femoral atherosclerotic plaques: a comparative study. *J. Biomech.* 49, 3697–3704.
- Demiray, H., 1972. A note on the elasticity of soft biological tissues. *J. Biomech.* 5, 309–311.
- Di Puccio, F., Celi, S., Forte, P., 2012. Review of experimental investigations on compressibility of arteries and introduction of a new apparatus. *Exp. Mech.* 52, 895–902.
- Erhart, P., Grond-Ginsbach, C., Hakimi, M., Lasitschka, F., Dihlmann, S., Ockler, D., Hyhlik-Dürr, A., 2014. Finite element analysis of abdominal aortic aneurysms: predicted rupture risk correlates with aortic wall histology in individual patients. *J. Endovasc. Ther.* 21, 556–564.
- Erhart, P., Hyhlik-Dürr, A., Geisbüsch, P., Kotelis, D., Müller-Eschner, M., Gasser, T.C., Von Tengg-Kobligh, H., Böckler, D., 2015. Finite element analysis in asymptomatic, symptomatic, and ruptured abdominal aortic aneurysms: In search of new rupture risk predictors. *Eur. J. Vasc. Endovasc. Surg.* 49, 239–245.
- Erhart, P., Roy, J., de Vries, J.-P.P.M., Liljeqvist, M.L., Grond-Ginsbach, C., Hyhlik-Du rr, A., Böckler, D., 2016. Prediction of rupture sites in abdominal aortic aneurysms after finite element analysis. *J. Endovasc. Ther.* 23, 115–120.
- Ferruzzi, J., Vorp, D. a., Humphrey, J.D., 2011. On constitutive descriptors of the biaxial mechanical behaviour of human abdominal aorta and aneurysms. *J. R. Soc. Interface* 8, 435–450.
- Gasser, T.C., Schulze-Bauer, C. a.J., Holzapfel, G. a., 2002. A three-dimensional finite element model for arterial clamping. *J. Biomech. Eng.* 124, 355.
- Gasser, T.C., Ogden, R.W., Holzapfel, G.A., 2006. Hyperelastic modelling of arterial layers with distributed collagen fibre orientations. *J. R. Soc. Interface* 3, 15–35.
- Gasser, T.C., Görgülü, G., Folkesson, M., Swedenborg, J., 2008. Failure properties of intraluminal thrombus in abdominal aortic aneurysm under static and pulsating mechanical loads. *J. Vasc. Surg.* 48, 179–188.
- Gasser, T.C., Gallinetti, S., Xing, X., Forsell, C., Swedenborg, J., Roy, J., 2012. Spatial orientation of collagen fibers in the abdominal aortic aneurysm's wall and its relation to wall mechanics. *Acta Biomater.* 8, 3091–3103.
- Hill, M.R., Duan, X., Gibson, G.A., Watkins, S., Robertson, A.M., 2012. A theoretical and non-destructive experimental approach for direct inclusion of measured collagen orientation and recruitment into mechanical models of the artery wall. *J. Biomech.* 45, 762–771.
- Hollander, Y., Durban, D., Lu, X., Kassab, G.S., Lanir, Y., 2011. Constitutive modeling of coronary arterial media—comparison of three model classes. *J. Biomech. Eng.* 133, 61008.
- Holzapfel, G.A., Stadler M., Schulze-Bauer C.A.J. A Layer-Specific Three-Dimensional Model for the Simulation of Balloon Angioplasty using Magnetic Resonance Imaging and Mechanical Testing. <<http://dx.doi.org/10.1114/1.1492812>>.
- Holzapfel, G.A., Gasser, T.C., Ogden, R.W., 2000. A new constitutive framework for arterial wall mechanics and a comparative study of material models. *J. Elast.* 61, 1–48.
- Holzapfel, G.A., Sommer, G., Regitnig, P., 2004. Anisotropic mechanical properties of tissue components in human atherosclerotic plaques. *J. Biomech. Eng.* 126, 657–665.
- Holzapfel, G.A., Sommer, G., Gasser, C.T., Regitnig, P., 2005. Determination of layer-specific mechanical properties of human coronary arteries with nonatherosclerotic intimal thickening and related constitutive modeling. *Am. J. Physiol. - Hear. Circ. Physiol.* 289.
- Holzapfel, G.A., Ogden, R.W., Holzapfel, G.A., Ogden, R.W., 2010. Constitutive modelling of arteries. *Proc. R. Soc. A* 466, 1551–1597.
- Holzapfel, G.A., Mulvihill, J.J., Cunnane, E.M., Walsh, M.T., 2014. Computational approaches for analyzing the mechanics of atherosclerotic plaques: a review. *J. Biomech.* 47, 859–869.
- Khosla, S., Morris, D.R., Moxon, J.V., Walker, P.J., Gasser, T.C., Gollidge, J., 2014. Meta-analysis of peak wall stress in ruptured, symptomatic and intact abdominal aortic aneurysms. *Br. J. Surg.* 101, 1350–1357.
- Lally, C., Dolan, P., Prendergast, P.J., 2005. Cardiovascular stent design and vessel stresses: a finite element analysis. *J. Biomech.* 38, 1574–1581.
- Lanir, Y., 1983. Constitutive equations for fibrous connective tissues. *J. Biomech.* 16, 1–12.
- Martufi, G., Gasser, T.C., 2011. A constitutive model for vascular tissue that integrates fibril, fiber and continuum levels with application to the isotropic and passive properties of the infrarenal aorta. *J. Biomech.* 44, 2544–2550.
- Mower W.R.J.Q.W., Gambhir S., 1997. Effect of intraluminal thrombus on local abdominal aortic aneurysm wall strength. In: *Proceedings of the first Jt BMES/EMBS Conf*, 27:244.
- Ohayon, J., Rioufol, G., Dubreuil, O., Lyon, D., 2005. A three-dimensional finite element analysis of stress distribution in a coronary atherosclerotic plaque. *Biomech. Appl. Comput. Assist Surg.* 661, 225–241.
- Polzer, S., Christian Gasser, T., Bursa, J., Staffa, R., Vlachovsky, R., Man, V., Skacel, P., 2013. Importance of material model in wall stress prediction in abdominal aortic aneurysms. *Med. Eng. Phys.* <http://dx.doi.org/10.1016/j.medengphy.2013.01.008>.
- Polzer, S., Gasser, T.C., Novak, K., Man, V., Tichy, M., Skacel, P., Bursa, J., 2015. Structure-based constitutive model can accurately predict planar biaxial properties of aortic wall tissue. *Acta Biomater.* <http://dx.doi.org/10.1016/j.actbio.2014.11.043>.
- Raghavan, M.L., Vorp, D.A., 2000. Toward a biomechanical tool to evaluate rupture potential of abdominal aortic aneurysm: identification of a finite strain constitutive model and evaluation of its applicability. *J. Biomech.* 33, 475–482.
- Raghavan, M.L., Webster, M.W., Vorp, D.A., 1996. Ex vivo biomechanical behavior of abdominal aortic aneurysm: assessment using a new mathematical model. *Ann. Biomed. Eng.* 24, 573–582.
- Raghavan, M.L., Hanaoka, M.M., Kratzberg, J.A., Higuchi, M., de, L., da Silva, E.S., 2011.

- Biomechanical failure properties and microstructural content of ruptured and unruptured abdominal aortic aneurysms. *J. Biomech.* 44, 2501–2507.
- Reeps, C., Gee, M., Maier, A., Gurdan, M., Eckstein, H.H., Wall, W.A., 2010. The impact of model assumptions on results of computational mechanics in abdominal aortic aneurysm. *J. Vasc. Surg.* 51, 679–688.
- Reeps, C., Maier, A., Pelisek, J., Härtl, F., Grabher-Meier, V., Wall, W.A., Essler, M., Eckstein, H.H., Gee, M.W., 2013. Measuring and modeling patient-specific distributions of material properties in abdominal aortic aneurysm wall. *Biomech. Model. Mechanobiol.* 12, 717–733.
- Schriefl, A.J., Zeindlinger, G., Pierce, D.M., Regitnig, P., Holzapfel, G. a., 2012a. Determination of the layer-specific distributed collagen fibre orientations in human thoracic and abdominal aortas and common iliac arteries. *J. R. Soc. Interface* 9, 1275–1286.
- Schriefl, A.J., Reinisch, A.J., Sankaran, S., Pierce, D.M., Holzapfel, G.A., 2012b. Quantitative assessment of collagen fibre orientations from two-dimensional images of soft biological tissues. *J. R. Soc. Interface* 9, 3081–3093.
- Skacel, P., Bursa, J., 2014. Comparison of constitutive models of arterial layers with distributed collagen fibre orientations. *Acta Bioeng. Biomech.* 16, 47–58.
- Skacel, P., Bursa, J., 2015. Poisson's ratio of arterial wall – inconsistency of constitutive models with experimental data. *J. Mech. Behav. Biomed. Mater.* 54, 316–327.
- Slazansky, M., Polzer, S., Man, V., Bursa, J., 2016. Analysis of accuracy of biaxial tests based on their computational simulations. *Strain*. <http://dx.doi.org/10.1111/str.12205>.
- Tong, J., Schriefl, A.J., Cohnert, T., Holzapfel, G.A., 2013. Gender differences in biomechanical properties, thrombus age, mass fraction and clinical factors of abdominal aortic aneurysms. *Eur. J. Vasc. Endovasc. Surg.* 45, 364–372.
- Tsamis, A., Phillippi, J.A., Koch, R.G., Pasta, S., D'Amore, A., Watkins, S.C., Wagner, W.R., Gleason, T.G., Vorp, D.A., 2013. Fiber micro-architecture in the longitudinal-radial and circumferential-radial planes of ascending thoracic aortic aneurysm media. *J. Biomech.* 46, 2787–2794.
- Vande Geest, J.P., Sacks, M.S., Vorp, D.A., 2006. The effects of aneurysm on the biaxial mechanical behavior of human abdominal aorta. *J. Biomech.* 39, 1324–1334.
- Vito, R.P., Dixon, S.A., 2003. Blood vessel constitutive models—1995–2002. *Annu. Rev. Biomed. Eng.* 5, 413–439.
- Volokh, K.Y., 2006. Compressibility of arterial wall in ring-cutting experiments. *Copyp. C. Tech. Sci. Press MCB* 3, 35–42.
- Weisbecker, H., Unterberger, M.J., Holzapfel, G.A., 2015. Constitutive modelling of arteries considering fibre recruitment and three-dimensional fibre distribution. *J. R. Soc. Interface* 12.
- Yeoh, O.H., 1993. Some forms of the strain energy function for rubber. *Rubber Chem. Technol.* 66, 754–771.
- Yoram Lanir, R.N., 2015. Reliability of structure tensors in representing soft tissues structure. *J. Mech. Behav. Biomed. Mater.* 46, 222–228.
- Zeinali-Davarani, S., Raguin, L.G., Vorp, D.A., Baek, S., 2011. Identification of in vivo material and geometric parameters of a human aorta: toward patient-specific modeling of abdominal aortic aneurysm. *Biomech. Model. Mechanobiol.* 10, 689–699.
- Zhang, Y., Xu, B., Chow, M.J., 2011. Experimental and modeling study of collagen scaffolds with the effects of crosslinking and fiber alignment. *Int. J. Biomater.* <http://dx.doi.org/10.1155/2011/172389>.

15 Appendix B

Table 10 Starting points of the Microfiber material model, constrained and unconstrained.

Parameters		Starting point Number				Free		Constrained	
Layer	Name	1	2	3	4	Min	Max	Min	Max
media	mu	1	5	500	50	0	-	0	-
	k	1	10	400	400	0	-	0	-
	l_min	1	1	1	1	1	-	Fix	Fix
	l_max	1,2	1,3	1,5	1,5	1	-	1	2
	b	0,1	0,5	1,5	1,5	0	-	0	1,5
adventitia	mu	0	0	0	0	Fix	Fix	Fix	Fix
	k	1	50	1,0E+07	1,0E+05	0	-	0	-
	l_min	1,1	1,2	1,1	1,3	1	-	1	1,5
	l_max	1,5	2	2	2	1	-	Fix	Fix
	b	0,1	0,5	0,5	0,5	0	-	0	1,5

Table 11 Starting points of the Microfiber material model with resulting fitted parameters and residuals R^2 and NRMSE for equibiaxial dataset.

Equibiaxial only		Starting Point 1		Starting Point 2		Starting Point 3		Starting Point 4	
Layer	Name	Start	Fit	Start	Fit	Start	Fit	Start	Fit
media	mu	1	74,301	5	0	500	44,887	50	44,665
	k	1	22,561	10	1168,768	400	515,722	400	472,406
	l_min	1	3,694	1	1,096	1	1,368	1	1
	l_max	1,2	1,829	1,3	5,9	1,5	1,006	1,5	1,359
	b	0,1	3,048	0,5	0	1,5	0,194	1,5	0,192
adventitia	mu	0	0	0	0	0	0	0	0
	k	1	0	50	357,138	1,0E+07	23302476	1,0E+05	160105
	l_min	1,1	7,198	1,2	1,064	1,1	5,398	1,3	1,263
	l_max	1,5	1	2	1	2	13,189	2	2,335
	b	0,1	3,143	0,5	0,098	0,5	0	0,5	0,016
		R2 / NRMSE 0,8525 / 0,3062		R2 / NRMSE 0,9772 / 0,1196		R2 / NRMSE 0,9969 / 0,0443		R2 / NRMSE 0,9974 / 0,0404	

Table 12 Starting points of the Microfiber material model with resulting fitted parameters and residuals R^2 and NRMSE for all datasets combined, unconstrained (free).

All protocols, free		Starting Point 1		Starting Point 2		Starting Point 3		Starting Point 4	
Layer	Name	Start	Fit	Start	Fit	Start	Fit	Start	Fit
media	mu	1	28,347	5	0	500	29,605	50	27,152
	k	1	254,287	10	180,127	400	369,391	400	551,009
	l_min	1	137,171	1	1	1	1	1	1
	l_max	1,2	1,398	1,3	1	1,5	1,232	1,5	1,304
	b	0,1	0,392	0,5	0,091	1,5	0,288	1,5	0,108
adventitia	mu	0	0	0	0	0	0	0	0
	k	1	622	50	2245,79	1,0E+07	26464120	1,0E+05	168845,4
	l_min	1,1	1	1,2	1,866	1,1	1,764	1,3	1,533
	l_max	1,5	1,34	2	1	2	1,396	2	2,978
	b	0,1	0	0,5	0,027	0,5	1,235	0,5	0,608
		R2 / NRMSE 0,964 / 0,147		R2 / NRMSE 0,9812 / 0,101		R2 / NRMSE 0,9526 / 0,1527		R2 / NRMSE 0,9669 / 0,1405	

Table 13 Starting points of the Microfiber material model with resulting fitted parameters and residuals R^2 and NRMSE for all datasets combined, constrained.

All protocols, constrained		Starting Point 1		Starting Point 2		Starting Point 3		Starting Point 4	
Layer	Name	Start	Fit	Start	Fit	Start	Fit	Start	Fit
media	mu	1	28,346	5	0	500	26,907	50	27,156
	k	1	622,081	10	268,27	400	535,665	400	551,088
	l_min	1	1	1	1	1	1	1	1
	l_max	1,2	1,34	1,3	1	1,5	1,297	1,5	1,304
	b	0,1	0	0,5	0,057	1,5	0,106	1,5	0,108
adventitia	mu	0	0	0	0	0	0	0	0
	k	1	0	50	1,091	1,0E+07	1,47E+08	1,0E+05	48799,92
	l_min	1,1	1,5	1,2	1,004	1,1	1,398	1,3	1,499
	l_max	1,5	1,5	2	2	2	2	2	2
	b	0,1	1,5	0,5	1,5	0,5	1,303	0,5	0,342
		R2 / NRMSE 0,964 / 0,147		R2 / NRMSE 0,8796 / 0,2604		R2 / NRMSE 0,9671 / 0,1401		R2 / NRMSE 0,9669 / 0,1405	

16 Appendix C

Process of fitting the measured data using the program Hyperfit

After starting the program, an empty working space shows up. In the left panel we choose Test data – Add (from file). It is possible to select multiple files in order to shorten the working time.

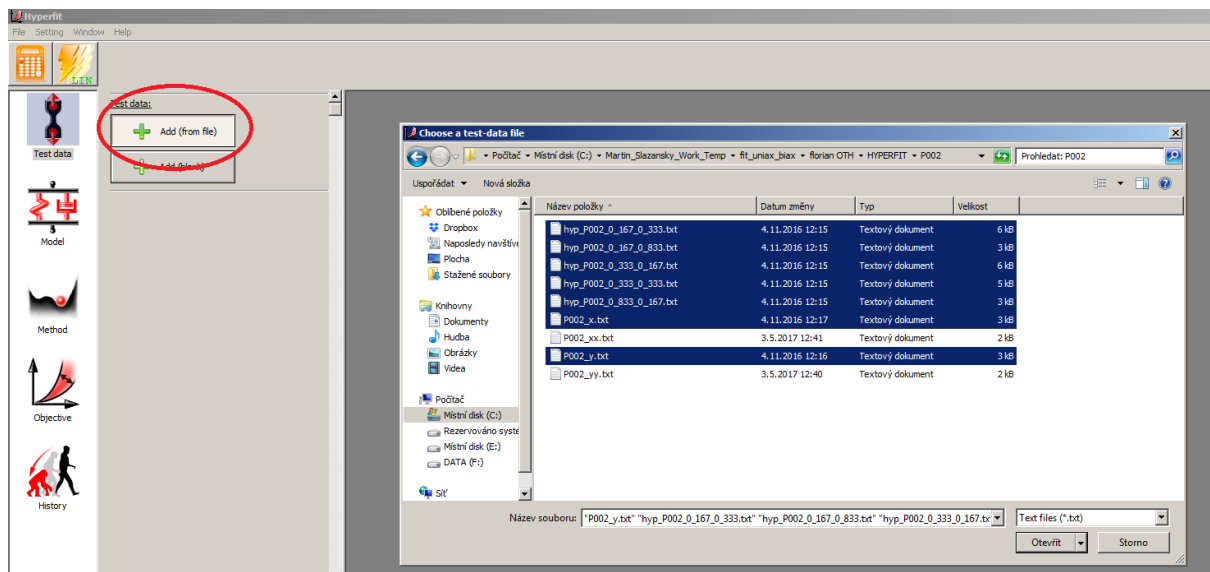


Figure 46 Adding data sets into the Hyperfit program.

The selected data sets show up in a form of stress strain graphs. In the heading we can see the type of experimental protocol, depending on the chosen data set. The main testing protocols are uniaxial, equibiaxial and biaxial. In relation to the analyses of aortic aneurysm, uniaxial and equibiaxial protocols are distant from the reality of aortic physiological stress – strain behaviour. Biaxial tension in axial and radial direction of the aortic tube is distributed normally in the ratio of ca 1:2 in case of healthy young person and in the ratio of approximately 1:5 in case of older people where the axial pretension decreases during the aging process.

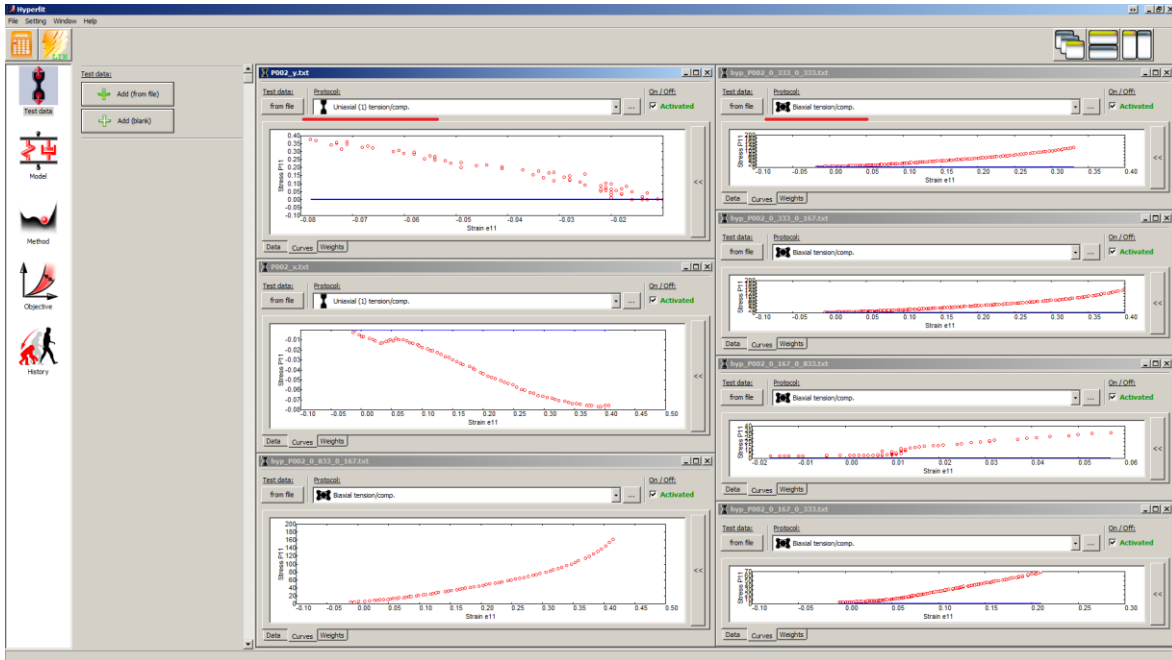


Figure 47 Loaded data sets. Underlined testing protocols.

For better representation of data sets, a sorting function is used. The experimental data obtained via uniaxial loading are on the left side of the window, the biaxial experimental data are on the other side.

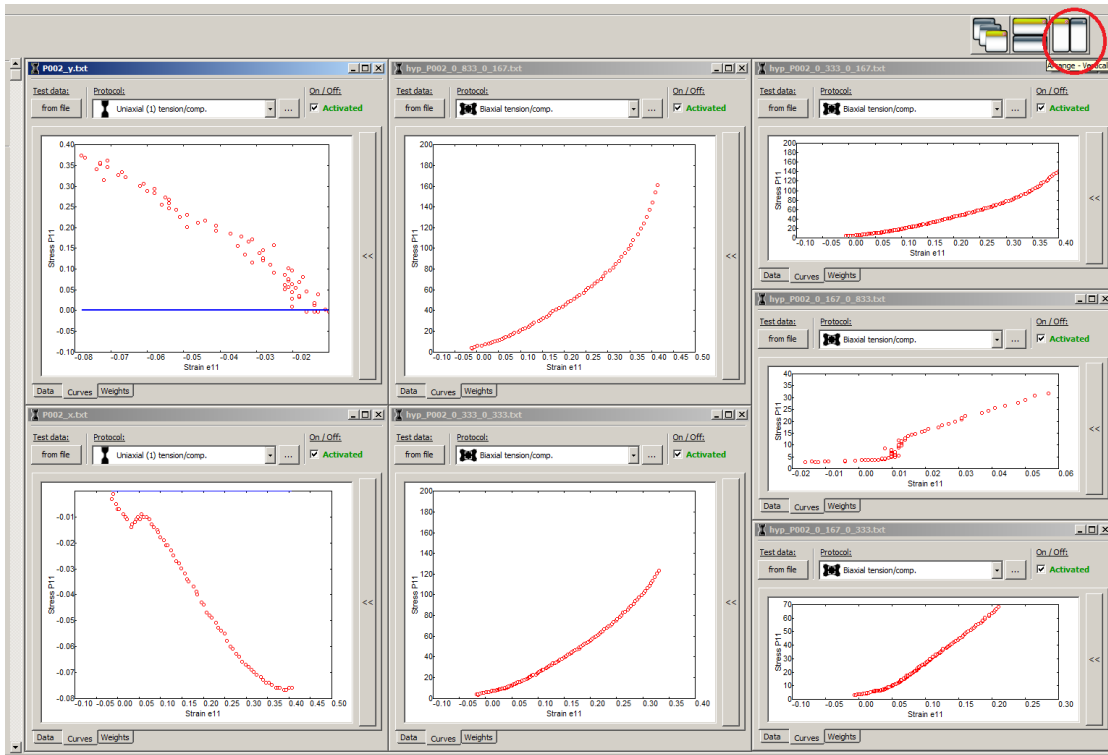


Figure 48 Sorted data sets.

Now we need to set up the uniaxial tension tests as biaxial tension tests with no perpendicular stress calculated, only strains in both axes and one stress, as explained in the relevant chapter. First, the type of experimental setup is changed from uniaxial to biaxial. In the upper case, the stress is practically zero in one axis; therefore we need to show the values of stress and strain in the other axis.

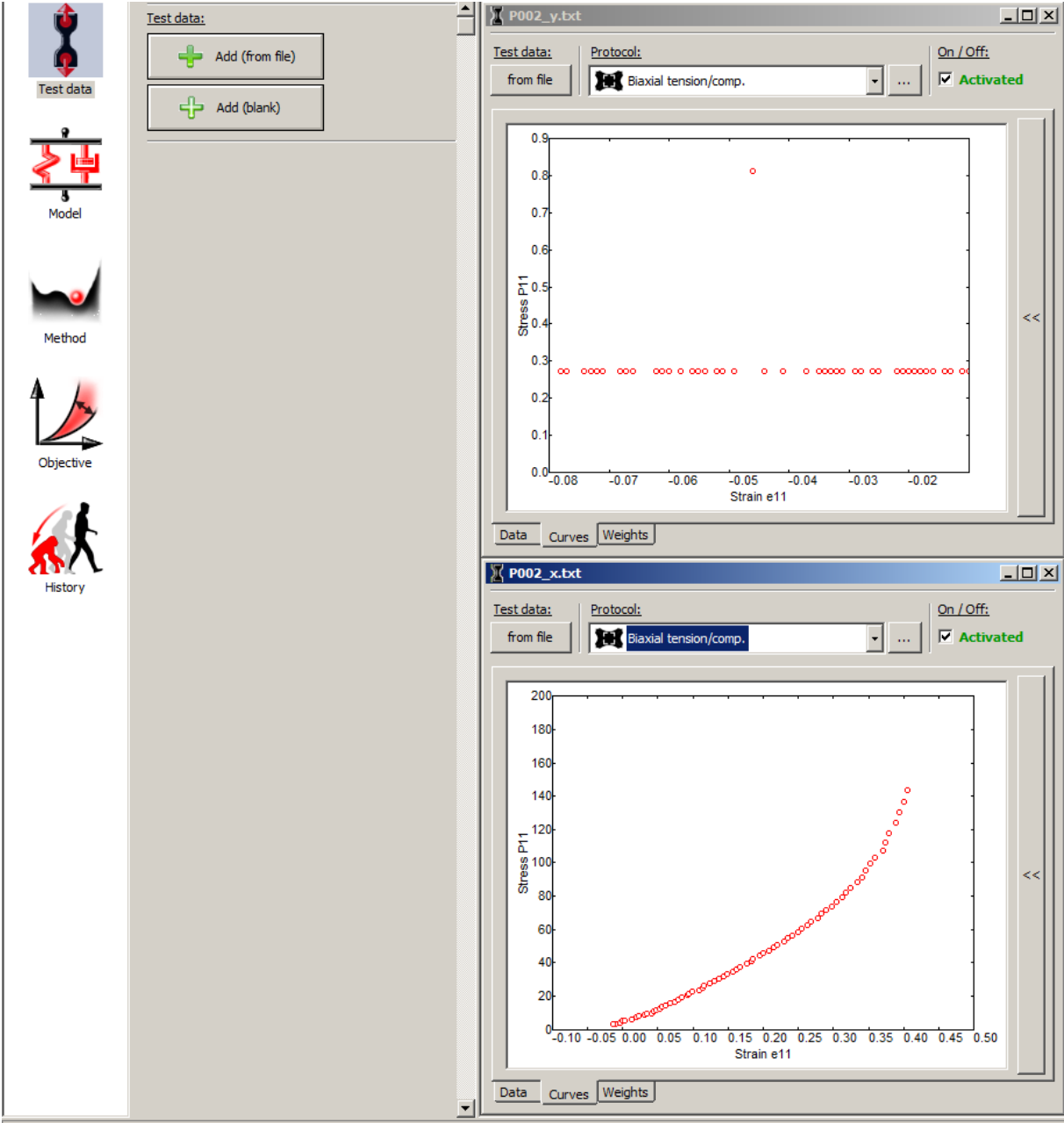


Figure 49 The two uniaxial data sets will be set up.

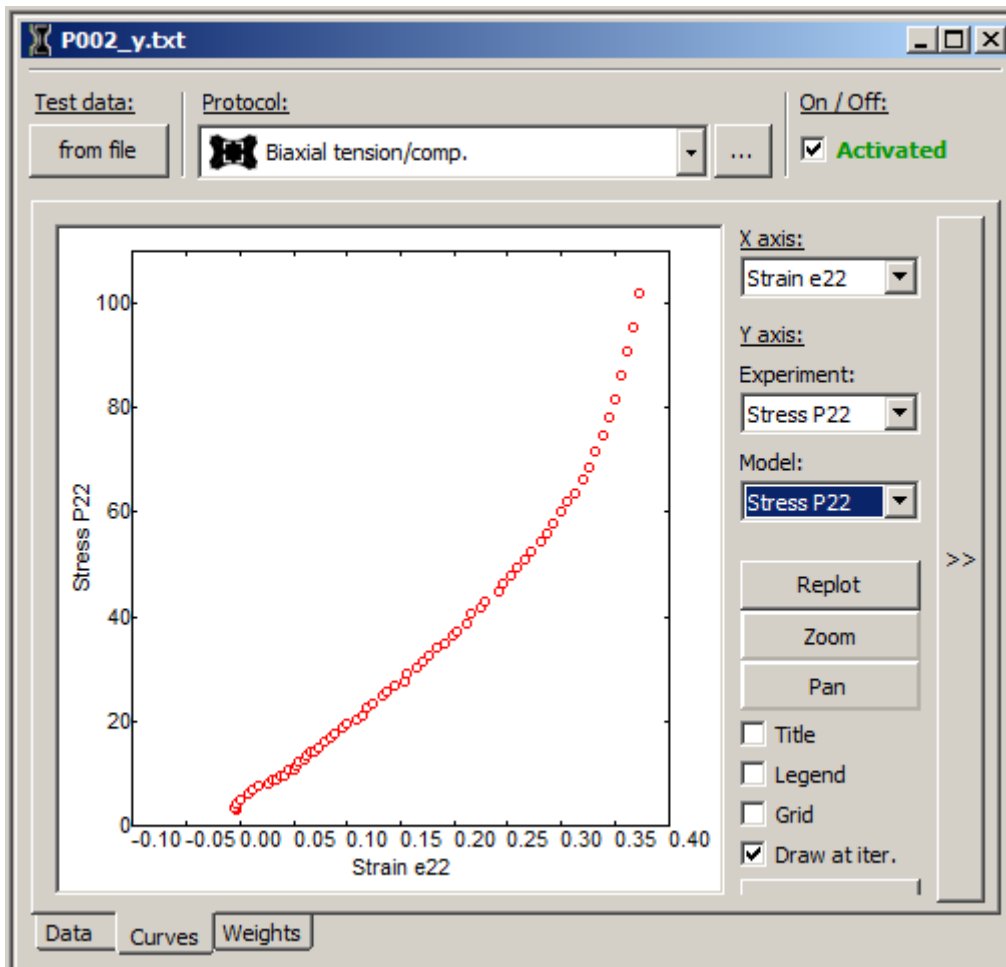


Figure 50 Changing X and Y axis to show the desired data.

Now we need to exclude the zero stress in perpendicular direction to loading vector. The weight of the values will therefore be zero. The data of strain in perpendicular direction influence the fitting process despite the exclusion of the corresponding stress.

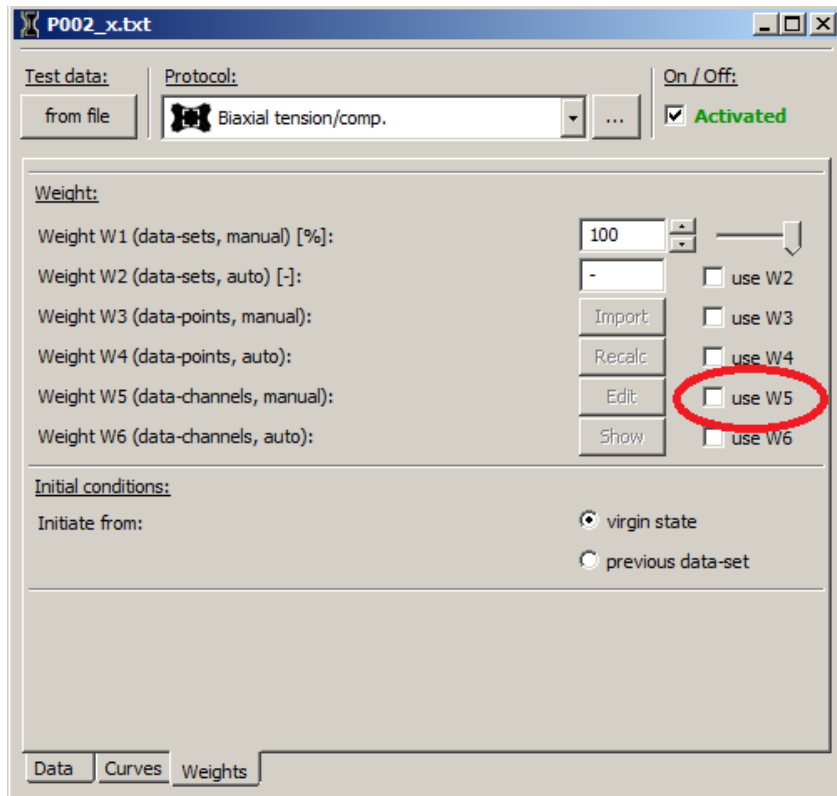


Figure 51 Setting the weight of chosen stress values to zero, first window.

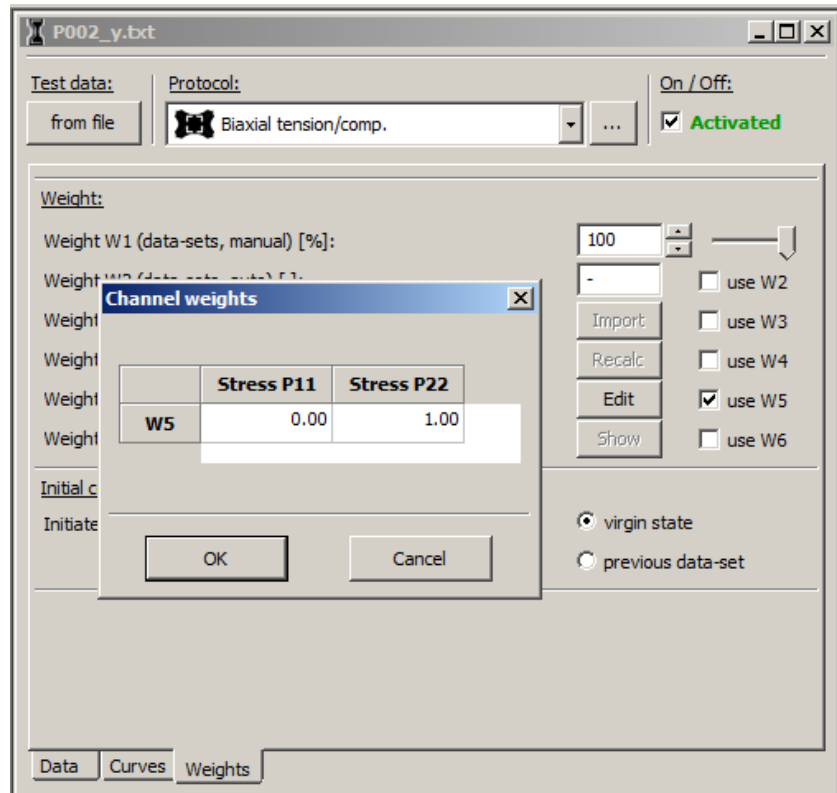


Figure 52 Setting the weight of chosen stress values to zero, second window

The setting needs to be done in both cases of uniaxial tests.

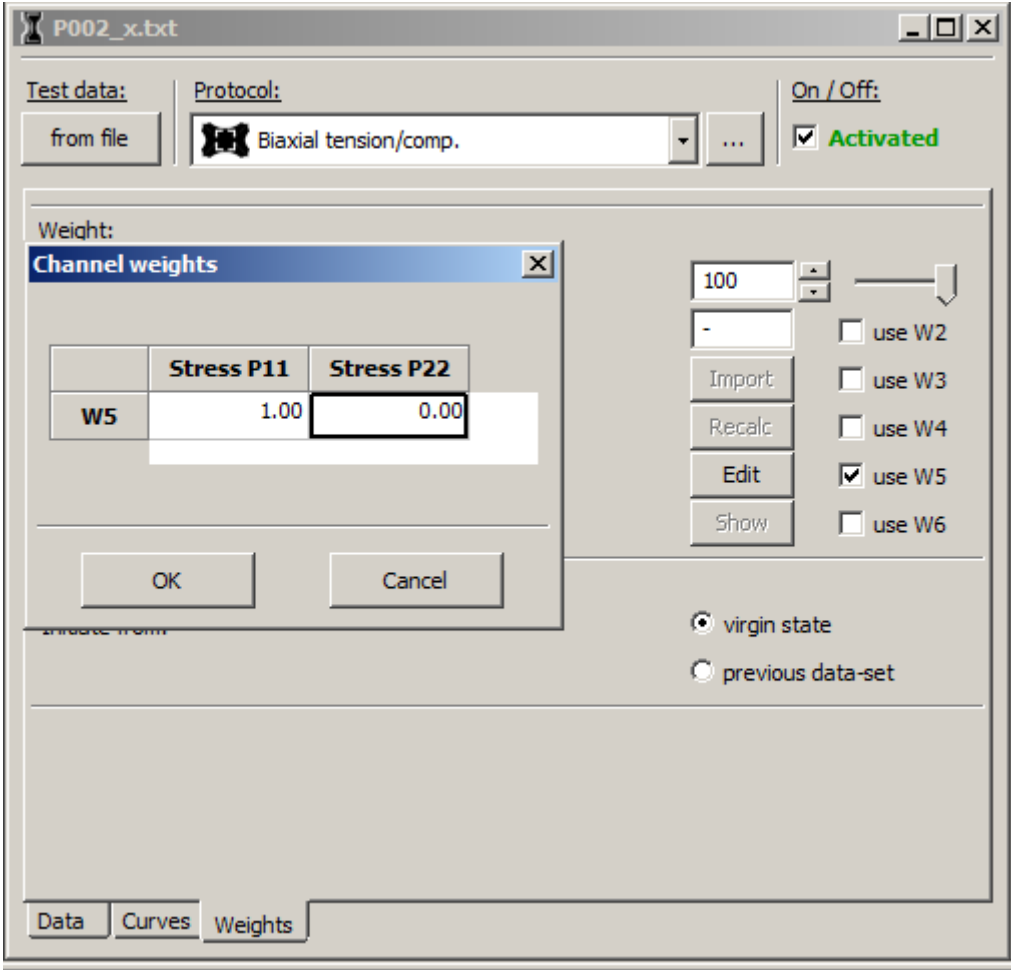


Figure 53 Setting the weight of chosen stress values to zero, second data set.

Now the data sets are ready to be fitted. First we start with the fitting of biaxial data. The uniaxial data sets on the left will be deactivated.

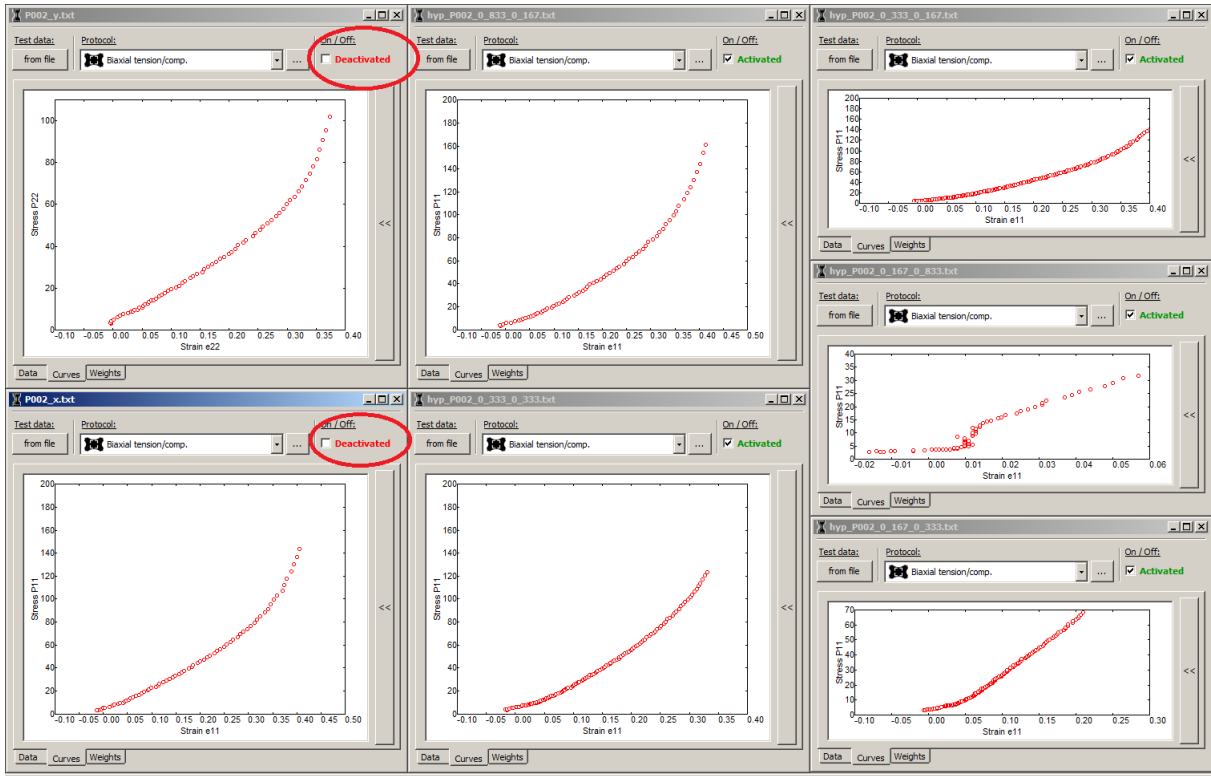


Figure 54 Deactivating of the uniaxial data sets.

Now another part of the program needs to be set up. The objective function which will be optimised (minimized or maximized) is in our case the Coefficient of determination R^2 .

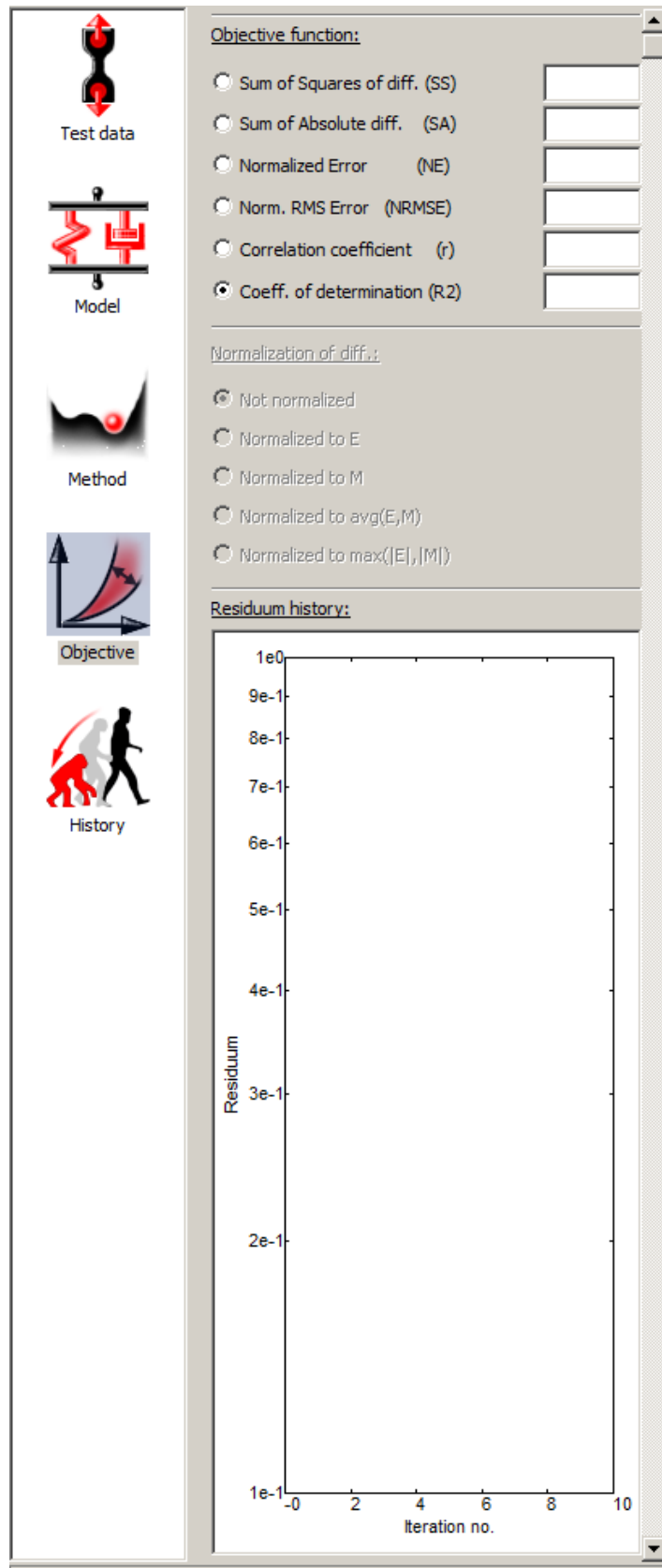


Figure 55 Setting the Coeff. of Determination as the objective function.

The numerical method used to find the best fit must be set up now. The used values are a compromise of time and accuracy.

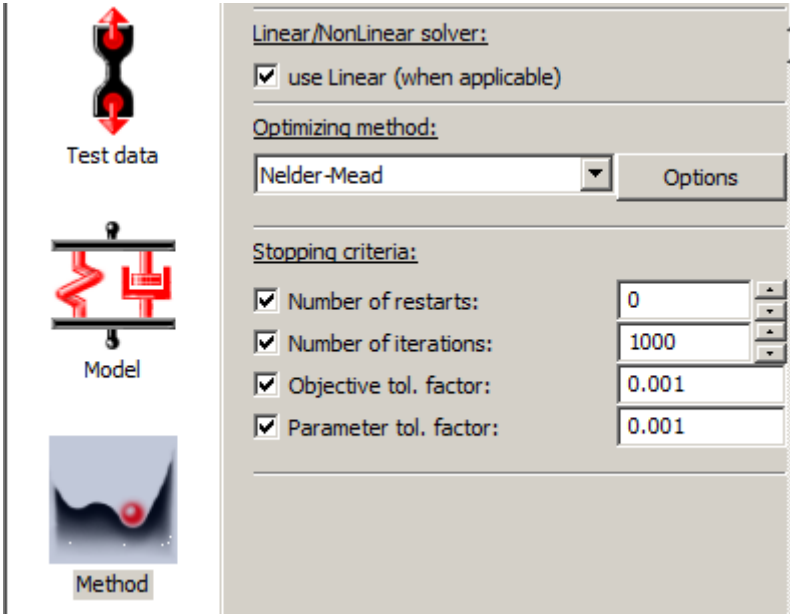


Figure 56 Setting the numerical method.

Lastly we need to choose and set the Model of material.

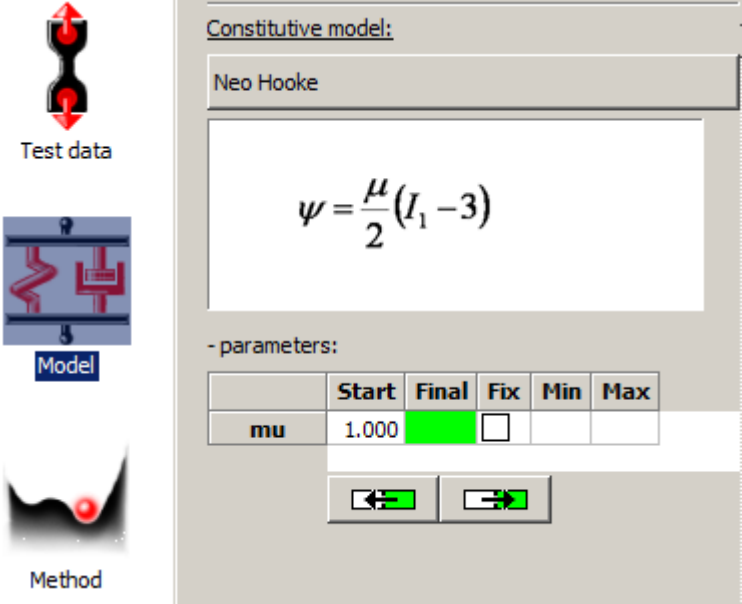


Figure 57 Choosing the material model.

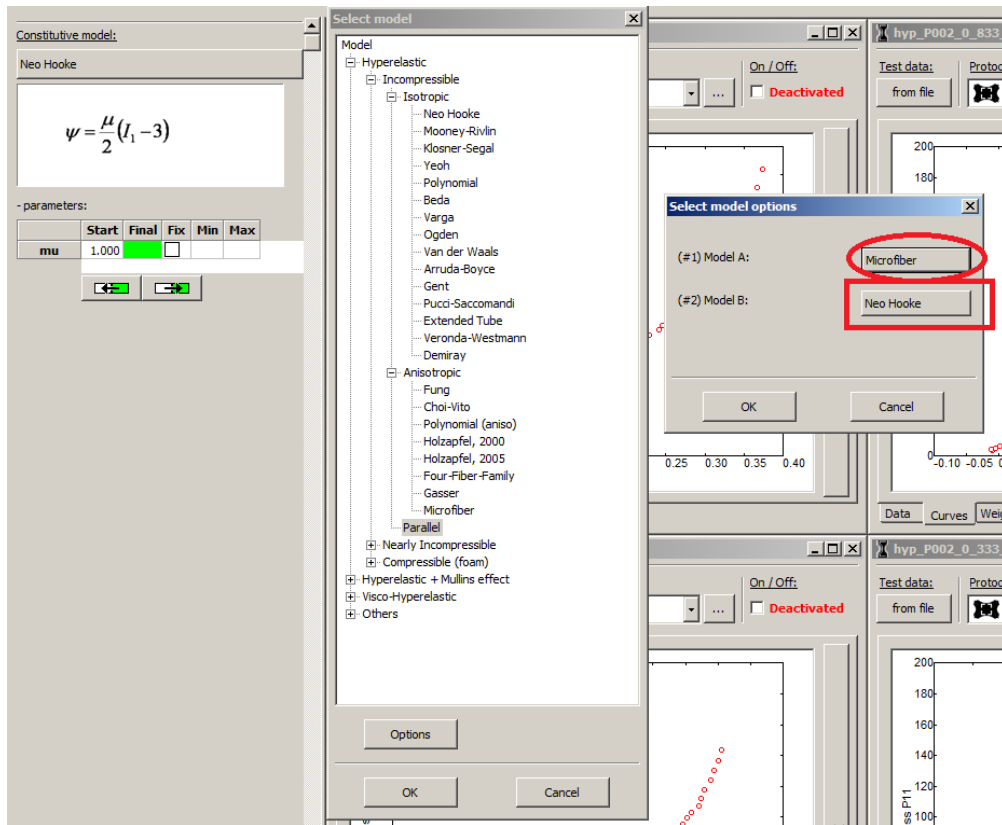


Figure 59 Choosing the second material model.

The second parallel model is getting set up.

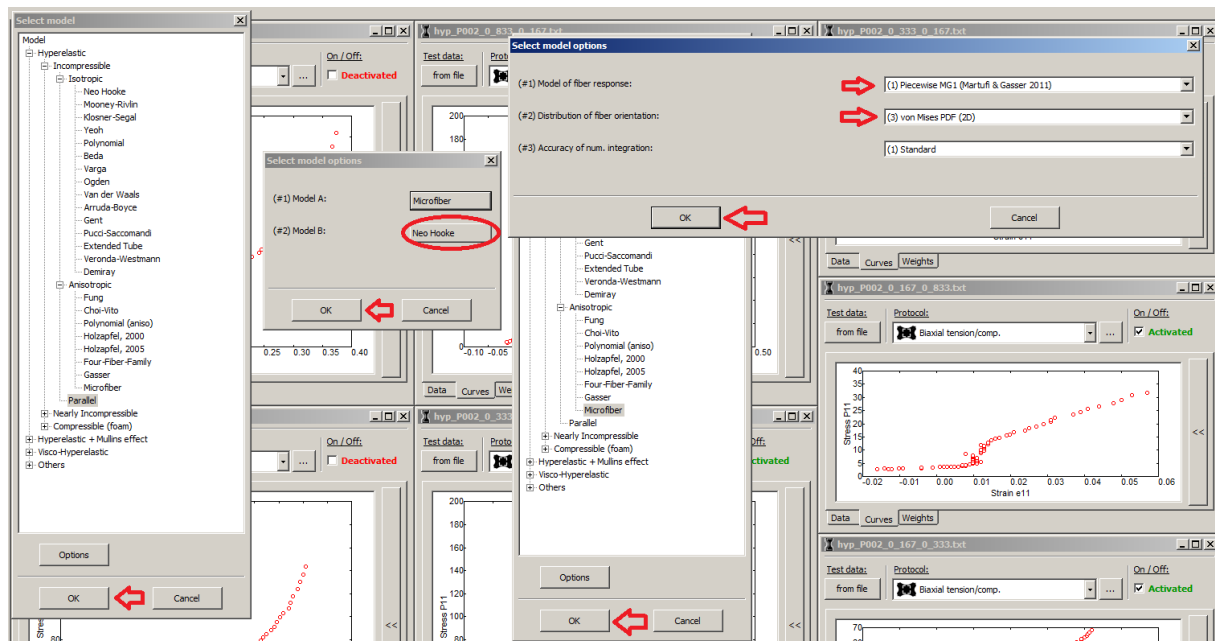
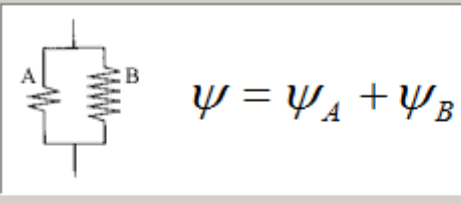


Figure 60 Detailed way how to set up the second chosen material model.

After having chosen the model, its name, description and coefficients are shown in a blank sheet.

Constitutive model:

Parallel



- parameters:

	Start	Final	Fix	Min	Max
mu	1.000		<input type="checkbox"/>	0.00	
k	1.000		<input type="checkbox"/>	0.00	
l_min	1.000		<input type="checkbox"/>	1.00	
l_max	1.500		<input type="checkbox"/>	1.00	
b	0.000		<input type="checkbox"/>	0.00	
mu	1.000		<input type="checkbox"/>	0.00	
k	1.000		<input type="checkbox"/>	0.00	
l_min	1.000		<input type="checkbox"/>	1.00	
l_max	1.500		<input type="checkbox"/>	1.00	
b	0.000		<input type="checkbox"/>	0.00	



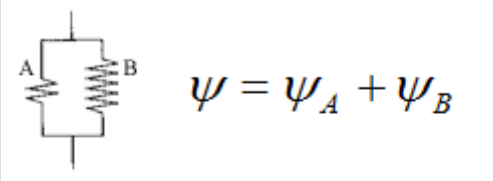
Navigation buttons:  

Figure 61 Table of parameters for chosen material model. Default values.

The Start and Min values are default values which are optional to change. The Microfiber parallel model works with two separate matrixes, but the overall matrix stiffness is just a sum of the two separate ones. Because of this, only one matrix constant is needed, the other one can be fixed to zero easing thus the process of fitting.

Constitutive model:

Parallel



$\psi = \psi_A + \psi_B$

- parameters:

	Start	Final	Fix	Min	Max
mu	1.000		<input type="checkbox"/>	0.00	
k	1.000		<input type="checkbox"/>	0.00	
l_min	1.000		<input type="checkbox"/>	1.00	
l_max	1.500		<input type="checkbox"/>	1.00	
b	0.000		<input type="checkbox"/>	0.00	
mu	0.000	0.000	<input checked="" type="checkbox"/>	0.00	<input type="text"/>
k	1.000		<input type="checkbox"/>	0.00	
l_min	1.000		<input type="checkbox"/>	1.00	
l_max	1.500		<input type="checkbox"/>	1.00	
b	0.000		<input type="checkbox"/>	0.00	



Navigation icons:  

Figure 62 Constraining one matrix stiffness parameter.

More about starting parameters and their influence on the resulting coefficient of determination is analysed after the explanation of fitting process in the chapter 6.2 below.

After successful setup of the program and material model we can start the fitting process using the icon in the left upper corner of the screen. While the fitting process is running, a graph of residuum is shown to illustrate the success of the fitting process.

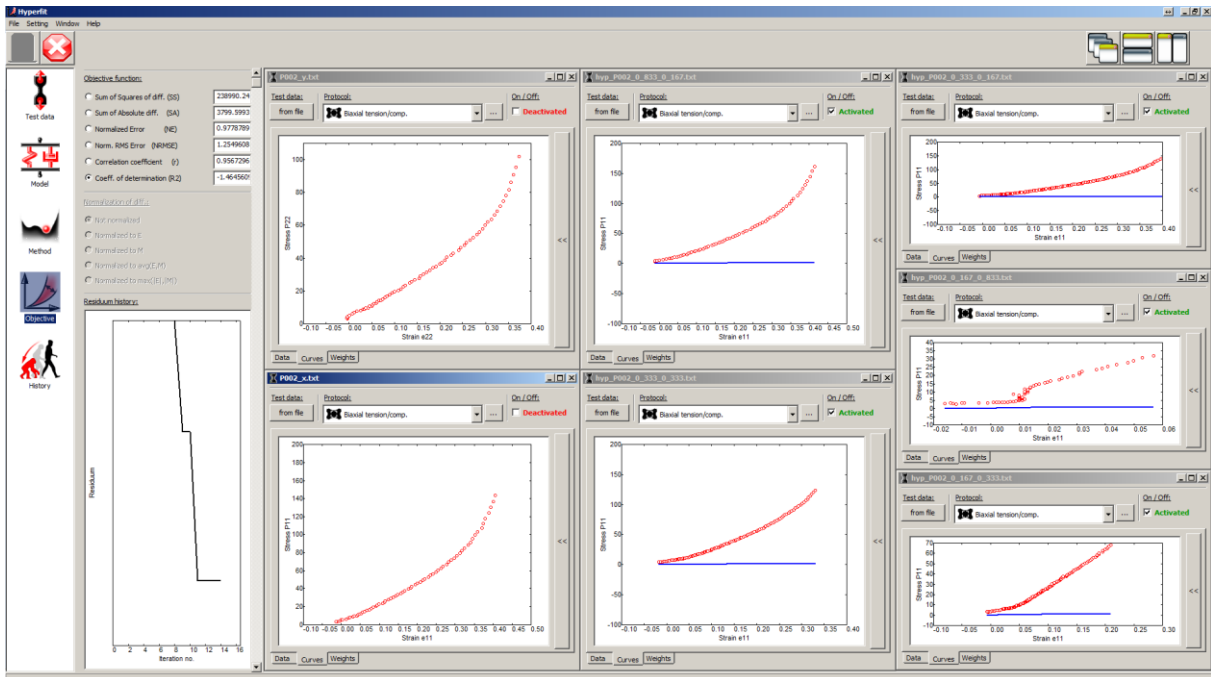


Figure 63 Start of the fitting proces.

After a number of iterations the blue model curves get near the red measured ones.

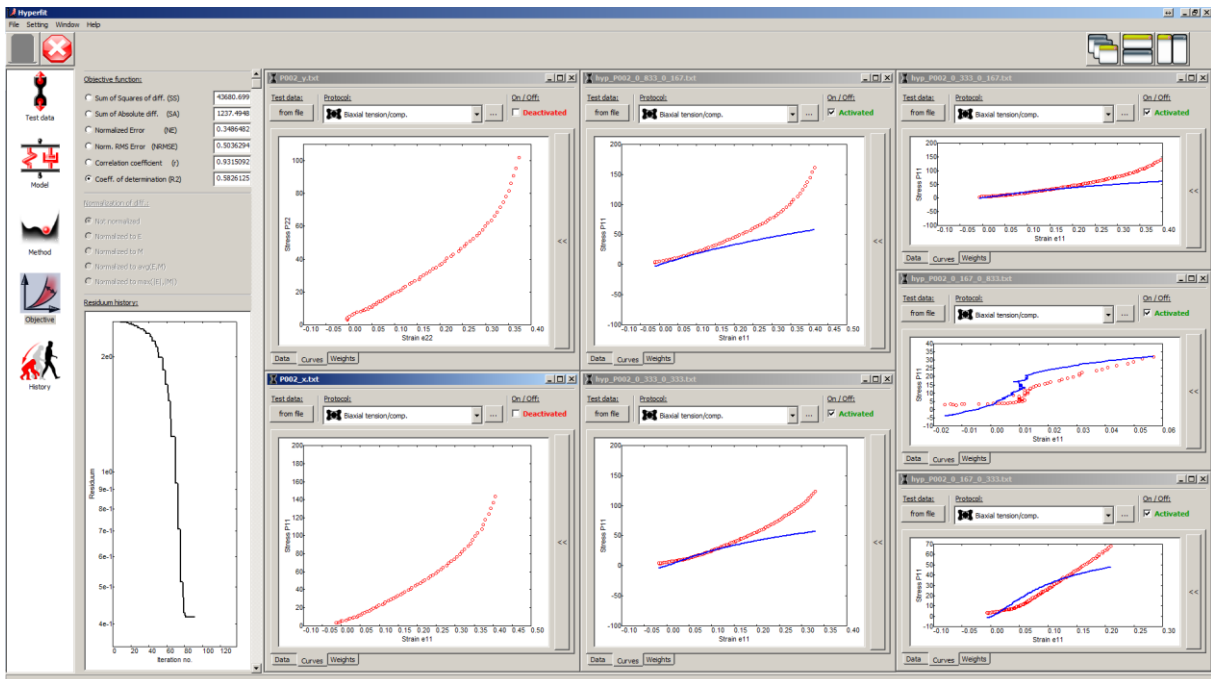


Figure 64 During the fitting proces the model curves (blue) are getting closer to the experimental data.

Once reaching the maximal possible value of the coefficient of determination, the fitting process stops. The values of the NRMSE and R2 are written down.

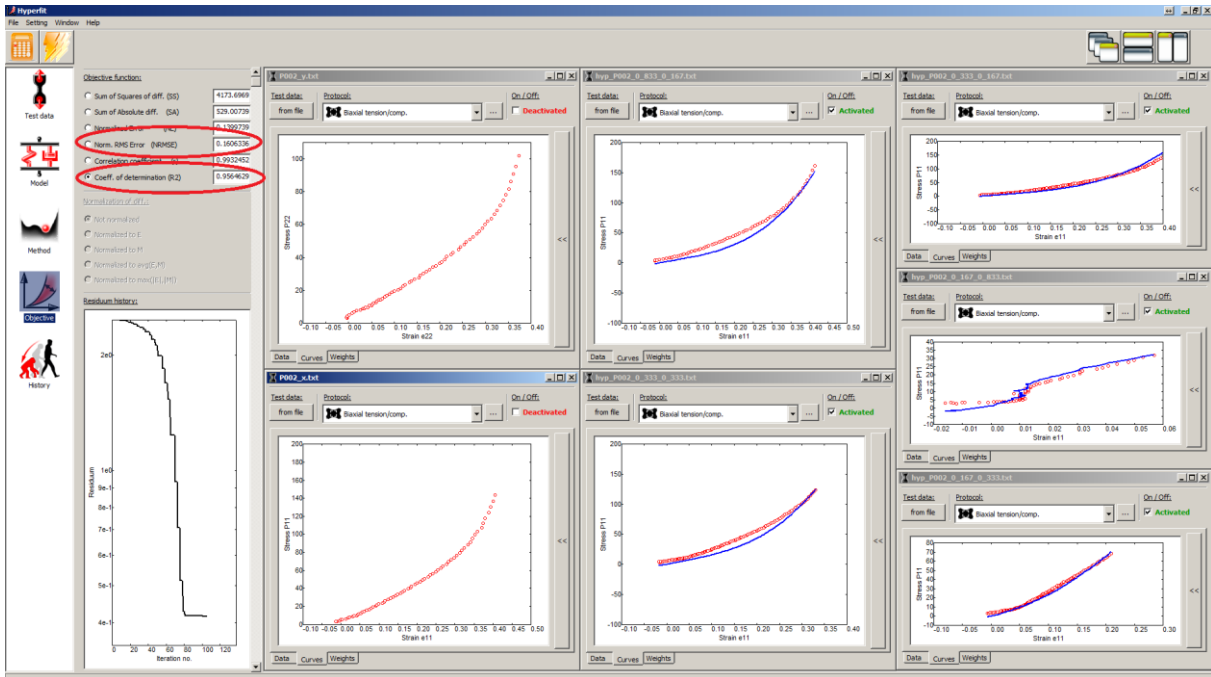


Figure 65 After the fitting process is finished, the values of R^2 and NRMSE are written down.

Also the values of all the coefficients of the material model are written down.

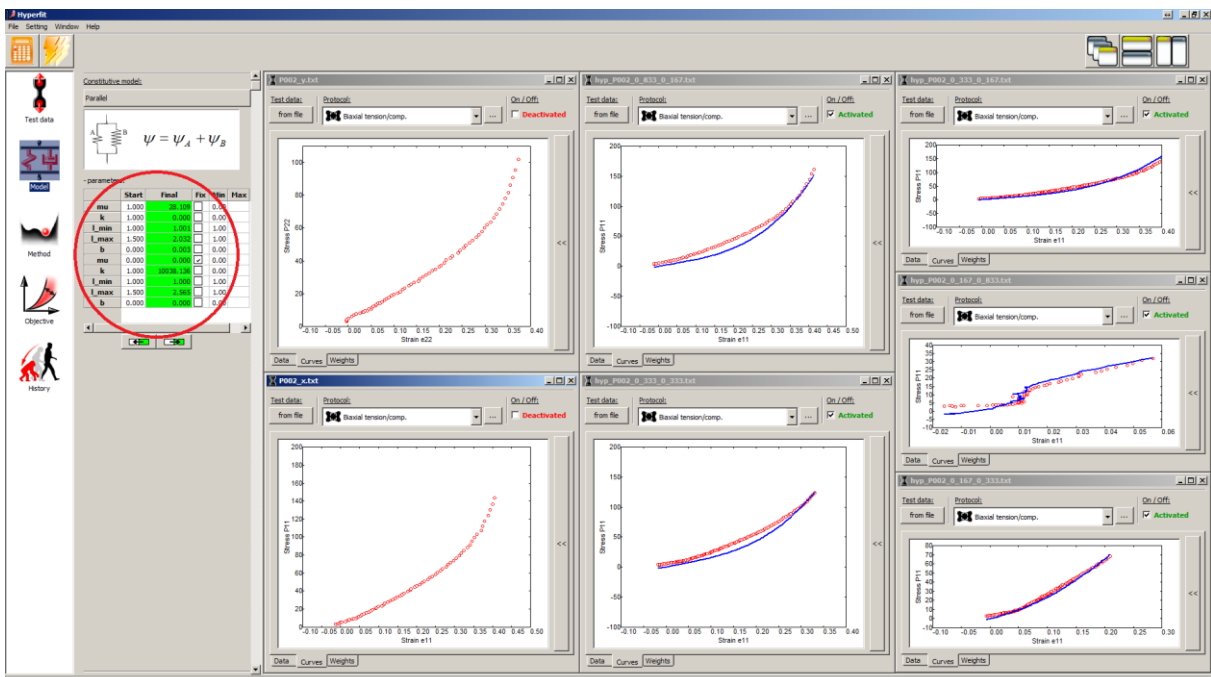


Figure 66 Also the model parameters are written down.

Now the uniaxial data will be fitted. In the first run using the recently fitted material model which was based on biaxial data and then using a new fitting process. Therefore the uniaxial data sets are activated and all the biaxial data sets are turned off. After clicking on the calculator icon in the upper left corner of the screen, the resulting NRMSE and R^2 are shown. These values represent the capability of the material model to predict the uniaxial response on the basis of biaxial experimental data.

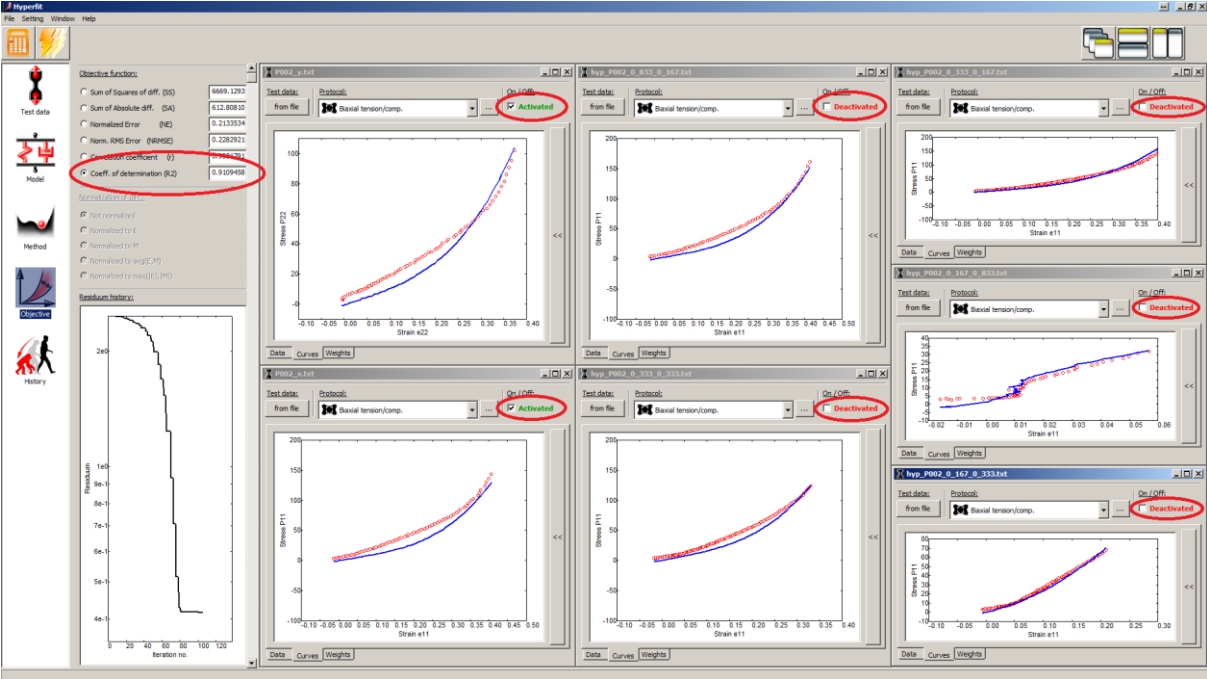


Figure 67 Switching the data sets. Writing down the R^2 and NRMSE.

After this evaluation a new fitting process starts. In this case we fit the material model to uniaxial data.

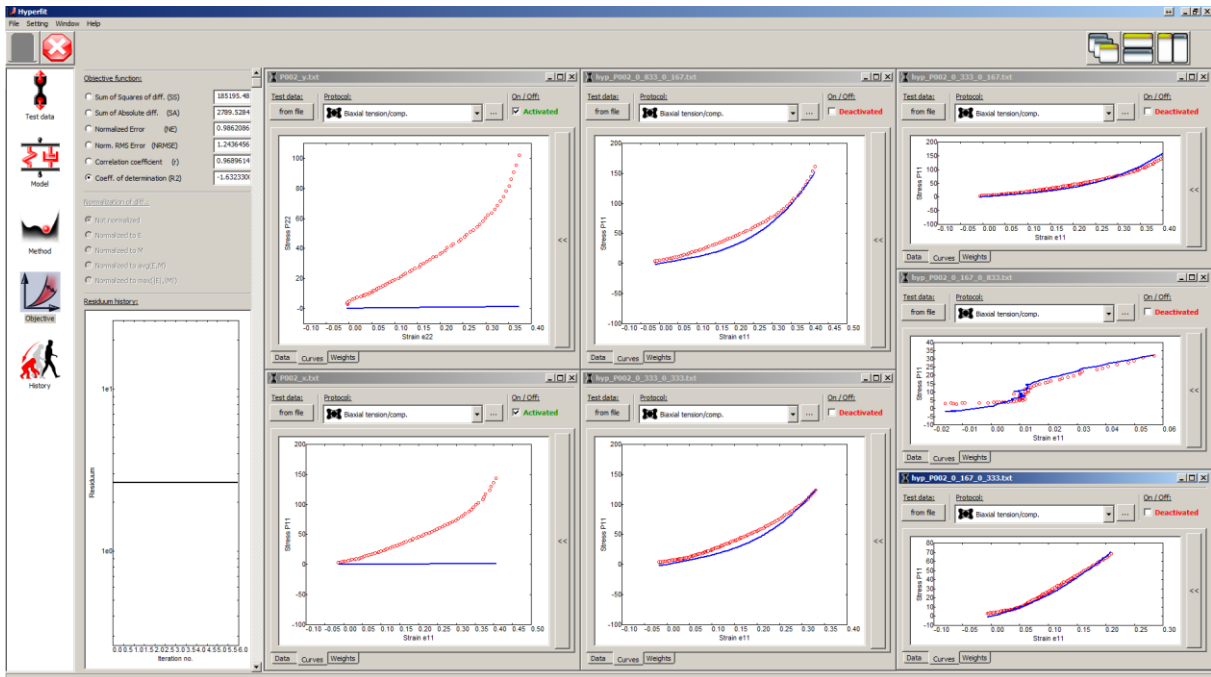


Figure 68 Fitting the other data sets (uniaxial).

After several iterations the blue model curves are getting near the measured data exactly in the same manner as before for the biaxial data. The only difference is the quicker fitting process caused by less data sets to be fitted.

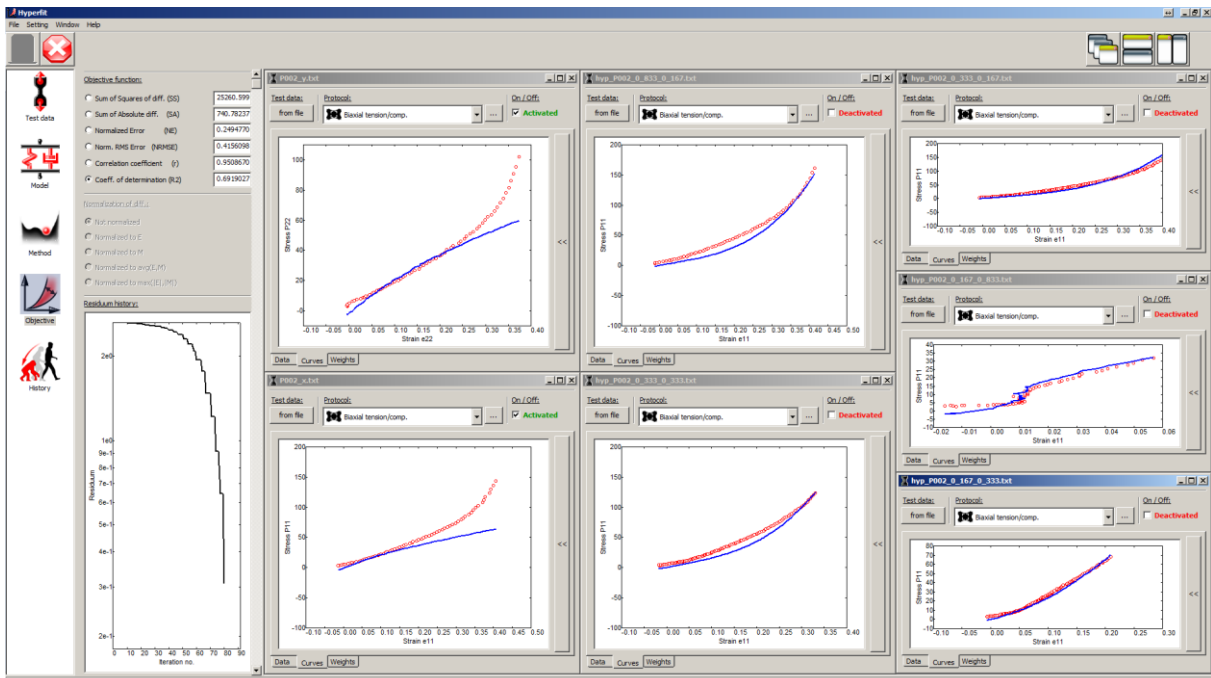


Figure 69 During the fitting process the model curves (blue) are getting closer to the experimental data (uniaxial).

After a short period of time the fitting process terminates. The values of the NRMSE and Coefficient of determination together with the model constants are written down.

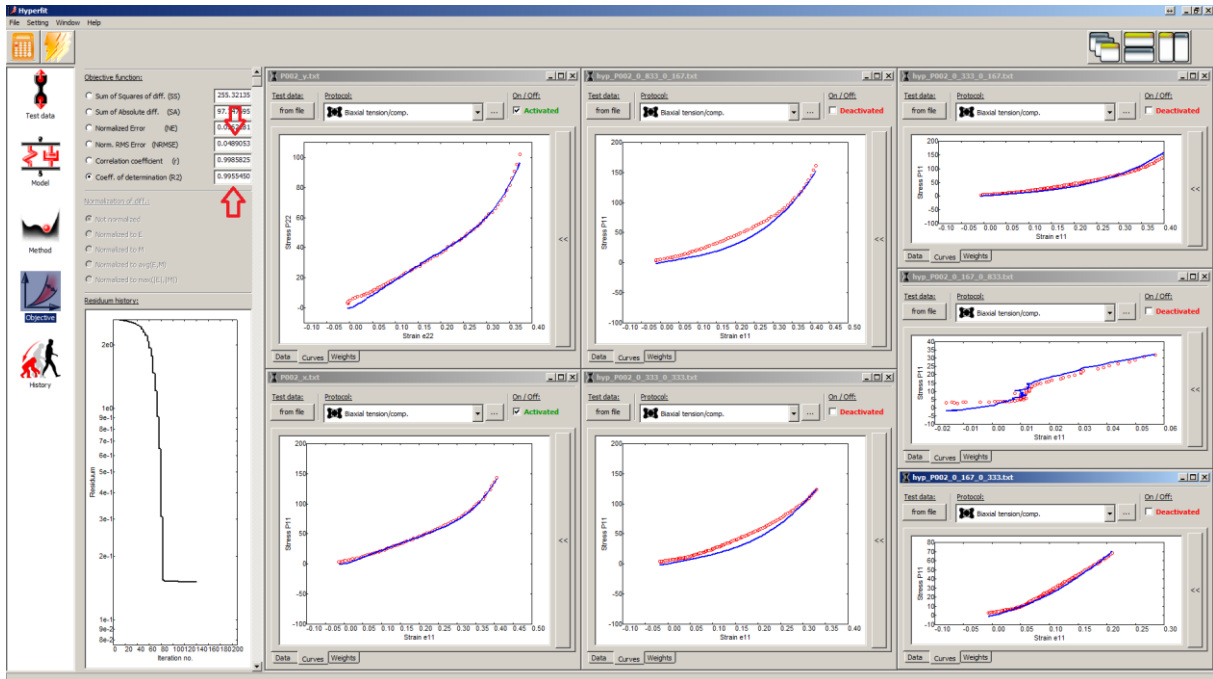


Figure 70 The fitting process is complete for all data sets. R^2 and NRMSE are written down.

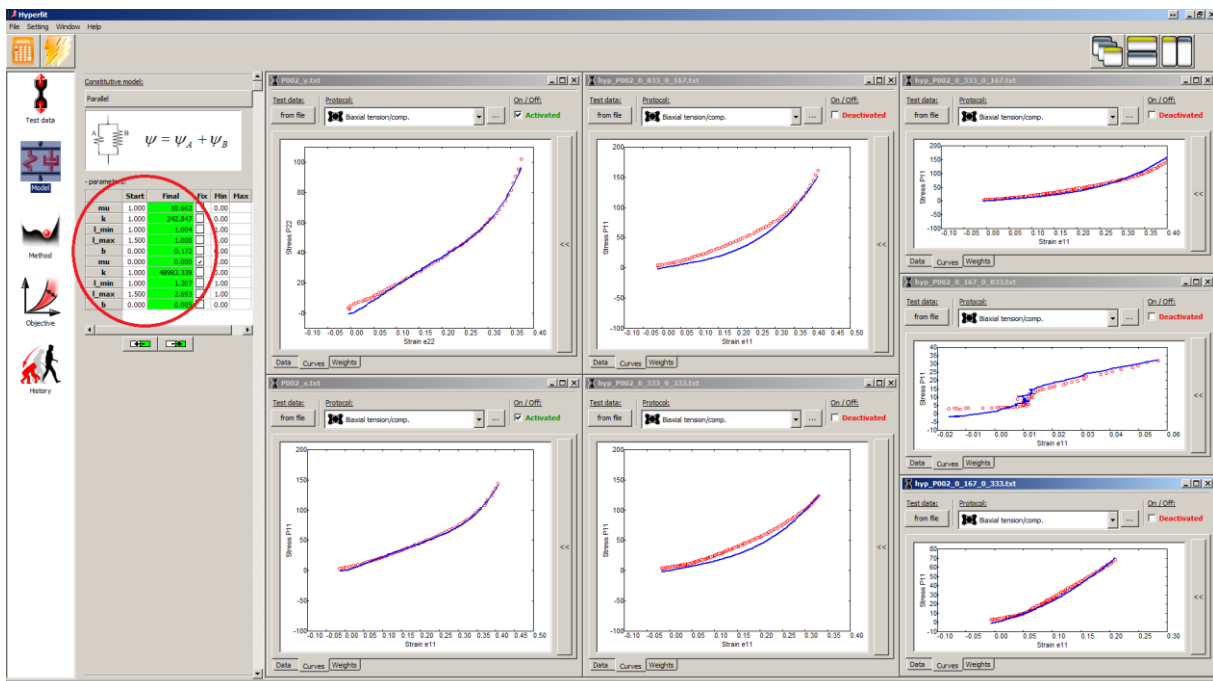


Figure 71 The model parameters are also written down.

When the material model based on uniaxial data is complete, we switch again all the data sets from Activated to Deactivated and vice versa. After having calculated the NRMSE and R^2 of the fitted material model based on uniaxial data which was now used to fit the biaxial data, we obtain and write down the values which represent the predictive capability of the model.

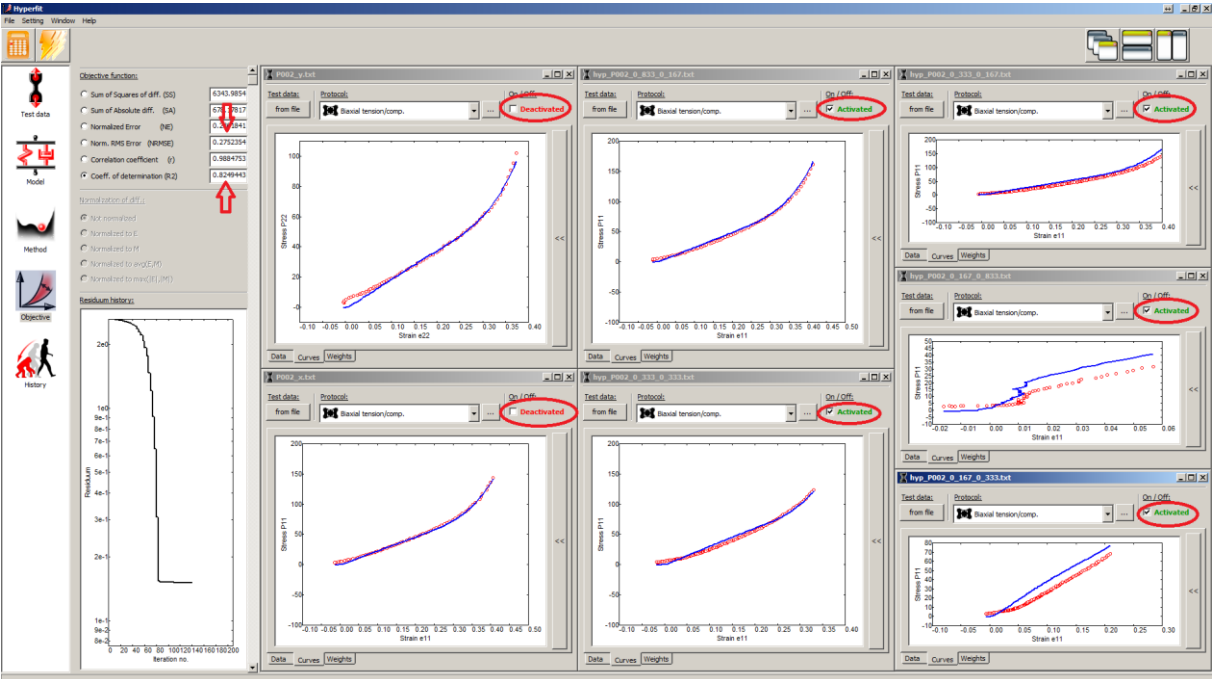


Figure 72 The data sets are switched again and the R^2 and NRMSE are written down.